

PREFACE

This report describes the research that was carried out as a graduation project as part of the curriculum of Civil Engineering at Delft University of Technology. The subject is the rear slope stability of rubble mound breakwaters.

During the research experiments were carried out in the laboratory of fluid mechanics at the subfaculty of Civil Engineering. I would like to thank all co-workers in the laboratory who have helped me during the construction of the experimental set-up.

I would also like to thank all members of the graduation committee, especially ir. H.J. Verhagen who always managed to get me back at "the right track".

Last but not least, I would like to thank my parents and the rest of my family for their mental support during this graduation project and the rest of my study.

Bas van Dijk
December 2001

SUMMARY

The hydraulic processes in and around rubble mound breakwaters as well as the response of the breakwater to these phenomena are not fully understood. Design rules for the required stone (or rock) size are therefore largely based on empirical relations, experience and rules of thumb.

From an economical point of view, it could be attractive to construct low-crested breakwaters, for which a considerable amount of overtopping of waves takes place. A lower crest implies that the crest riprap and the rear slope (or inner slope) armour layer have to withstand a larger amount of wave energy. As a consequence, the front slope armour layer stone size can be reduced, while the stone size of the crest and the rear slope armour layer has to be enlarged. In general, the stone size of the rear slope's armour layer of low-crested breakwaters is taken equal to the (reduced) stone size of the front slope's armour layer. This rule of thumb however lacks a theoretical (and physical) basis. Former research with random waves indicates an overdimensioning of the rear slope when use is made of this rule of thumb.

Above-mentioned research with random waves provides a direct relation between the (significant) wave height and the rear slope stability. In reality however, the wave height is only indirectly responsible for the rear slope stability. The interaction of the waves with the front slope and the crest determines the parameters of the overtopping waves and thus the forces to which the rear slope is subjected. Seepage is considered to be of secondary influence. In this research it is tried to provide a better understanding of the physics of the rear slope. For this, use is made of physical experiments.

In the experimental set-up, it is tried to relate the rear slope stability to the characteristics of overtopping waves (seepage is discarded). In this research waves itself were not considered. Overtopping waves ('plunges') were simulated with water flowing out of a reservoir. The breakwater model was reduced to the rear slope armour layer only. In this way the amount of influencing parameters was minimised. Implicitly, this lead to a simple laboratory model instead of a complicated scale model of a prototype of reality.

In the experiments the rear slope was subjected to plunges of which the sizes were increased with certain steps by increasing the water volume in the reservoir. One step consisted of three plunges of the same size. After each plunge the number and location of the displaced stones were recorded. The experiment ended when rear slope collapse occurred. With this approach, the cumulative damage is considered and not the damage due to individual plunges. One serie of experiments was carried out with individual plunges to compare both approaches.

From the experiments it can be concluded that a distinction has to be made between the occurrence of damage and the collapse behaviour of the rear slope.

First, the occurrence of damage is considered. As long as the rear slope is not collapsed, the damage can be related to the quotient of the maximum instantaneous discharge of the plunge and the maximum layer thickness of the plunge. This parameter is defined as the

characteristic velocity of the plunge. The volume of the plunge does not influence the rear slope stability.

The damage increases progressively, with increasing characteristic velocity. The spread in damage between repeated experiments also increases with increasing characteristic velocity. A minimum of five repeated experiments is required to obtain a minimum reliability of the results. The damage mostly occurred just below the waterline and due to the loss of support as a consequence also above the waterline. Under water the damage quickly decreases.

The crest freeboard significantly influences the rear slope damage development. Similar series of experiments were carried out for three different crest freeboards by varying the water level in the flume. The rear slope stability is least for an intermediate crest freeboard. On average, the sum of the stabilising damping effect of the tailwater and the destabilising lifting effect of the tailwater is least favourable in this situation.

One serie of experiments was carried out with individual plunges. The rear slope proved to be less stable. At an arbitrary plunge size, the damage due to an individual plunge was larger than the damage due to a plunge preceded by several smaller plunges. This difference quickly increases with increasing plunge size. It seems that the damage due to individual plunges plotted against the plunge size has an exponential development.

Second, the collapse behaviour is considered. It was observed that in some experiments collapse occurred at relatively small values of the plunge size, while in other experiments the rear slope could resist fairly large values of the plunge size. The probability of collapse increased with increasing plunge size. Taken into account the limited amount of experiments carried out, it seems that this probability resembles a Gaussian-like curve.

According to the experiments, the crest freeboard seems to influence the collapse behaviour. Especially in the case of a very low crest freeboard, the rear slope seems less sensitive to collapse than in the case of a high crest freeboard or an intermediate one.

It is recommended that in future research a standard experiment is repeated many times (approximately a hundred times), in order to better investigate the occurrence of damage as well as the collapse behaviour. This standard experiment can be used to endorse above conclusions.

The great influence of the waterline relative to the crest justifies more research into the influence of the crest freeboard. Especially the crest freeboard for which the rear slope stability is lowest, is important to establish. Furthermore, the influence of other breakwater parameters should be investigated, for instance the rear slope angle, the stone size, the stone shape and the roughness of the filter layer. Finally, more knowledge about the stability of single stones on a rubble slope could contribute to a better understanding of the rear slope physics and is therefore an interesting field of future research.

TABLE OF CONTENTS

PREFACE	1
SUMMARY	2

TABLE OF CONTENTS	3
LIST OF SYMBOLS	6
LIST OF FIGURES	8
LIST OF TABLES	10
1 BACKGROUND	11
1.1 INTRODUCTION	11
1.2 BREAKWATER TYPES	11
1.3 BREAKWATER STABILITY	12
1.4 LOW-CRESTED BREAKWATERS	13
1.5 TECHNICAL AND ECONOMICAL RELEVANCE	13
1.6 OUTLINE	14
2 PROBLEM ANALYSIS	15
2.1 INTRODUCTION	15
2.2 MAIN GOAL	16
2.3 SCOPE	16
2.4 PROBLEM DESCRIPTION	17
2.5 OBJECTIVE	17
3 LITERATURE STUDY	18
3.1 INTRODUCTION	18
3.2 WAVE PARAMETERS	19
3.3 BREAKWATER PARAMETERS	21
3.4 HYDRAULIC RESPONSE	23
3.5 STRUCTURAL RESPONSE REAR SLOPE	29
3.6 GENERAL REMARKS	32
4 EXPERIMENTS	34
4.1 INTRODUCTION	34
4.2 CONCEPTUAL DESIGN OF EXPERIMENTAL SET-UP	36
4.3 EXPERIMENTAL SET-UP	38
5 DATA PROCESSING	50
5.1 INTRODUCTION	50
5.2 PLUNGE CHARACTERISTICS	50
5.3 REAR SLOPE DAMAGE	55
6 ANALYSIS OF EXPERIMENTS	63
6.1 INTRODUCTION	63
6.2 REAR SLOPE DAMAGE VS REAR SLOPE COLLAPSE	63
6.3 RELATION BETWEEN CUMULATIVE DAMAGE AND PLUNGE CHARACTERISTICS	64
6.4 PROBABILITY OF COLLAPSE	70
6.5 INFLUENCE CREST FREEBOARD ON REAR SLOPE DAMAGE	72
6.6 INFLUENCE CREST FREEBOARD ON DAMAGE LOCATION	74
6.7 INFLUENCE CREST FREEBOARD ON COLLAPSE BEHAVIOUR	76
6.8 DAMAGE DUE TO INDIVIDUAL PLUNGES	77
6.9 COMPARISON DAMAGE RESULTS WITH FORMER RESEARCH	79

7	CONCLUSIONS / RECOMMENDATIONS	85
7.1	CONCLUSIONS	85
7.2	RECOMMENDATIONS	86
8	REFERENCES	87
ANNEX I – LITERATURE		
ANNEX I.A	VAN GENT’S EQUATIONS FOR WAVE RUN-UP	89
ANNEX I.B	PERIODIC WAVE OVERTOPPING - BATTJES	91
ANNEX I.C	PERIODIC WAVE OVERTOPPING - PERDIJK	93
ANNEX I.D	COMPARISON AVG. OVERTOPPING EQUATIONS	95
ANNEX I.E	DISTRIBUTION OF OVERTOPPING WAVES	100
ANNEX I.F	WAVE OVERTOPPING – VAN GENT	101
ANNEX I.G	REAR SLOPE STABILITY - WALKER	104
ANNEX I.H	REAR SLOPE STABILITY - VIDAL	106
ANNEX I.I	REAR SLOPE STABILITY - VAN DER MEER	107
ANNEX I.J	REAR SLOPE STABILITY – DE JONG	108
ANNEX I.K	REAR SLOPE STABILITY - ANDERSEN	110
ANNEX I.L	REAR SLOPE STABILITY – KOBAYASHI	113
ANNEX II – EXPERIMENTS		
ANNEX II.A	RESERVOIR OUTFLOW	116
ANNEX II.B	DERIVATION OF MAXIMUM DISCHARGE	118
ANNEX II.C	DERIVATION OF MAX. LAYER THICKNESS	124
ANNEX II.D	DERIVATION OF FRONT VELOCITY	130
ANNEX II.E	DERIVATION OF CHARACTERISTIC VELOCITY	133
ANNEX II.F	DATA ON CUM. DAMAGE DEVELOPMENT	136
ANNEX II.G	DAMAGE DUE TO INDIVIDUAL PLUNGES	139
ANNEX II.H	DAMAGE INCLUDING RELIABILITY INTERVALS	140
ANNEX III – ROUGH ESTIMATES OF DIMENSIONS OF EXPERIMENTAL SET-UP		
ANNEX III.A	SCHATTING PARAMETERWAARDEN	143
ANNEX III.B	DIMENSIES PROEFOPSTELLING	147
ANNEX III.C	FORMULES VAN GENT	150
ANNEX III.D	FORMULES PERDIJK	152
ANNEX III.E	STABILITEITSFORMULES VAN DER MEER	153

LIST OF SYMBOLS

α	Front slope angle	[-]
A_r	Water surface of reservoir	[m ²]
β	Rear slope angle	[-]
b	Normalised overtopping volume	[-]
B	Width of experimental set-up	[m]
B_c	Crest width	[m]
d	Layer thickness	[m]
d_{\max}	Maximum layer thickness	[m]
d_{Ru}	Layer thickness of run-up	[m]
D_n	Diameter of stone / block	[m]
$d_{2\%}$	Maximum layer thickness of overtopping volume at the rear side of the crest, exceeded by 2% of the incident waves	[m]
f_f	Roughness of filter layer	[-]
g	Gravitational acceleration	[m/s ²]
γ_β	Reduction factor, taking into account angular wave attack	[-]
γ_f	Reduction factor, taking into account the structure's friction	[-]
γ_{f-c}	Crest roughness reduction factor	[-]
h	Water level in front of the structure	[m]
H	Incident wave height in front of structure	[m]
H_s	Significant wave height	[m]
ϑ_m	Normalised run-up volume	[-]
$k = \frac{2\pi}{L}$	Wave number	[m ⁻¹]
κ	Fractional distance along the front slope	[-]
L	Wave length	[m]
L_0	Wave length at deep water	[m]
L_{Ru}	Run-up length	[m]
M_n	Stone mass, which is exceeded by n % of the stones	[kg]
N	Number of waves	[-]
N_{ow}	Number of overtopping waves	[-]
N_w	Number of incoming waves	[-]
N_{od}	Damage parameter	[-]
P	Permeability factor (of Van der Meer)	[-]
\bar{q}	Average overtopping discharge	[m ³ /ms]
$q_{2\%}$	maximum overtopping discharge at the rear side of the crest, exceeded by 2% of the incident waves	[m ³ /ms]
$P_{ow} = \frac{N_{ow}}{N_w}$	Probability of overtopping per wave	[-]

P_V	Probability of the overtopping volume per wave \underline{V} being less than or similar to V	[-]
Q	Discharge	[m ³ /s]
Q_b	Dimensionless discharge parameter breaking waves	[-]
Q_n	Dimensionless discharge parameter non-breaking waves	[-]
Q_{\max}	Maximum discharge	[m ³ /s]
R_c	Crest freeboard related to SWL	[m]
$R_{u2\%}$	Wave run-up height exceeded by 2% of incident waves	[m]
$s = \frac{H}{L}$	wave steepness	[-]
s_{op}	Wave steepness, using the peak period T_p and the significant wave height H_{os} at deep water (off-shore)	[-]
s_{om}	Average wave steepness at deep water (off-shore)	[-]
S	Damage parameter	[-]
t_a, t_f	Thickness of armour layer and filter layer	[m]
T	Incident wave period	[s]
\bar{T}	Average wave period	[s]
ρ_s	Mass density of stone	[kg/m ³]
$u_{2\%}$	maximum overtopping velocity at the rear side of the crest, exceeded by 2% of the incident waves	[m/s]
u_{char}	Characteristic velocity ($= \frac{Q_{\max}}{B \cdot d_{\max}}$)	[m/s]
u_f	Front velocity	[m/s]
v_{Ru}	Run-up velocity	[m/s]
$V_{2\%}$	Overtopping volume exceeded by 2% of the incident waves	[m ³ /m]
V_{over}	Overtopping volume	[m ³]
W_f	Front slope stone weight divided by rear slope stone weight	[-]
$\omega = \frac{2\pi}{T}$	Wave frequency	[s ⁻¹]
ξ	Irribarren parameter	[-]
ξ_{op}	Irribarren parameter, using the peak period T_p and the significant wave height H_{os} at deep water (off-shore)	[-]
θ_{u_f}	Shields parameter with front velocity	[-]
$\theta_{u_{char}}$	Shields parameter with characteristic velocity	[-]
θ_q	Shields parameter with maximum discharge per unit width	[-]

LIST OF FIGURES

Figure 1: The classical rubble mound breakwater	12
Figure 2: Differences in response of front slope and rear slope	15
Figure 3: Interaction between wave parameters and breakwater parameters	18
Figure 4: Breakwater parameters	21
Figure 5: Definition of wave run-up	23
Figure 6: The schematised shape of an overtopping wave ('plunge')	28
Figure 7: Test results of De Jong and Van der Meer	30
Figure 8: Field of interest	35
Figure 9: Sketch of experimental set-up	39
Figure 10: Overview of experimental set-up	39
Figure 11: The transition between the crest and the rear slope	40
Figure 12: Solution for transition	40
Figure 13: Eight coloured strips, including strip numbers	41
Figure 14: Stone size of the three different stone-classes.	42
Figure 15: The length-width ratio of the three different stone-classes	43
Figure 16: WHM2 and WHM3	45
Figure 17: Collision of plunge with WHM	46
Figure 18: The three configurations of the reservoir (not on scale)	51
Figure 19: Volume versus the water level inside the reservoir	51
Figure 20: Relation between water level in reservoir and maximum discharge for the three reservoir configurations.	52
Figure 21: Relation between water level inside the reservoir and maximum layer thickness for the three reservoir configurations.	53
Figure 22: Relation between water level in reservoir and front velocity for the three reservoir configurations.	54
Figure 23: Relation between water level in reservoir and characteristic velocity for the three reservoir configurations.	55
Figure 24: Cumulative damage for Configuration I, crest freeboard = 10 cm	57
Figure 25: Cumulative damage for Configuration II, crest freeboard = 10 cm	57
Figure 26: Cumulative damage for Configuration III, crest freeboard = 10 cm	58
Figure 27: Cumulative damage for Configuration I, crest freeboard = 7 cm	58
Figure 28: Cumulative damage for Configuration I, crest freeboard = 3 cm	59
Figure 29: Damage per strip, crest freeboard = 10 cm, experiment 3	60
Figure 30: Damage per strip, crest freeboard = 7 cm, experiment 3	60
Figure 31: Damage per strip, crest freeboard = 3 cm, experiment 1	61
Figure 32: Damage due to individual plunges for Configuration I	62
Figure 33: Cumulative damage development plotted against θ_{u_f}	66
Figure 34: Cumulative damage development plotted against θ_q	67
Figure 35: Layer thickness plotted against θ_q	69
Figure 36: Cumulative damage development plotted against $\theta_{u_{char}}$	70
Figure 37: Probability of collapse	71
Figure 38: Average damage development for all data (second approach)	72
Figure 39: Three different water levels (not on scale)	73
Figure 40: Influence of crest freeboard on cumulative damage development.	73
Figure 41: Damage per strip for Configuration I and crest freeboard of 10 cm	75
Figure 42: Damage per strip for Configuration I and crest freeboard of 7 cm	75
Figure 43: Damage per strip for Configuration I and crest freeboard of 3 cm	76
Figure 44: Comparison of collapse behaviour of three dimensionless crest freeboards	77
Figure 45: Comparison between cumulative damage and damage due to individual plunges	78

Figure 46: 'Exponential' character of damage due to individual plunges	78
Figure 47: Burger's relation between significant wave height and rear slope stability ($S=0.5$)	79
Figure 48: Relation between overtopping velocity and significant wave height for different crest freeboards	82
Figure 49: Dimensionless overtopping velocity vs dimensionless significant wave height	82
Figure 50: Comparison of experimental data with Burger's data	83
Figure 51: Wave run-up according to Van Gent	90
Figure 52: Comparison of equations that predict overtopping ($H_s = 8$ m)	99
Figure 53: Rear slope stability results of Walker	104
Figure 54: Forces acting on a single stone, according to Andersen	111
Figure 55: Overtopping wave according to Kobayashi	113
Figure 56: Forces on stone according to Kobayashi	114
Figure 57: Examples of data on discharge	119
Figure 58: 'Translation wave' in reservoir	120
Figure 59: Average maximum discharge vs initial water level in reservoir	122
Figure 60: Reliability of data	123
Figure 61: Typical example of data	124
Figure 62: Comparison of the two methods to determine maximum layer thickness	125
Figure 63: Examples of data on layer thickness	126
Figure 64: Maximum layer thickness vs initial water level in reservoir	128
Figure 65: Reliability of data	129
Figure 66: Front velocity vs initial water level in reservoir	131
Figure 67: Reliability of data	132
Figure 68: Characteristic velocity vs initial water level in the reservoir	134
Figure 69: Reliability of data	135
Figure 70: Cumulative damage vs u_f	140
Figure 71: Cumulative damage vs q	140
Figure 72: Cumulative damage vs. u_{char}	141
Figure 73: Cumulative damage for three different crest freeboards (Configuration I)	141
Figure 74: Cumulative damage vs individual damage	141

LIST OF TABLES

Table 1: Features of the different stone-classes _____	42
Table 2: Reservoir configurations _____	47
Table 3: Experiments on cumulative damage _____	48
Table 4: Experiments on damage due to individual plunges _____	48
Table 5: Experiments on cumulative damage _____	56
Table 6: Combinations of parameters considered _____	65
Table 7: Values of other plunge characteristics for an arbitrary value of front velocity _____	66
Table 8: Values of other plunge characteristics for arbitrary value of maximum discharge _____	68
Table 9: Variables used in the comparison _____	98
Table 10: Damage vs. water level; $R_c = 10$ cm; Configuration I _____	136
Table 11: Damage vs water level; $R_c = 10$ cm; Configuration II _____	136
Table 12: Damage vs water level; $R_c = 10$ cm; Configuration III _____	137
Table 13: Damage vs water level; $R_c = 7$ cm; Configuration I _____	137
Table 14: Damage vs water level; $R_c = 3$ cm; Configuration I _____	138
Table 15: Individual damage vs water level; $R_c = 10$ cm; Configuration I _____	139

1 BACKGROUND

1.1 Introduction

The subject of this report is the static stability of the rear slope armour layer of classical breakwaters. In this first chapter the subject's background is presented, in which emphasis is put on the technical relevance as well as on the economical relevance of this report.

1.2 Breakwater types

Basically, breakwaters are used to provide a sheltered area from the action of wind waves and swell. This area mostly concerns the entrance channel and basin of a port, but it can also concern for instance a beach section or a water intake facility for a power plant. The breakwater is expected to reduce the wave energy in the protection area to a certain acceptable value. Other functions of breakwaters comprise the guidance of currents, protection against shoaling and the provision of quay facilities.

Next to their functional requirements, breakwaters can be categorised according to their structural features, e.g.:

- *Monolithic type* structure that acts as one solid block.
- *Rubble mound type* structure that consists of loose non-cohesive elements.
- *Composite type* structure that consists of a solid block, with a berm composed of loose material.

In this report only the "classical" rubble mound type breakwater is considered. This type of breakwater consists of several layers of stone. The armour layer has to withstand the wave forces and therefore consists of heavy blocks. The core, which is protected from wave attack by the armour layer, can be constructed with smaller stones. In between the core and the armour layer a filter layer of intermediate stone size prevents the core from getting washed out. In *Figure 1* an example of a classical rubble mound breakwater is presented.

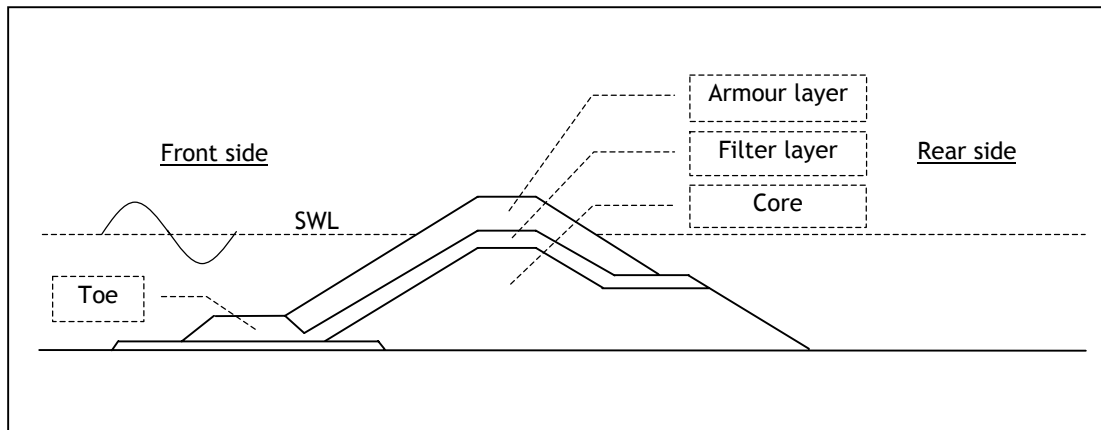


Figure 1: The classical rubble mound breakwater

1.3 Breakwater stability

As breakwaters are rather expensive, extensive research into breakwater design has been carried out. The research on rubble mound breakwaters can be divided into two parts:

- *Hydraulic research*, which describes the transmission of wave energy through and over the breakwater
- *Structural research*, which describes the response of the rubble mound breakwater to waves

This report discusses research of the second type.

The response of a breakwater to incoming waves is indicated as the breakwater stability. A breakwater should be constructed in such a way that its stability is secured under certain normative conditions, the so-called Ultimate Limit State (ULS). This can be seen as the most unfavourable situation to which the breakwater is subjected in its lifetime.

Next to the ULS, the Serviceability Limit State (SLS) is distinguished, which is defined as the state at which the breakwater can still fulfil its functions. In general the ULS and the SLS are not the same. For instance, it is quite common that a port is allowed to have a few days 'down-time' a year, during which the wave height in the port exceeds the permissible wave height for normal (un)loading activities. However, during this SLS the breakwater is not allowed to lose its stability. In this report only the ULS is considered.

Several failure mechanisms can lead to instability of the breakwater. Examples are "instability of armour layer", "instability of toe", "settlement of subsoil" and "displacement of crest element". In this report only the failure mechanism "instability of armour layer" is considered.

The primary stabilising parameter of the armour layer is the weight of the blocks. As long as the weight of the blocks in the armour layer exceeds the force of the incoming waves, the stability of the blocks is secured. This report only treats the static stability of the

armour layer of a breakwater. Dynamically stable rubble mound breakwaters, for which some “reshaping” of the breakwater’s slope is allowed, are not discussed.

1.4 Low-crested breakwaters

Breakwaters are characterised as “low-crested” when the crest freeboard of the breakwater is low compared to the wave height and considerable overtopping takes place.¹ Recent studies proved that lowering the crest of a rubble mound breakwater positively affects the stability of the front slope armour layer. This can be explained by the fact that part of the wave energy is transported over the breakwater. Accordingly, the wave attack on the crest and on the rear slope armour layer increases. In this report a first attempt is made to describe the static stability of the rear slope armour layer of low-crested breakwaters. Instead of the terms “front slope armour layer” and “rear slope armour layer” simply the terms “front slope” and “rear slope” will be used in this report.

At first sight, it is not expected that low-crested breakwaters are suitable for the protection of a port basin. Low-crested structures seem more appropriate to protect areas, for which only partial protection is needed, like beach sections. However, in certain areas around the world, the difference between the SLS and ULS is very large due to rarely occurring situations, which determine the ULS, like typhoons. It is imaginable that in the ULS the constructed breakwater is characterised as low-crested, while this is not the case under normal wave conditions (or during the SLS). According to the above this could mean a reduction of the stone size needed for the armour layer, which leads to a more economical design.

1.5 Technical and economical relevance

The construction costs of the breakwater’s armour layer depend to a great extent on the amount and the size of the material used. In general it can be stated that the amount of stones used is positively correlated to the construction costs. This also applies for the size of stones used. On the other hand, the maintenance costs are negatively correlated to the stone size used. The economically optimum design amounts to the lowest total costs, which equals the sum of construction costs and maintenance costs.

With complete understanding of all hydraulic processes around the breakwater and the breakwater’s response to these phenomena, this economically optimum design could be found. Principally, all structural research in the field of breakwater design is performed to attain this economic optimum.

The most commonly used equations in the design of the armour layer’s stone size of rubble mound breakwaters are the equations of Van der Meer [2]. These equations mainly concentrate on the stability of the front slope of non-overtopped rubble mound breakwaters. Van der Meer provides reduction factors for the required mass of stone on the front slope of statically stable low-crested rubble mound breakwaters, but he did not perform extensive research on the stability of rear slopes. In general, the armour size on

¹ The crest freeboard is taken relative to the Still Water Level (SWL). A breakwater with a negative freeboard is called “submerged”. In this report only breakwaters with positive freeboards are considered.

the rear slope of low-crested breakwaters is taken equal to the (reduced) armour on the front slope. This rule of thumb however lacks a theoretical (and physical) basis.

From the above it can be concluded that from an economical point of view it is desirable to reduce the size of the material needed for construction of the breakwater's armour layer as much as possible. A fair estimate of the minimum stone size needed can only be given when the physics that control the stability of the stones is completely clear. For the rear slope of a low-crested rubble mound breakwater this insight is not yet available in literature. The simple design rules seem somewhat arbitrary and could lead to an uneconomical design. This report tries to explain the physics of the rear slope of a low-crested breakwater. In doing so, the report will fill up part of the gap in existing literature on rubble mound breakwater design. This should contribute to more economic breakwater designs in the future.

1.6 Outline

In Chapter 2 the problem analysis is dealt with, resulting in the problem description and the objective to be reached in this report. In Chapter 3 previous research in the field of wave overtopping and rear slope stability is discussed. In Chapter 4 this is followed by the description of the experimental set-up that is used for physical tests. In Chapter 5 the processing of experimental data is dealt with, followed by the analysis of those data in Chapter 6. This finally leads to the conclusions and recommendations in Chapter 7.

2 PROBLEM ANALYSIS

2.1 Introduction

The front slope stability of a breakwater is determined by the front slope strength and the hydraulic load caused by incoming waves. For low-crested breakwaters, the front slope stability is also affected by the crest freeboard relative to the water level.

The rear slope stability of a low-crested breakwater is determined by the rear slope strength and the hydraulic load caused by waves overtopping the crest (from here on referred to as 'plunges') and seepage flowing through the breakwater.

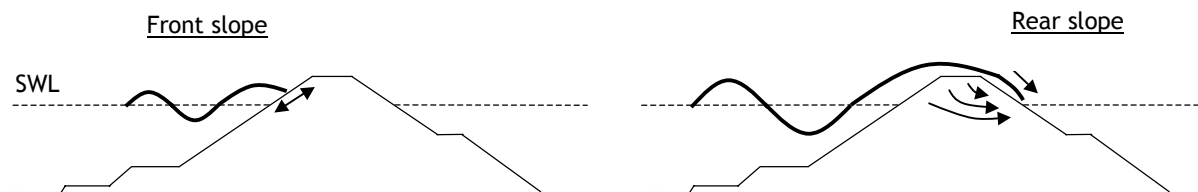


Fig. 2.1.1. Front and rear slope stability analysis

As can be concluded from the above, little similarity is found between the response of the front slope and the response of the rear slope on waves attacking the breakwater. The discrepancies can be summed up as follows:

- The wave impacts due to collapsing waves which occur at the front slope do not appear at the rear slope
- The amount of plunges subjected to the rear slope is (much) lower than the amount of waves subjected to the front slope
- The primary hydraulic force on the rear slope acts in almost the same direction as the gravity force, while the primary hydraulic force on the front slope acts in almost opposite direction of the gravity force
- At the front slope wave down-rush has to be accounted for as an extra (secondary) destabilising force downward the slope
- At the rear slope seepage has to be accounted for as an extra (secondary) destabilising force

Above-mentioned discrepancies between the hydraulic loads on the front slope and on the rear slope of low-crested rubble mound breakwaters justify a separate study of the rear slope stability. It is quite probable that the physical processes determining the rear slope stability differ considerably from the physical processes that determine the front slope stability. Therefore, the normative wave conditions for the rear slope are not necessarily the same as for the front slope.

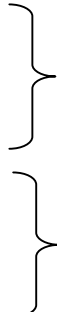
2.2 Main goal

With the information acquired so far, the main goal can be determined:

“To understand the physical processes concerning the stability of the rear slope of low-crested rubble mound breakwaters and defining a stability parameter to be used in future more economic breakwater designs.”

2.3 Scope

The main goal described in the previous section can be divided into four partial studies. These studies comprise hydraulic research as well as structural research:

- | | | |
|--|--|---|
| <ol style="list-style-type: none"> 1. The translation of incoming wave characteristics into “plunge characteristics” for the rear slope 2. The translation of incoming wave characteristics into “seepage characteristics” for the rear slope 3. The description of the response of the rear slope to the plunge characteristics 4. The description of the response of the rear slope to the seepage characteristics |  | <p>Hydraulic research</p>

<p>Structural research</p> |
|--|--|---|

These four studies joint together will produce the desired insight to equationte a physically based stability parameter for the rear slope as a function of the incoming wave characteristics. In order to avoid a so-called black-box model, in which the rear slope stability is directly linked to the incoming wave characteristics, without any physical basis, it is vital to describe the response of the rear slope to plunges and seepage first. Without a fair physical description of these phenomena the response of the rear slope to incoming waves cannot be determined physically.

In order to achieve useful results as soon as possible it is common in hydraulic research to study the most predominate processes first. Less influential processes can be looked upon in later stages. It is therefore decided to study the response of the rear slope to the plunge characteristics at first, followed by the translation of the incoming wave characteristics into plunge characteristics. It is assumed that the seepage characteristics will only play a secondary role in the rear slope stability of rubble mound breakwaters. The scope of this report comprises the physics of a rubble rear slope subjected to overtopping waves (plunges).

2.4 Problem description

This report tries to tackle the following problem:

“The stability of the rear slope of low-crested rubble mound breakwaters subjected to plunges is not well-described in existing literature.”

2.5 Objective

The objective of this report can be formulated as follows:

“To physically describe the response of the rear slope of rubble mound breakwaters to plunges.”

3 LITERATURE STUDY

3.1 Introduction

This Chapter describes previous research that is relevant to the subject discussed in this report. The research comprises empirical as well as theoretical studies, although it was observed by the author that most research performed in this field is of empirical nature.

As mentioned earlier, the interaction between the rear slope strength and the hydraulic load determines the rear slope stability.² The hydraulic load is determined by the response of wave parameters to the breakwater's breakwater parameters. The rear slope strength is determined by the breakwater parameters on the rear slope. This process is visualised in *Figure 3*. In this scheme seepage is discarded.

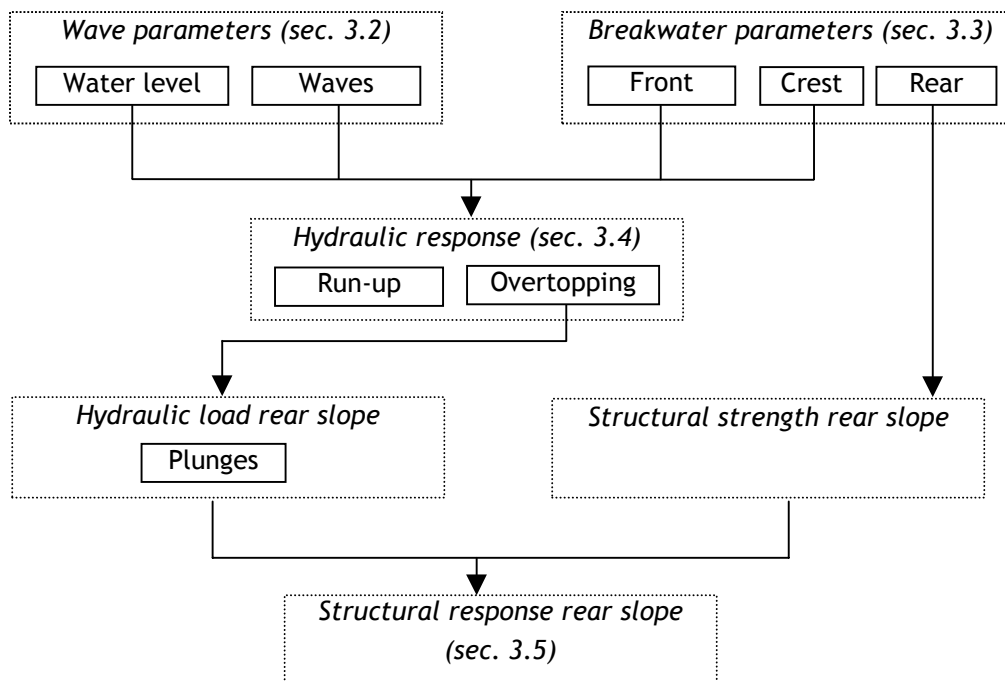


Figure 3: Interaction between wave parameters and breakwater parameters

In section 3.2 the wave parameters are discussed, followed by a discussion of the breakwater parameters in section 3.3. Next, the hydraulic response of the incoming waves to the breakwater parameters is discussed in section 3.4. Research on the structural response of the rear slope of breakwaters to the hydraulic load is discussed in section 3.5. Finally, in section 3.6 some conclusions are presented.

² Geo-technical parameters like subsoil characteristics and permeability of the core, are not considered in this report.

3.2 Wave parameters

In literature it is stated that in principle three wave parameters determine the hydraulic processes on breakwaters:³

- h water level in front of the structure [m]
- H incident wave height in front of structure [m]
- T incident wave period [s]

These three parameters will be discussed further in the following sections.

3.2.1 Water level

The water level in front of the structure h is not constant. Usually the term Still Water Level (SWL) is used, which is defined as the instantaneous mean water level in the absence of waves. The SWL during high spring tide is called Highest High Water level, or HHW. The SWL during low spring tide is called Lowest Low Water level, or LLW. The SWL shifts between HHW and LLW. In general it can be said, that the water level has two effects on the hydraulic processes:

- A shallow foreshore causes the highest waves to break, before reaching the breakwater, which decreases the wave attack on the breakwater.
- A high water level at the breakwater toe causes waves to overtop, which decreases the wave attack on the front side of the breakwater, but increases the wave attack on crest and rear slope.

3.2.2 Waves

A wave at sea is the result of wind interacting with the water surface. ⁴ In the idealised case, this interaction results in a periodic, sine-shaped wave. However, wind is a stochastic parameter, with fluctuations in velocity and direction. The wave conditions at a fixed point at sea can therefore not be characterised by a simple sine-shape, but are the result of numerous sine-shaped waves, produced by numerous gusts of wind of various velocities and from various directions.

3.2.2.1 Wave height

The wave height H is defined as the highest crest minus the lowest trough between two zero-crossings. It is evident that the wave height is not constant in time. For practical purposes however, a measure is wanted to characterise a wave field. Usually, the significant wave height is used, which is defined as the mean value of the highest third part of the waves. This wave height agrees well with the visually observed wave heights from the past. Usually it is assumed that the wave height distribution can be described with the Rayleigh-distribution:

$$P(\underline{H} > H) = e^{-2\left(\frac{H}{H_s}\right)^2} \tag{1}$$

³ The hydraulic processes inside the breakwater are not considered in this report.

⁴ It is also possible that an underwater earthquake generates a wave field. This is called a Tsunami.

in which

H_s The significant wave height [m]

It must be kept in mind that this distribution only appears in water deeper than $3 - 4 \cdot H_s$. In shallow water, the highest waves will break and the distribution deviates from the theoretical Rayleigh distribution.

The wave height of a random wave field is not determined by the significant wave height alone. The storm duration also plays a role. When considering two storms with equal significant wave heights, the storm with the longer duration has a greater probability of larger waves to occur.

3.2.2.2 Wave period

Just like the wave height, also the wave period features irregularity in a random wave field. To characterise a particular wave field, sometimes the significant wave period T_s is used, which is defined as the mean value for the highest third part of the waves. However, more frequently other characteristic wave periods are used in calculations, like the average wave period T_m or the peak period T_p .

The average wave period T_m is simply defined as the total number of waves divided by the total elapsed time. The peak period T_p of a random wave field is defined as the period for which the energy density spectrum of the wave field has its maximum. The energy density spectrum can be interpreted as the distribution of energy over the various wave periods. As the wave energy is a function of the wave height, a wave registration can be transformed into an energy density spectrum. This is done with use of spectral analysis.

3.2.2.3 Wave steepness

The random wave steepness s is an important parameter in breakwater stability and is defined as a characteristic wave height divided by a characteristic wave length. The wave length L depends on the wave period and on the water level. Using the dispersion relation for free periodic waves from the linear wave theory yields:

$$\omega^2 = gk \cdot \tanh kh \tag{2}$$

in which

$$\omega = \frac{2\pi}{T} \quad = \text{the wave frequency} \quad [s^{-1}]$$

$$k = \frac{2\pi}{L} \quad = \text{the wave number} \quad [m^{-1}]$$

This relation can be rewritten with L en T instead of k and ω :

$$L = \frac{gT^2}{2\pi} \tanh \frac{2\pi h}{L} \tag{3}$$

In deep water ($kh \rightarrow \infty$), the wavelength equals $\frac{gT^2}{2\pi}$, also described as L_0 . In shallower

water, L decreases with a factor $\tanh \frac{2\pi h}{L}$. The wave steepness is mostly expressed in

terms of the significant wave height H_s and the deep water wave length L_0 , using the peak period T_p . The resulting wave steepness is formulated as s_p :

$$s_p = \frac{2\pi \cdot H_s}{gT_p^2} \tag{4}$$

From field measurements it was observed that this wave steepness seldom exceeds 5% or becomes less than 1%.

3.3 Breakwater parameters

In literature it is stated that a rubble mound breakwater can be characterised by a large number of parameters. These parameters can be summed up as follows (see also *Figure 4*):

- D_n Diameter of stone / block [m]
- α Front slope angle [-]
- β Rear slope angle [-]
- R_c Crest freeboard related to SWL [m]
- B_c Crest width [m]
- P Permeability factor (of Van der Meer) [-]
- t_a, t_f Thickness of armour layer and filter layer [m]
- f_f Roughness of filter layer [-]

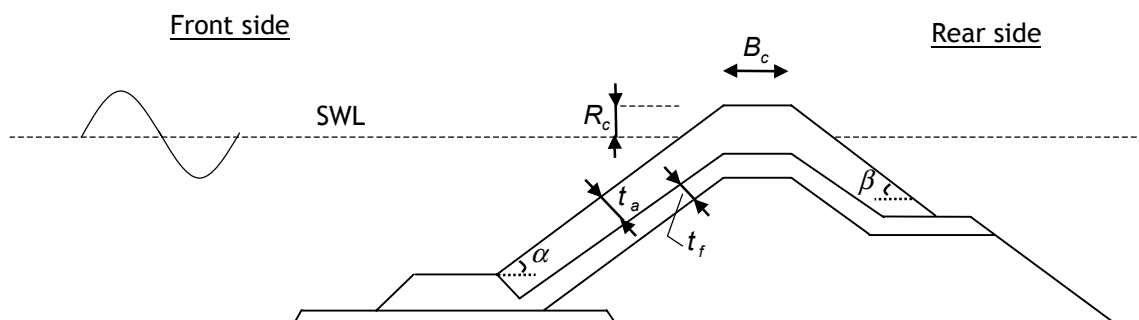


Figure 4: Breakwater parameters

3.3.1 Stone parameters

The nominal stone diameter of the armour layer, the filter layer or the core, is related to its average weight. That is the 50% value on the mass distribution curve:

$$D_{n50} = \left(\frac{M_{50}}{\rho_s} \right)^{\frac{1}{3}} \tag{5}$$

in which:

M_n	Stone mass, which is exceeded by n % of the stones	[kg]
ρ_s	Mass density of stone	[kg/m ³]

A specific stone gradation is not characterised by the nominal stone diameter alone. The width of the gradation w also plays a role, as well as the stone shape. The width of the gradation can be formulated as follows:

$$w = \frac{D_{n85}}{D_{n15}} = \frac{\left(\frac{M_{85}}{\rho_s}\right)^{\frac{1}{3}}}{\left(\frac{M_{15}}{\rho_s}\right)^{\frac{1}{3}}} \quad (6)$$

Many authors studied the influence of the stone shape. It turns out that rounded stones reduce interlocking and the layer's porosity.

Next to these parameters, also the layer thickness t and the filter layer's roughness f_f plays a role. An increased layer thickness reduces the probability of failure, while an increasing filter layer's roughness increases the interlocking between filter layer and armour layer.

3.3.2 Front slope angle and rear slope angle

The front slope as well as the rear slope cannot be constructed steeper than the material's angle of repose. A steeper angle implies lower construction costs, but higher maintenance costs. In practice the angle will be somewhere between 1:1.5 and 1:3.5.

3.3.3 Crest freeboard and crest width

The minimum crest width is about 3 blocks and the minimum crest freeboard for low-crested breakwaters is 0 m⁵. The maximum crest freeboard for low-crested breakwaters is about 1 to 1.5 times H_s (as long as considerable overtopping takes place). It must be kept in mind that breakwaters are often constructed of huge concrete blocks or rocks. Therefore, it is hard to determine the crest freeboard and the crest width accurately.

3.3.4 Permeability

The permeability of a breakwater is hard to determine. Van der Meer introduced the permeability factor P (without any physical meaning), which he used in his stability equations for the front slope armour layer. Van der Meer used the following values for the permeability factor:

- $P \approx 0.1$ impermeable breakwater [-]

⁵ Submerged breakwaters, for which the crest freeboard is negative, do exist in practice, but in this report only breakwaters with positive freeboards are considered, see section 1.4.

- $P \approx 0.4$ breakwater with core, filter and armour layer [-]
- $P \approx 0.5$ breakwater with only core and armour layer [-]
- $P \approx 0.6$ homogeneous structure, which consists of armour rocks [-]

A higher value of P implies a more stable front slope. The influence of P on the rear slope stability is not known.

3.4 Hydraulic response

When waves approach a breakwater, the waves will respond to the structure. The incoming waves will run-up and some waves will overtop the breakwater. This results in a hydraulic load on the rear slope, known as plunges.⁶ In this section the hydraulic response of incoming waves to the breakwater's parameters is discussed. The wave run-up is determined by the wave parameters and the breakwater parameters on the front slope, while the wave overtopping is determined by the wave parameters and the breakwater parameters of the front slope and of the crest.

3.4.1 Wave run-up

The wave run-up R_u is defined as the maximum height above Still Water Level reached by a wave rushing up the slope. This definition of wave run-up is visualised in *Figure 5*.

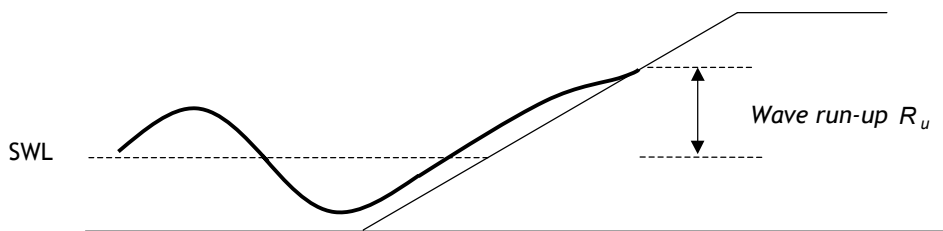


Figure 5: Definition of wave run-up

Wave run-up depends on the surf similarity parameter or Iribarren parameter, which can be seen as the steepness of the slope relative to the steepness of the incident wave:

$$\xi = \frac{\tan \alpha}{\sqrt{s}} \quad (7)$$

in which

ξ	Iribarren parameter	[-]
α	front slope angle	[rad]
$s = \frac{H}{L}$	wave steepness	[-]

⁶ Seepage is not considered in this report.

The Irribarren parameter determines the form of wave breaking on a beach or structure. The transition between breaking and non-breaking lies around $\xi = 2.5-3$. For values of $\xi > 3$ the wave motion is called 'surging' (the wave surges up and down the slope with minor air entrainment). For values of ξ between 0.5 and 3 the wave motion is called 'plunging', characterised by curling waves. In between these two types of breaking waves is the collapsing wave, which causes the most damage on the front slope of breakwaters. For values of ξ smaller than 0.5, spilling breaking waves occur, which causes only minor wave attack on the structure.

3.4.1.1 Run-up of periodic breaking waves

Hunt [7] has given the following empirical equation for the run-up of periodic waves of perpendicular incidence waves breaking on a smooth slope ($\xi < 2.5-3$):

$$R_u = \sqrt{HL_0} \cdot \tan \alpha \quad (8)$$

Above-mentioned equation can be rewritten using the Irribarren parameter:

$$\frac{R_u}{H} = \xi \quad (9)$$

For rough slopes the run-up is about 50% of the run-up on a smooth slope.

3.4.1.2 Run-up of random waves

A lot of research is performed into the prediction of run-up of random waves. The commonly used equation is developed by De Waal and Van der Meer [15] and can be expressed as follows:

$$\frac{R_{u2\%}}{H_s} = \gamma_f \cdot \gamma_\beta \cdot 1.5 \cdot \xi_{op} \quad \text{with a maximum of } \frac{R_{u2\%}}{H_s} = 3.0 \quad (10)$$

in which

$R_{u2\%}$	the wave run-up height exceeded by 2% of the incoming waves [m]	
ξ_{op}	the Irribarren parameter, using the peak period T_p and the significant wave height H_{os} at deep water (off-shore)	[-]
γ_f	reduction factor, taking into account the friction of the structure	[-]
γ_β	reduction factor, taking into account angular wave attack	[-]

For design purposes De Waal and Van der Meer advised to use 1.6 and 3.2 instead of 1.5 and 3.0 respectively in above equation.

The derived relation shows the same form as the equation of Hunt. Simply applying the Rayleigh distribution for the 2% highest waves on the expression for regular waves, results in the equation of De Waal and Van der Meer, with a constant of 1.4 instead of 1.6.

Deviation of the wave height from the Rayleigh distribution due to shallow water conditions could be the cause for this difference.

Another approach was followed by Van Gent [6]. With the use of numerical modelling and physical model investigations, Van Gent investigated the run-up of random waves on impermeable dikes with shallow foreshores. Van Gent found that the wave run-up is better predicted using the spectral wave period $T_{m-1,0}$ instead of the peak period T_p as used by De Waal and Van der Meer. Van Gent found less scatter around his equations and a better prediction for larger values of ξ . The equations of De Waal and Van der Meer imply a maximum run-up value for $\xi_{op} > 2$, while the run-up calculated with the equations of Van Gent rises monotonously with increasing $\xi_{s,-1}$. In Annex I.A, a more thorough discussion of the research of Van Gent is presented, including his equations.

3.4.2 Wave overtopping

An extensive literature study is carried out into the complex hydraulics of wave overtopping. In this stage of the research to improve the understanding of the physics of the rear slope subjected to overtopping waves, the outcome of this literature study is only used as background. However, for future research in this field, this section is most relevant.

First, in section 3.4.2.1, the overtopping of periodic waves is discussed, in order to get an idea of the parameters that are involved with overtopping. Most literature tries to find an expression for the *average* overtopping discharge. Four of these equations are described and compared in section 3.4.2.2. However, the stability of the rear slope of low-crested breakwaters is not determined by the *average* overtopping discharge. The *momentary* values of the overtopping parameters determine the rear slope stability (probably the larger values). Van der Meer [10] enhanced his average overtopping equations by providing a "translation" of the average overtopping discharge into momentary values of overtopping volumes, discussed in section 3.4.2.3. In section 3.4.2.4 the findings of Van Gent [9] are discussed. Van Gent found expressions for the layer thickness, the overtopping discharge, the overtopping volumes and the overtopping velocity exceeded by 2% of the incoming waves. Finally section 3.4.2.5 discusses the shape of the overtopping wave.

3.4.2.1 Periodic overtopping waves

Battjes [8] derived a mathematical expression for the overtopping volume V_{over} of a periodic wave rushing up a smooth, gentle slope, which he verified with physical tests. He found that the overtopping volume of a wave could be expressed as a function of hydraulic and breakwater parameters. Battjes states that the overtopping volume depends on the incident wave height H , the wave period T , the front slope angle α and the crest height R_c . The influence of roughness and oblique waves was not taken into account. A more thorough discussion of Battjes' findings on periodic wave overtopping is presented in Annex I.B. Battjes' equations on random wave overtopping are not discussed in this report.

Perdijk [13] performed physical tests to describe the overtopping parameters of periodic overtopping waves as well as random overtopping waves over dikes. In this report only Perdijk's findings on periodic overtopping waves will be discussed. Tests were performed on

a smooth, gentle slope and with perpendicular wave attack. Perdijk measured the overtopping parameters (maximum layer thickness d , maximum overtopping velocity u , overtopping time τ and overtopping volume V_{over}) at one fixed point on the dike crest.

Perdijk's expression for V_{over} more or less confirms Battjes' computations. According to Perdijk all of the other overtopping parameters depend on the incident wave height H , the wave period T and the front slope angle α . The layer thickness as well as the overtopping time also depend on $\left(\frac{R_c}{R_u}\right)$. This parameter does not significantly influence the overtopping velocity. In Annex I.C a more thorough discussion of Perdijk's equations is presented.

3.4.2.2 Random overtopping waves - average discharge

Experimental studies into overtopping of dikes and breakwaters in the past have led to a number of empirical equations that predict the average overtopping discharge during a storm. Many of them relate a dimensionless average discharge Q to a dimensionless crest

freeboard $R = \frac{R_c}{H_s}$. Examples are the equations of:

- Owen (originally derived for dike design)
- De Waal / Van der Meer (dike design and breakwater design)
- Bradbury et al (breakwater design)
- Hebsgaard, Sloth and Juhl (breakwater design)

A critical examination and comparison of these equations is presented in Annex I.D. From this examination it can be concluded that the equations are not very accurate for low crest freeboards. None of the equations are validated for a dimensionless crest freeboard R smaller than 0.5. Calculation results for R smaller than 0.5 should therefore be questioned. Next to that, the scatter in calculated values for $0.5 < R < 1$ is also considerable. It is not clear to the author which equation represents the average overtopping discharge best for crest freeboards lower than the significant wave height. It is therefore decided not to use this approach in determining the rear slope stability.

Moreover, it should be questioned whether it is the right approach to describe the rear slope stability using the average overtopping discharge. It is more likely that the (larger) momentary values of overtopping volumes or overtopping velocities determine the rear slope stability of low-crested breakwaters. The following sections will deal with these momentary values.

3.4.2.3 Random overtopping waves - wave overtopping distribution

Van der Meer [10] states that the average overtopping discharge can be used to compute the probability distribution function of the overtopping volumes per wave. It was found by Van der Meer that the distribution of the overtopping volumes follows the Weibull distribution. This distribution is determined by the average overtopping volume per wave ($V_{average} = \bar{q} \cdot \bar{T}$) and the probability of a wave overtopping a breakwater (P_{ow}).

The probability of a wave overtopping a breakwater (P_{ow}) can be described by the Rayleigh distribution. This distribution is determined by the crest height R_c and the run-up height $R_{u2\%}$.

From the above it can be concluded that four parameters determine the probability of a certain water volume overtopping a breakwater:

- \bar{q} average overtopping discharge [m³/ms]
- \bar{T} average wave period [s]
- R_c crest freeboard [m]
- $R_{u2\%}$ run-up level, exceeded by 2% of the incident waves [m]

In Annex I.E a more thorough discussion of the equations of Van der Meer is presented.

3.4.2.4 Random overtopping waves - momentary values

Van Gent [9] investigated the overtopping of random waves with the use of a numerical model and some physical model tests. He did not consider the permeability of the structure. Instead of concentrating on finding an expression for the average value of the overtopping discharge, like was done by previous authors (see 3.4.2.2), Van Gent tried to provide more information on individual wave overtopping events. He states that a random overtopping wave field can be characterised by the following four parameters:

- $d_{2\%}$ maximum layer thickness of overtopping volume at the rear side of the crest ⁷, exceeded by 2% of the incident waves [m]
- $u_{2\%}$ maximum overtopping velocity at the rear side of the crest, exceeded by 2% of the incident waves [m/s]
- $q_{2\%}$ maximum overtopping discharge at the rear side of the crest, exceeded by 2% of the incident waves [m³/ms]
- $V_{2\%}$ overtopping volume exceeded by 2% of the incident waves [m³/m]

Van Gent derived four equations, which describe the four overtopping parameters in terms of three breakwater parameters:

- $\frac{(R_{u2\%} - R_c)}{H_s}$ Dimensionless crest freeboard relative to the run-up height [m]
- B_c Crest width [m]
- γ_{f-c} Crest roughness reduction factor [-]

Van Gent relates the overtopping parameters to $\frac{(R_{u2\%} - R_c)}{H_s}$. It must be emphasised that for the calculation of the average overtopping discharge, Van der Meer [14] compared this

⁷ As Van Gent performed his research for wave overtopping of sea dikes he uses the expression 'land side' instead of 'rear side'. Although the appearance of a breakwater is somewhat different from dikes, it is assumed that Van Gent's equations also apply for low-crested breakwaters.

approach to an approach in which the average overtopping discharge is related to $\frac{R_c}{H_s}$. He found that for low crest freeboards, the first approach is less reliable.

According to the equations of Van Gent especially the crest level influences the overtopping parameters to a great extent. The crest width has only a minor influence on the overtopping parameters, probably due to the limitation to impermeable structures. More information on the above is presented in Annex I.F.

3.4.2.5 Random overtopping waves - shape of overtopping wave

Perdijk [13] and Van der Meer [14] measured the shape and velocity of overtopping waves at the crest. Perdijk considered periodic waves as well as random waves. Van der Meer only considered random waves. Van der Meer also measured the development of the overtopping wave at the rear slope. Perdijk as well as Van der Meer only considered impermeable structures.

From their measurements it can be concluded that at a fixed point on the crest the layer thickness of the overtopping wave quickly increases to its maximum value and then slowly decreases to zero. Consequently, the development of the layer thickness at a fixed point is schematised as a triangular shape. The overtopping velocity at a fixed point can also be schematised as a triangular shape. Most of the times, the maximum layer thickness at the crest occurred at the same time as the maximum overtopping velocity. The time for the layer thickness to reach its maximum t_1 in proportion to the total overtopping time t_2 varies considerably per overtopping wave. Roughly spoken, it can be stated that t_1 is about 10% - 50% of t_2 . In Figure 6, the schematised shape of the overtopping wave is presented.

Unlike Van der Meer, Perdijk did not measure the development of the overtopping waves on the rear slope. Van der Meer found that the layer thickness decreases in the direction of the rear slope, while the wave length increases. In other words: the overtopping wave becomes longer and thinner in the direction of the rear slope. This is accompanied by an increase in the wave front velocity, according to the measurements of Van der Meer.

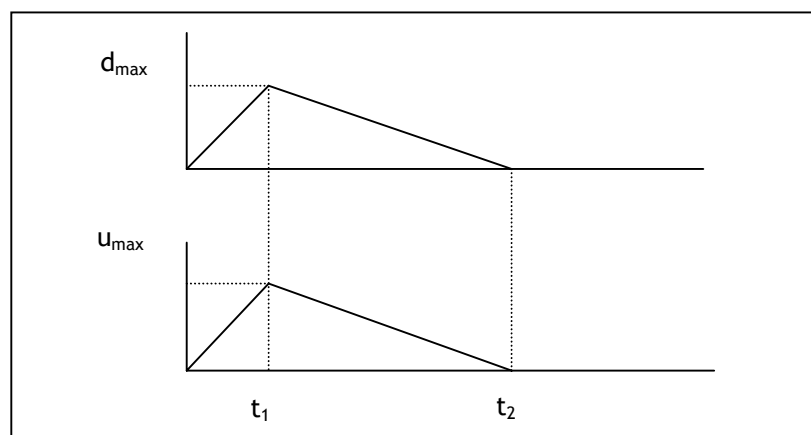


Figure 6: The schematised shape of an overtopping wave ('plunge')

3.5 Structural response rear slope

In the following sections several authors are discussed who have performed research into rear slope stability. In section 3.6, these investigations are evaluated.

3.5.1 Walker

Walker [3] investigated the rear slope stability of low-crested breakwaters subjected to periodic overtopping waves. Walker performed several tests in which he varied two dimensionless parameters:

- $\frac{R_c}{H}$ crest freeboard divided by the wave height [-]
- $\frac{W_f}{W_b}$ front slope stone weight divided by the rear slope stone weight [-]

According to Walker, the experimental data appear to indicate that when $\frac{R_c}{H}$ exceeds approximately 0.7, the armour units on the rear slope may be reduced relative to those on the front slope. When $\frac{R_c}{H}$ is less than 0.7, larger units or better placement may be required on the rear slope. In Annex I.G, a more thorough discussion of the research of Walker is presented.

3.5.2 Vidal, Van der Meer, Burger and De Jong

Burger [1] revised the test results of Vidal [4] and Van der Meer [2] on low-crested rubble mound breakwaters. His findings as well as the conclusions of Vidal and Van der Meer are elaborated in this section. Next to this, also the findings of De Jong [5] are discussed in this section. Finally, a closer look is taken at the observations of Van der Meer and De Jong.

Burger compared the test results of Vidal (see Annex I.H) and Van der Meer (see Annex I.I). His findings are concentrated on the influence of the crest freeboard on the rear slope stability. He visualised the slope stability using the dimensionless parameters $\frac{R_c}{D_{n50}}$ and

$\frac{H_s}{\Delta D_{n50}}$. The most important conclusion that can be drawn from Burger's analysis is that the rear slope stability is least at an intermediate crest freeboard. His conclusions for the rear slope can be summarised as follows:

- $\frac{R_c}{D_{n50}} < 2.5$ increasing rear slope stability with decreasing crest freeboard
- $\frac{R_c}{D_{n50}} = 2.5$ the rear slope is least stable
- $\frac{R_c}{D_{n50}} > 2.5$ increasing rear slope stability with increasing crest freeboard

It was further observed by Van der Meer that the rear slope stability was never normative for the total breakwater stability. This indicates an overdesign of the rear slope.

Among other things, De Jong [5] investigated the rear slope stability of a low-crested breakwaters armoured with tetrapods subjected to a random wave field. Just like Vidal and Van der Meer, also De Jong used the same size of armour on the front slope and the rear slope.

Although De Jong’s research comprises an armour layer constructed of tetrapodes instead of rock, as was studied by Vidal and Van der Meer, his results resemble their observations to a great extent (see Figure 7). Also De Jong concluded that the rear slope stability was never normative for the total breakwater stability. In Annex I.J, a more thorough discussion of the research of De Jong is presented.

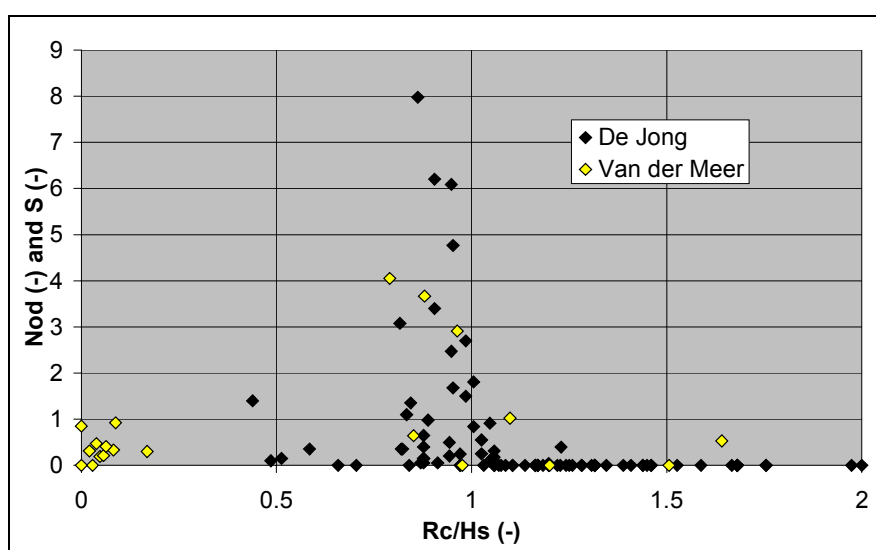


Figure 7: Test results of De Jong and Van der Meer

After studying the results of Van der Meer and De Jong, some additional remarks can be made. First, from the test results of both De Jong and Van der Meer it was found that the rear slope is very sensitive to changes in the relative crest freeboard for $\frac{R_c}{H_s} \approx 1$ (see Figure 7). From this it can be concluded that the damage development at the rear slope is more abrupt than at the front slope, in other words: a slightly higher significant wave height causes much more damage.

Secondly, De Jong concludes that in general, a longer storm duration causes more damage to the rear slope. It is unclear however, if this increase in damage is induced by more overtopping waves, or by larger overtopping waves. The test results of Van der Meer indicate that the rear slope damage after 3000 incident waves is slightly larger than after 1000 incident waves.

3.5.3 Andersen

Andersen [12] investigated the rear slope stability of berm breakwaters subjected to random waves. For berm breakwaters a dynamic equilibrium exists between the wave

attack and the armour stone. Some reshaping of the armour layer is allowed, in contrary to a statically stable construction.

Andersen used a simple equation for the fictitious run-up to predict the overtopping velocity, which is assumed to be the only determining factor in describing the rear slope stability. For the armour stone stability a force balance between the drag and lift forces of the overtopping wave and the mass of the stone is used. Andersen derived an equation in which the rear slope stability is directly linked to the incoming wave parameters.

Andersen states that the rear slope stability can be increased in several ways:

- increase of the crest freeboard
- increase of the stone diameter
- increase of relative density
- decrease of rear slope angle

The last statement is completely the opposite of Walker's [3] conclusions. However, it should be noted that in Andersen's experiments, the stone diameter as well as the relative density and the rear slope angle were kept constant. Therefore, statements about these parameters could be questioned.

For a more thorough investigation on the equations of Andersen, see Annex I.K.

3.5.4 Van der Meer and Veldman

Among other things, Van der Meer and Veldman [18] investigated the stability of berm breakwaters using physical tests in a wave flume with a random wave field. It was found that the crest freeboard, the wave height and the wave period determine the rear slope stability. Van der Meer and Veldman investigated breakwaters with a relative crest freeboard $\frac{R_c}{H_s}$ of 0.6 up to 1.2. Three damage levels were distinguished, 'start of damage', 'moderate damage' and 'severe damage'. These damage levels are not quantified by Van der Meer and Veldman. The following equations are recommended for the design of the rear slope of berm breakwaters:

$$\frac{R_c}{H_s} \cdot s_{op}^{\frac{1}{3}} = 0.25 \quad \text{'start of damage'} \quad (11)$$

$$\frac{R_c}{H_s} \cdot s_{op}^{\frac{1}{3}} = 0.21 \quad \text{'moderate damage'} \quad (12)$$

$$\frac{R_c}{H_s} \cdot s_{op}^{\frac{1}{3}} = 0.17 \quad \text{'severe damage'} \quad (13)$$

Above-mentioned equations imply that the rear slope of a breakwater, subjected to a wave field with a wave steepness s_{op} of 1%, will feature 'start of damage' when the dimensionless crest freeboard $\frac{R_c}{H_s}$ equals 1.2 and 'severe damage' when the dimensionless

crest freeboard equals 0.8. For a wave field with a wave steepness s_{op} of 5%, these values are 0.7 and 0.5 respectively. It can be concluded that the influence of the wave period on the rear slope stability is considerable, according to above equations.

Van der Meer and Veldman did not consider the influence of other breakwater parameters than the crest freeboard on the rear slope stability. In their tests, the relation between the significant wave height and the stone size was not varied much ($\frac{H_s}{\Delta D_{n50}} = 2.5 - 3.5$). The initial rear slope angle was taken equal to 1:1.5.

3.5.5 Kobayashi

Kobayashi [19] investigated the rear slope stability using numerical model tests, calibrated with physical tests performed by Vidal [4]. Kobayashi used a numerical flow model that predicts the flow characteristics on rough slopes. The velocity and layer thickness of the overtopping jet⁸ at the rear side edge of the crest were the input of the stability analysis of the rear slope armour layer. Kobayashi assumed that the jet velocity primarily determines the destabilising force. Kobayashi considered only impermeable breakwaters and the static stability of the rear slope.

Kobayashi expressed the stability of the armour units using the stability number $N_s = \frac{H_s}{\Delta D_{n50}}$. With the expressions of all forces, a static stability relation was formulated.

The non-dimensional force coefficients in this relation are calibrated using physical experiments performed by Vidal. With above calibrated stability equation, the influence of several parameters on the rear slope stability was determined.

Kobayashi found that the rear slope stability is increased with:

- Decreasing front slope angle
- Decreasing rear slope angle
- Increasing crest width
- Decreasing wave period
- Increasing water level (for the same $\frac{R_c}{H_s}$ ratio, deep water results in better stability than shallow water)

For a more thorough investigation on the equations of Kobayashi, see Annex I.L.

3.6 General remarks

After studying the above investigations, some general remarks are made regarding the research on the rear slope stability of breakwaters.

⁸ Kobayashi uses the term 'jet' for the overtopping wave. In this section the same formulation as Kobayashi is used.

For a proper physical representation of the rear slope stability of breakwaters, the approach as given in section 3.1 is needed. This approach consists of two steps. First, the interaction of the wave parameters with the front slope is considered, resulting in wave run-up and possible overtopping of the waves. Second, the overtopping waves are considered, which cause rear slope instability. None of the authors discussed earlier uses this approach, as the amount of parameters involved make the hydraulic processes too complex.

Walker [3] as well as Van der Meer [2], Vidal [4], De Jong [5] and Van der Meer and Veldman [18] relate the rear slope stability to the wave parameters and (some of) the breakwater parameters. In this approach a clear representation of the hydraulic response is missing and therefore the hydraulic processes are considered as a black box.

Although these studies contribute greatly in establishing design criteria for the rear slope armour layer, it lacks a proper physical base for the rear slope stability. It is unclear what overtopping parameter(s) cause(s) the stone on the rear slope to move.

Andersen [12] as well as Kobayashi [19] are the only authors who relate the rear slope stability to a parameter of the overtopping waves. In their investigations, they both state that the overtopping velocity is the primary parameter that determines the destabilising force of the rear slope. They do not consider all overtopping parameters, like the layer thickness, the discharge and the total overtopping volume. However, it is quite probable that these parameters do influence the rear slope stability.

Above-mentioned considerations lead to the conclusion that the rear slope stability is related to the characteristics of the overtopping waves (plunges)⁹. With an experimental set-up in which these plunges are simulated, the complex interaction of random waves with the front slope and the crest can be discarded. In this way, the complexity of the research is reduced considerably. Furthermore, the influence of all characteristics of the overtopping wave on the rear slope stability can be better examined. This approach is further elaborated in Chapter 4.

⁹ Seepage is discarded in this report.

4 EXPERIMENTS

4.1 Introduction

For a description of the rear slope response to plunges, physical modelling is indispensable. Use of a numerical model in this stage of the research would be too much influenced by the a priori assumptions on the governing hydraulic processes made by the researcher. Only physical testing will lead to more insight in the physical processes. Therefore, physical tests have been carried out.

Former research was concentrated on the relation between the significant wave height and the rear slope stability of the armour layer (see Chapter 3). In that approach, the hydraulic processes in and on the breakwater are considered as a black box.

A different approach is followed in the research described in this report. The wave itself is considered as a black box and the hydraulic processes on top of the breakwater are simulated by plunges.¹⁰

One advantage of this approach is the reduction of the number of influencing parameters (such as the wave height, the wave period, the front slope angle, the crest freeboard etc.). Another advantage of this approach is that the number, the size and the characteristics of the plunges can be varied. Implicitly, this leads to a laboratory model with variable plunges instead of a scale model of a prototype with random overtopping waves.

Two major starting-points were formulated (see section 3.6):

- The hydraulic behaviour of the overtopping wave is reduced to a plunge with certain characteristics.
- Only the breakwater's rear slope armour layer is modelled.

The above is presented in Figure 8.

¹⁰ The hydraulic processes inside the breakwater (seepage) are considered to be of secondary influence and are therefore not taken into account in the current research (see also Chapter 2).

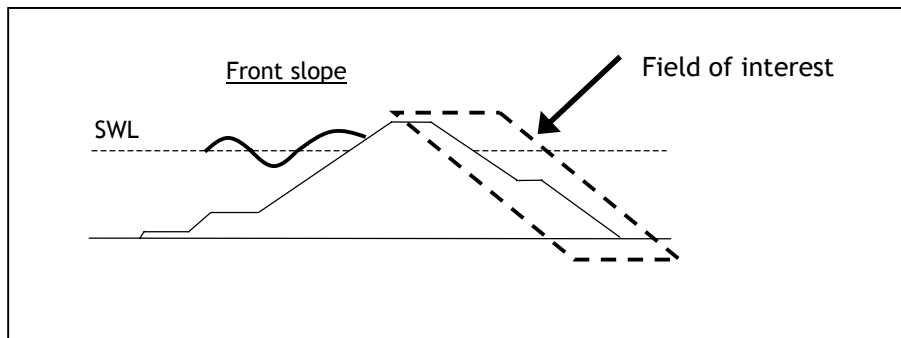


Figure 8: Field of interest

According to Perdijk [13] and Van der Meer [10], a plunge features the following behaviour (see also 3.4.2.5):

- The layer thickness of the plunge increases from zero to maximum in a short period of time and then decreases to zero in a longer period of time
- The same accounts for the velocity and therefore also for the discharge
- The maximum layer thickness and the maximum velocity usually occur simultaneously.

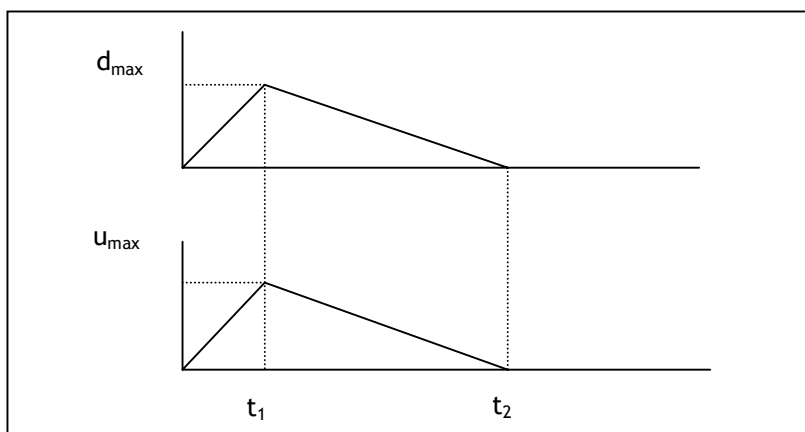


Figure 6: The schematised shape of an overtopping wave ('plunge')

The above presented schematised plunge is defined by four characteristics: the maximum layer thickness, the maximum velocity and the time durations t_1 and t_2 . Other plunge characteristics like the volume and the discharge can be derived from these characteristics.

The strength of the rear slope armour layer is defined by six characteristics (see section 3.3): the rear slope angle, the average stone size, the stone shape, the gradation of the stones, the characteristics of the filter layer (roughness, stone size etc.) and the crest freeboard.

In the experimental set-up, it is required that above-mentioned characteristics of the plunges as well as the rear slope strength can be varied and measured.

4.2 Conceptual design of experimental set-up

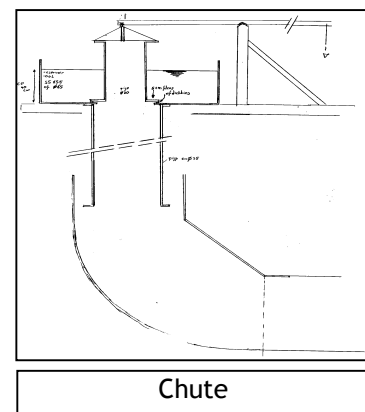
Before commencing on the conceptual design of the experimental set-up, some rough calculations were made to estimate the dimensions of the experimental set-up. These calculations were used as a basis for the design process described in the rest of this section. These calculations are presented in Annex III (in Dutch).

4.2.1 Plunge machine

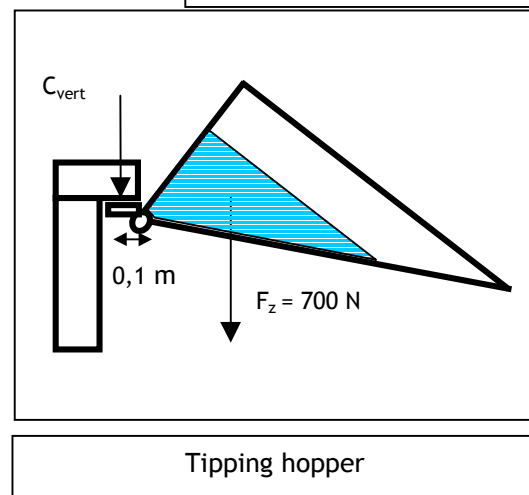
Four concepts of the “plunge machine” were investigated:

- A chute
- A tipping hopper
- A large reservoir with a valve
- A small reservoir with a gate

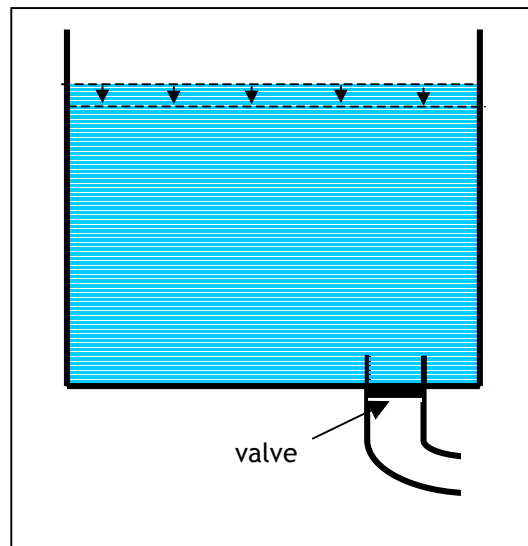
In the first concept, the plunge is simulated with a chute. The minimum height of the chute above the crest is determined by the pipe bend. Calculations were carried out and it turned out that the minimum velocity of the water that could be generated was too high for the dimensions of the rear slope. Therefore, this concept was not chosen.



In the second concept, it was investigated whether the plunge could be simulated by turning over a reservoir, a so-called tipping hopper. After an estimate of the plunge sizes needed, calculations were carried out to determine whether this concept was feasible. It turned out that the dynamics of the overturning mechanism required a heavy installation, for which the available location in the laboratory was not suitable. Conceptually however, the tipping hopper seems to be a good solution.

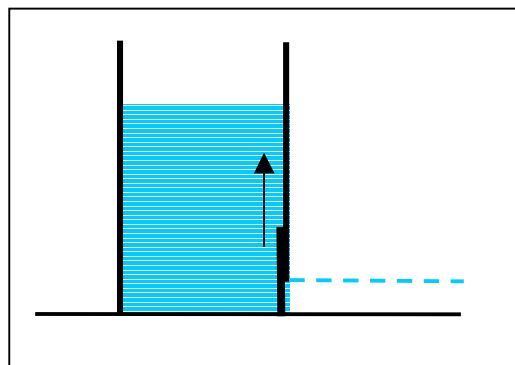


In the third concept, the water pressure inside a relatively large reservoir is used to generate the plunge velocity, by opening and closing a valve. Different plunge sizes can be generated with different water levels. Due to the size of the reservoir, the outflow velocity is more or less constant (the volume inside the reservoir has to be large enough so that a plunge does not significantly influence the height of the water inside the reservoir). The problem of a simple valve is the closing of the valve, due to the water pressure. This problem can be solved when use is made of a butterfly valve. It turned out that the plunge characteristics as formulated in the last section could not be simulated with this type of valve, due to the duration of the opening time. Therefore, this concept was not chosen.



Large reservoir with valve

In the fourth concept, the water pressure in a relatively small reservoir is used to generate the plunge velocity, by opening and closing of a vertical sliding gate. After opening of the gate, the water level and the configuration of the reservoir determines the development of the plunge velocity and the discharge. Because the gate can be lifted quickly, the required plunge characteristics can be simulated.



Small reservoir with a sliding gate

The concept of the reservoir with a vertical sliding gate is chosen as the best feasible of the four concepts described above. In the chosen concept, two parameters can be varied, namely the water level inside the reservoir and the 'shape' of the reservoir (by reduction of the water surface or by varying the opening height). These two parameters influence the plunge characteristics, described in section 4.1. However, the way these parameters influence the plunge characteristics is not known and therefore considered as a "black box".

4.2.2 Rear slope

The rear slope stability can be considered in two ways:

- The stability behaviour of a single stone on a rubble slope
- The stability behaviour of the rear slope as a whole

In the first consideration the research is concentrated on 'stone level'. This implicates measuring of (hydraulic and other) forces on the stone and of the resulting movement. In this approach, stability of a single stone is defined as the ratio of the force due to the plunge and a critical hydraulic force above which the stone starts to move.

In the second consideration the research is concentrated on 'slope level'. This implicates measuring of the amount of displaced stones, which is defined as damage. In this consideration, the stability of the slope is defined by the damage level: the higher the damage, the smaller the slope stability.

The objective of this research is to physically describe the rear slope response to plunges. This objective is not directly pursued when following the first approach. Information about the physics on stone level alone cannot describe the stability of the rear slope as a whole: a translation from stone level to slope level is needed. This translation however is very complex and therefore, as a first step, in this research it is chosen to apply the second approach.

4.3 Experimental set-up

4.3.1 Introduction

With the conceptual design of the plunge machine and the rear slope, the experimental set-up is designed. In section 4.3.2 a general description of the experimental set-up is given. In section 4.3.3, 4.3.4 and 4.3.5 important features of the experimental set-up, the measuring equipment and the experiments are taken into further consideration.

4.3.2 General description

The experimental set-up consists of the following components (see Figure 9 and Figure 10):

- Several *flume elements*, which are connected to each other. In the flume, all other components are placed.
- A *weir*, to establish a constant *water level* in the flume.
- *The rear slope*, which is constructed of a plate of ply wood (slope angle 1:1.5). A layer of small stones is glued onto this plate, which represents the filter layer of the rear slope. On top of this filter layer, loose stones are placed in two layers. These stones represent the rear slope armour layer. The toe consists of the same stone size as the armour layer.
- *The crest*, which is constructed of ply wood. In contrary to a real breakwater crest, the surface of the crest in the experimental set-up is kept smooth, in order to reduce the influence of the crest friction on the plunge. In this experimental set-up, the only purpose of the crest is to measure the plunge characteristics. It is important to note that the crest is not part of the breakwater model. On top of the crest two Wave Height Meters (WHM) are placed. The crest is situated 35 cm above the flume bottom.
- *The reservoir*, which is constructed of ply wood. The reservoir can be filled using a hose. Inside the reservoir a WHM is placed. The reservoir can be opened by lifting the vertical *gate*. In order to make the gate (more or less) watertight, butylene kit was applied as sealing.
- *Opening mechanism* (not drawn in figure below), constructed of ply wood. The gate is opened with a lever.

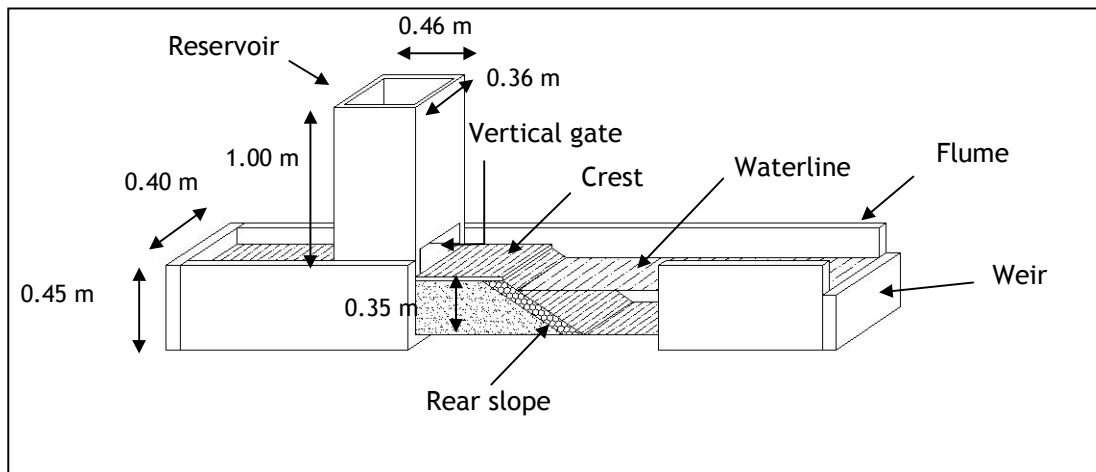


Figure 9: Sketch of experimental set-up

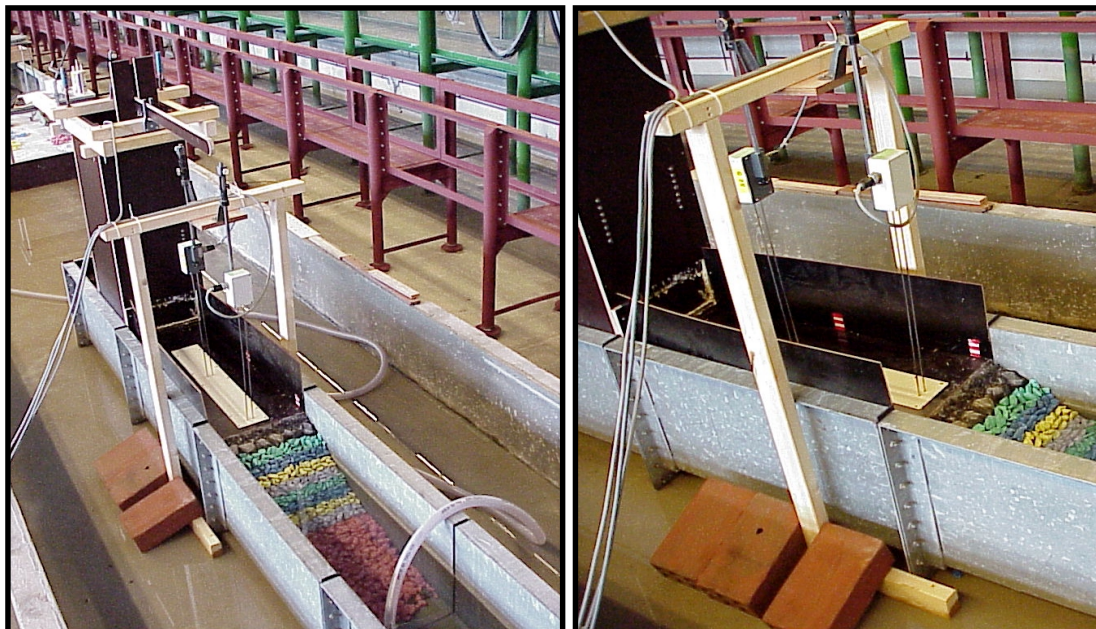


Figure 10: Overview of experimental set-up

As mentioned above, the crest in the experimental set-up is not part of the breakwater model. This leads to a problem in modelling the transition between crest and rear slope. This problem is explained in Figure 11.

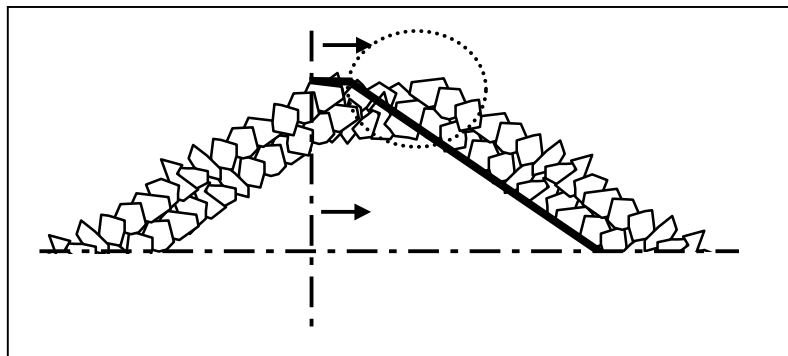


Figure 11: The transition between the crest and the rear slope

The crest is constructed as a smooth plane instead of applying stones. As a consequence, stones on the rear slope that are firstly hit by the plunge do not have any protection from other stones. That is why these stones start to move, even at small plunge sizes, resulting in a “stone avalanche”. This problem is solved by gluing large stones to the filter layer of the rear slope (see Figure 12). These large stones represent the transition between crest and rear slope. As a consequence this transition cannot be considered in this research.

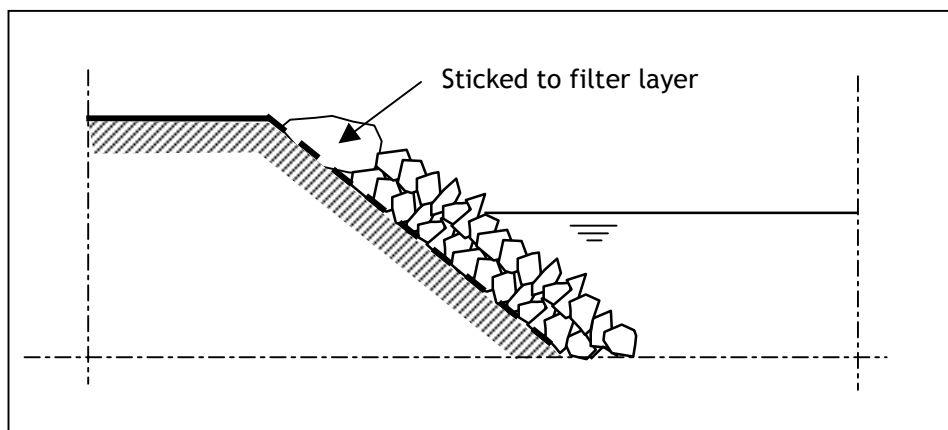


Figure 12: Solution for transition

In the experiments, use is made of coloured stones. Stones of equal colours are placed in strips with a width of two times D_{n50} (see Figure 13). This approach has a two-fold advantage in relation to the use of non-coloured stones:

- The displaced stones are easy to distinguish
- Use can be made of the definition of damage as defined by Van der Meer:
 - Damage can be expressed in the number of displaced stones
 - A stone is displaced when it has moved for more than two times the stone diameter.

So, in the experimental set-up a stone displaced from one coloured strip to another is considered as one unit of damage.

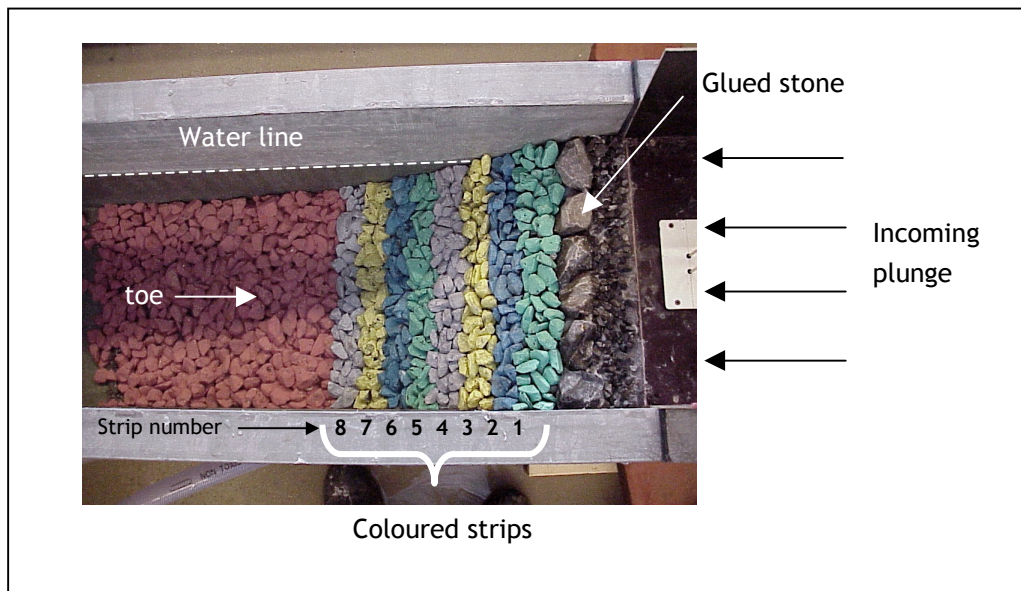


Figure 13: Eight coloured strips, including strip numbers

4.3.3 Dimensions

4.3.3.1 Boundary conditions

For the experimental set-up two boundary conditions have to be taken into account:

- The available location and space inside the laboratory (about 15 x 5 meter)
- The dimensions of the flume elements:
 - outer dimensions: $L \times B \times H = 1.0 \times 0.53 \times 0.515$ m
 - inner dimensions: $L \times B \times H = 1.0 \times 0.40 \times 0.45$ m

In total five flume elements were used and connected to each other. With this number of elements, the width and the length of the total flume and thus the experimental set-up becomes: $L \times B = 5.0 \times 0.53$ m

4.3.3.2 Stone size

The filter layer consists of stones with $D_{n50} = 0.8$ cm. This stone size was not varied and therefore the filter layer's roughness was a constant value in the experiments.

For the armour layer three stone-classes were distinguished ¹¹. Some important features of the different stone-classes were investigated ¹² :

- The average stone density, ρ_s , defined by the stone mass, m_s , divided by the stone volume, V : $\rho_s = \frac{m_s}{V}$
- D_n , defined as the cubic root of the stone mass divided by the average stone density:

$$D_n = \sqrt[3]{\frac{m}{\rho}}$$
- D_{n50} , defined as the stone size for which 50% of the measured stones in mass is smaller.
- $\frac{D_{n85}}{D_{n15}}$, the width of the stone-class.
- $\frac{Length}{Width}$, the ratio of the length of the stone and the width of the stone (the length of the stone is measured over the longest axis and the width is measured over the shortest axis).

Above features of the different stone-classes are presented in Table 1, Figure 14 and Figure 15.

Table 1: Features of the different stone-classes

Stone-class	Stone density (kg/m ³)	D_{n50} (cm)	$\frac{D_{n85}}{D_{n15}}$ (-)	Average length/width (-)
Small	2729	1.15	1.23	1.57
Intermediate	2682	1.86	1.32	1.74
Large	2721	2.76	1.34	1.59

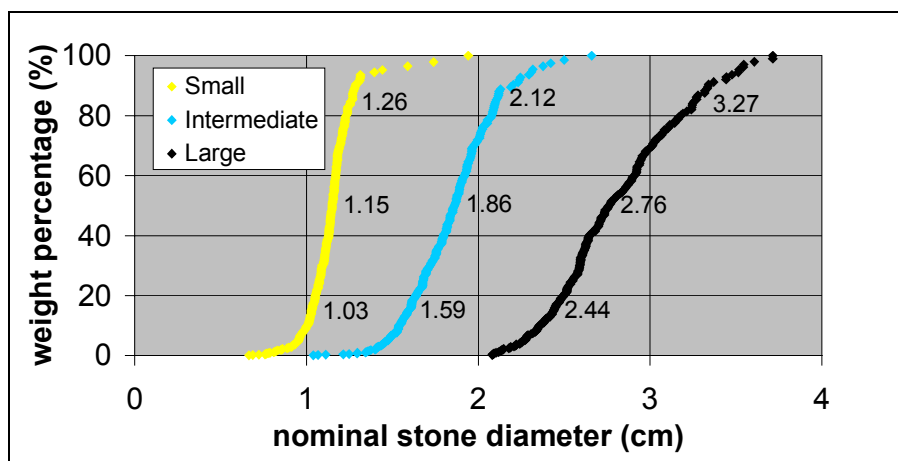


Figure 14: Stone size of the three different stone-classes.

¹¹ Only an armour layer with a thickness of two stones is considered.

¹² For this investigation a number of 250 randomly chosen stones of the particular stone-class was used.

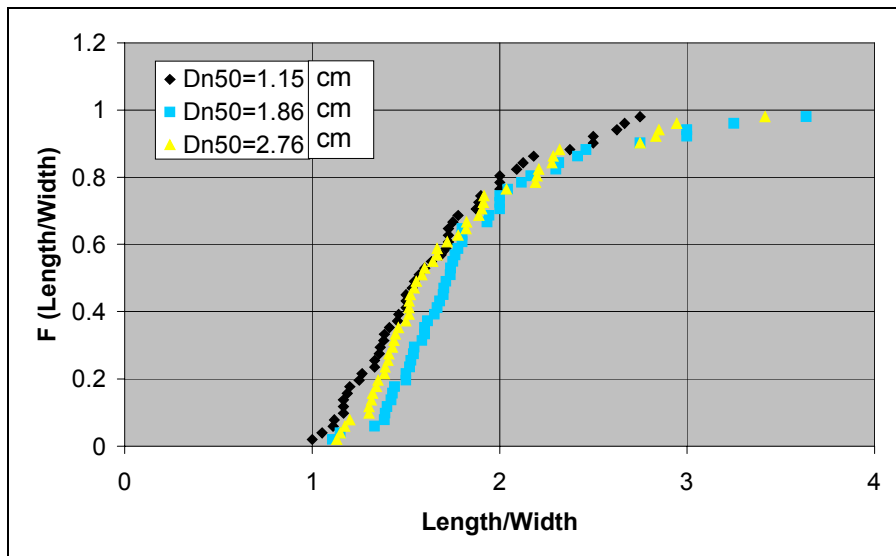


Figure 15: The length-width ratio of the three different stone-classes

4.3.3.3 Reservoir

The dimensions of the reservoir had to be chosen in such a way that the characteristics of the plunges that are created by opening the reservoir are realistic. However, the magnitudes of and the relation between the plunge characteristics are not known.

In this report an estimate is made of the magnitudes of the plunge characteristics using two sets of equations. First of all, with the equations of Van der Meer [2] the relation between the wave parameters and the size of the stones on the front slope is determined (assuming the same size of the stones on front slope and rear slope). Second, with the information of the wave parameters, the equations of Van Gent [10] are used to estimate the magnitude of the plunge characteristics.

However, the amount of parameters that can be varied in above approach is very large. The plunge characteristics are sensitive to variations in the value of these parameters (eg. the wave height and the crest freeboard). That applies to the maximum layer thickness and especially to the discharge and the overtopping volume. The maximum overtopping velocity was less sensitive to variations of those parameters.

The above approach did not produce a clear view of the magnitudes of the plunge characteristics, but a rough estimate could be established. With a maximum stone size of 3 cm, a larger velocity than 2.5 m/s seems unlikely to appear, as well as a layer thickness larger than 7 cm and a volume larger than 100 l.

Bearing above considerations in mind, and taking into account the uncertainty of the above estimates, it is sensible to dimension the reservoir with a certain oversize. The dimensions of the reservoir eventually were taken equal to $L \times B \times H$: $46 \times 36 \times 100 \text{ cm}^3$ (inner dimensions) and $L \times B \times H = 50 \times 40 \times 102 \text{ cm}^3$ (outer dimensions)

In the above dimensions the surface of the reservoir is taken relatively large, so that adaptations to this surface and therefore the volume easily can be made. The height of the reservoir is large enough to produce any realistic outflow velocity and even more. Finally,

the vertical gate is constructed in such a way that the height of the opening can be easily varied (removable bolts are used to fix the opening height of the gate) and therefore the magnitude of the layer thickness can be influenced.

The placement of the reservoir and the WHM's on the crest is a compromise between the required distance between two WHM's and the distance between the reservoir opening and the rear slope. It was decided to place the reservoir at a distance of 1 meter from the rear slope. This distance was not varied in the experiments.

4.3.3.4 Crest height and water level in the flume

The crest was situated 0.35 m above the bottom of the flume (inner dimensions). The water level in the flume was varied, by using weirs with different dimensions: 0.10 m under the crest, 0.07 m under the crest and 0.03 m under the crest (0.25 m, 0.28 m and 0.32 m above flume bottom, respectively).

4.3.4 Measuring equipment

The schematised plunge is defined by the maximum layer thickness, the maximum velocity and the time durations t_1 and t_2 (see section 4.1). In the experimental set-up, these parameters should be measured. The layer thickness as a function of time is relatively easy to measure on the crest using a Wave Height Meter (WHM). However, it is difficult to measure the velocity of the plunge as a function of time.

An estimate of the plunge velocity can be established with use of measurements of two Wave Height Meters on the crest. In this way, the front velocity is measured, which could be a good estimate of the plunge velocity.

Another approach is with use of a WHM inside the reservoir. Such a WHM indirectly produces data on the outflow discharge. If this information is combined with the measurements of the layer thickness, another estimate of the plunge velocity can be given.

Both methods do not lead to the plunge velocity as a function of time, but only to an estimate of the plunge velocity, independent of time. Both methods are used in the experimental set-up.

When furthermore the volume of the plunge is measured (which is relatively easily), all necessary information of the schematised plunge is available.

In the experimental set-up the following plunge characteristics have to be measured, according to above considerations:

- The volume
- The outflow discharge
- The layer thickness on the crest (two times)

Above-mentioned considerations result in the use of three Wave Height Meters. The first one was placed in the middle of the reservoir (WHM1) and was used to measure the development of the water level inside the reservoir. With this information, the volume and

the development of the discharge was calculated. The second meter was placed on the crest, 50 cm from the reservoir opening (WHM2). The third meter was placed on the crest, 92 cm from the reservoir (WHM3). Both these WHM's measured the development of the layer thickness in time. The data from WHM3 was used to determine the plunge's layer thickness at the rear slope. With the data from WHM2 and WHM3 the front velocity was calculated.

The used WHM's measure the electrical resistance of the water between two vertical conductors (metal bars). As long as the WHM is at least 4 cm immersed, a linear relation exists between its immersed length and the output voltage. Therefore, two separate rectangle boxes with a depth of about 10 cm are constructed below the crest in which WHM2 and WHM3 are placed. The boxes were filled with water and closed off by a lid. Small holes were made through the lid for the conductors (see Figure 16).

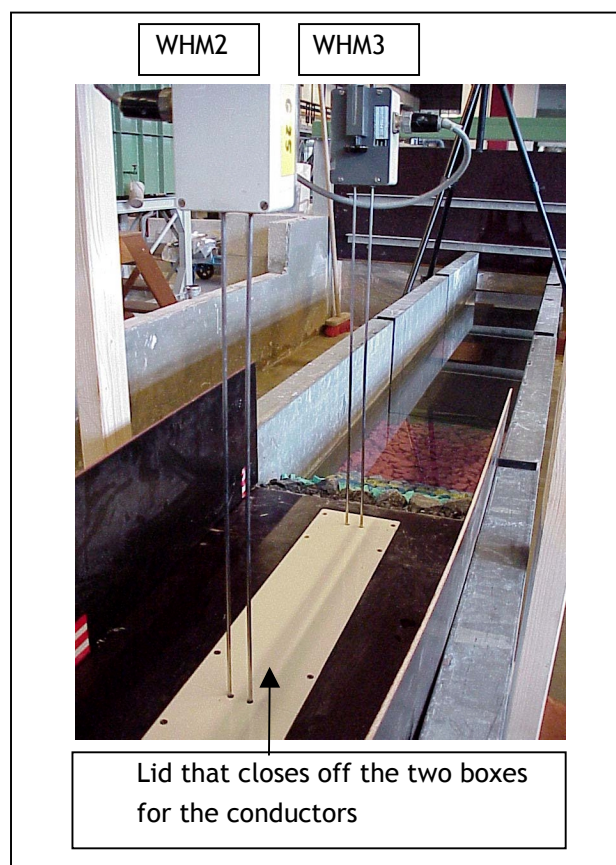


Figure 16: WHM2 and WHM3

The WHM's were calibrated in two ways, statically and dynamically. The static calibration was very straightforward. The flume was entirely filled with water, after which the WHM's were lifted in steps of 1 cm. All measurements of the WHM's were very reliable and equal for all three WHM's. This static calibration is carried out two times, the first time before the measurements began and the second time halfway the experiments.

The dynamic calibration was carried out for WHM2 and WHM3 by comparison of the measured maximum value of the layer thickness with the observed value of the maximum layer thickness. Within the reliability of this method, the results of this calibration showed

reasonable results: the measured value of the layer thickness differed not more than about 20% from the observed values.

According to the manual of the WHM's, fluctuations of the water level with a frequency higher than 10 Hz are not accurately measured by the WHM's. The data-acquisition program DasyLab, which is used to translate the analogue values of the WHM's into digital values, was programmed to carry out this translation with a frequency of 50 Hz. It must be kept in mind that fluctuations in the computer data, at a higher frequency than 10 Hz, must be handled with care. It is doubtful whether such fluctuations are correct.

A last remark about the measurements of the layer thickness must be made. Due to the collision of the plunge with WHM2 and WHM3, run-up of the water occurs around the conductor (see Figure 17). The response of the WHM's to these phenomena and the resulting effect on the measurements are not known and could be of influence.

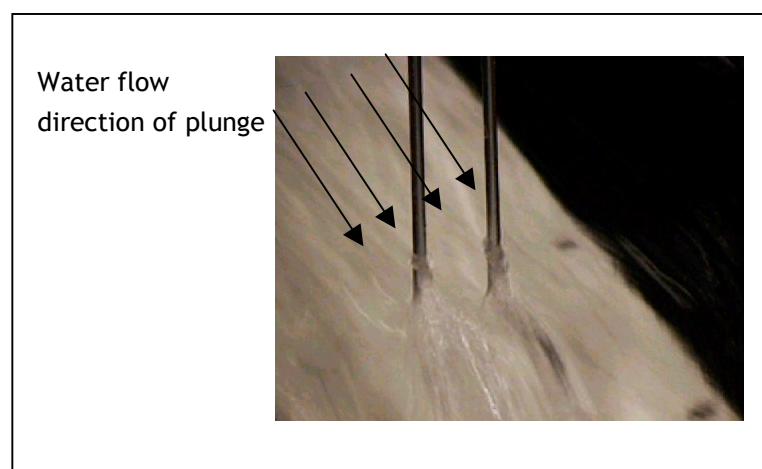


Figure 17: Collision of plunge with WHM

4.3.5 Experimental program

4.3.5.1 Pre-testing

Before starting with the experiments, a number of pre-testings were carried out. Apart from general knowledge about the best way to carry out the experiments, this was done to establish to what extent the shape of the schematised plunge as described in paragraph 3.4.2.5 is simulated correctly with the current experimental set-up. Furthermore, it was checked whether the dimensions of the experimental set-up are correct.

Some important findings of these tests can be summed up as follows:

- The shape of the plunge resembles the schematised plunge, described in section 4.1, especially the front part of the plunge. The decrease of the layer thickness after the maximum layer thickness is reached, is somewhat slower than described in the schematised plunge. However, as most damage is inflicted by the front part of the plunge, this deviation is considered to be not important.

- The small stones ($D_{n50} = 1.15$ cm) were not suitable for the current experimental set-up. These stones were flushed away even at small plunge sizes. The intermediate-size stones and the large stones were suitable. In the experiments described in this report only the intermediate-size stones were used.
- The spread in damage results was great.
- The stability of the rear slope increases when a large plunge is preceded by several smaller plunges.
- In almost all tests, the rear slope was not affected anymore after more than three plunges of the same size.

4.3.5.2 Cumulative damage vs individual plunges

The last two observations during pre-testing lead to the idea that it is questionable whether the experiments should concentrate on individual plunges. In this research it is decided to concentrate on the damage due to different plunge-sizes. This choice is made, because in real-life situations the probability of damage due to a single large plunge is small. It is more likely that this “super-plunge” is preceded by smaller plunges.

With above considerations, the experiments were carried out as follows. Starting with the smallest plunge size (4 cm water inside the reservoir ¹³), the number of displaced stones were recorded after every plunge. After three plunges of the same size, a picture was taken of the rear slope and the plunge size was raised (the water level inside the reservoir was raised with 1.25 cm). This procedure was carried out until rear slope collapse, defined as the condition at which the filter layer is visible over an area of four times D_{n50} .

Four series of experiments were carried out with individual plunges to consider the difference between damage due to individual plunges and cumulative damage. The plunge in these experiments was preceded by five very small plunges that did not cause any rear slope damage. In this way, the starting situation of the rear slope strength was likely to be more similar for the different experiments.

4.3.5.3 Plunge characteristics

The objective of the research was to describe the physics of the rear slope response to plunges. It is therefore necessary in the research to consider all plunge characteristics that could influence this response: the volume, the discharge, the layer thickness and (an estimate of) the plunge velocity, see section 4.3.4.

In order to investigate these plunge characteristics separately, different configurations of the reservoir are necessary in the experiments. Three reservoir configurations were used, as described in Table 2.

Table 2: Reservoir configurations

	Configuration I	Configuration II	Configuration III
Surface of reservoir (cm ²)	1590	1140	1590
Height of opening (cm)	4	4	8

¹³ The plunge size is related to the water level inside the reservoir. The smallest possible plunge size is determined by WHM1. For a water level below 4 cm, WHM1 does not produce reliable data.

4.3.5.4 Rear slope characteristics

All characteristics of the rear slope can be varied in the current experimental set-up: the stone size and shape, the slope angle, the roughness of the filter layer and the crest freeboard. In this research only the crest freeboard is varied in the experiments, due to the limited amount of time available. This rear slope characteristic is chosen, because, according to literature, the influence of the crest freeboard is considered to be of great influence to the rear slope stability (see Burger [1], Van der Meer [2], Vidal [4], de Jong [5] and Andersen [12])

Three different water levels in the flume were used in the experiments: 10 cm, 7 cm and 3 cm under the crest. The experiments with different reservoir configurations were carried out with the water level 10 cm under the crest.

4.3.5.5 Overview of experiments

In Table 3 and Table 4 all experiments are summed up. The experiments on cumulative damage are repeated five times. Only serie 1 of the experiments is repeated nine times, due to the large spread in the results. This spread reduced in experiments later on, probably due to more experience in constructing the rear slope. Furthermore, experiment number 6 of serie 1 was carried out with ten plunges instead of three plunges.

Table 3: Experiments on cumulative damage

Serie nr. of experiments	Configuration nr.	Crest freeboard (cm)	Repetitions
1	I	10	9
2	II	10	5
3	III	10	5
4	I	7	5
5	I	3	5

Table 4: Experiments on damage due to individual plunges

Serie nr. of exp.	Config. nr.	Water level res.	Crest freeboard	Repetitions
6	I	4	10	5
7	I	5.25	10	5
8	I	6.5	10	5
9	I	7.75	10	5

4.3.6 Testing procedure (cumulative damage)

PREPERATIONS

The rear slope

- Remove (all) water in the flume
- Remove primary armour layer
- Remove secondary armour layer (only if secondary armour layer is affected)

- Place secondary armour layer (white)
- Place primary armour layer in strips of two rows of coloured stones
- Fill flume with water (gently) until water flows over the weir
- Take a picture of the slope

Measuring equipment

- Check the slots for water
- Check the computer
- Run the program 'Dasylab'
- Fill water reservoir to check the measuring equipment (water flows through the gate)

The water reservoir

- Remove (all) water from the water reservoir
- Add butylene-kit on the gate to make it watertight, if necessary
- Place the screw bolt on the right height, if necessary
- Place (concrete) blocks in reservoir, if necessary
- Fill reservoir with water up to required volume

THE EXPERIMENT

- Quickly lift the gate
- Note down the number and strip number of displaced stones
- Fill the reservoir up to the required volume
- Repeat the first three steps another two times
- Take a picture of the rear slope
- Repeat the first five steps with a larger water level inside the reservoir until rear slope collapse occurs

AFTERWARDS

- Verify the number of displaced stones observed with the number of displaced stones on the pictures
- Translate the number of displaced stones into the damage number N_{od}
- Process the saved data of the plunge from Dasylab

5 DATA PROCESSING

5.1 Introduction

In this Chapter the rough data of WHM1, WHM2 and WHM3 are translated into the plunge characteristics. These plunge characteristics are plotted against the water level inside the reservoir. Furthermore, the data on the rear slope damage is dealt with. The rear slope damage is also plotted against the water level inside the reservoir. With this information, the rear slope damage can be related to the plunge characteristics, as is dealt with in Chapter 6.

5.2 Plunge characteristics

As described in section 4.3.4, five plunge characteristics are considered. In the next sections the (possible) influence of these five plunge characteristics on the rear slope stability is discussed:

- *The Volume (V)*
- *The maximum discharge (Q_{\max})*
- *The maximum layer thickness (d_{\max})*
The maximum of the discharge and the layer thickness is chosen as the characteristic value for these parameters.
- *The front velocity (U_f)*
The front velocity resembles the propagation velocity of the plunge. The front velocity is not necessarily a good representative of the water velocity. Therefore, it is tried to find a better characteristic of the velocities in the plunge, using a combination of above characteristics:
- *The characteristic velocity ($u_{char} = \frac{Q_{\max}}{B \cdot d_{\max}}$)*

Above-mentioned plunge characteristics are induced by lifting the gate of the reservoir. The resulting hydraulic processes on the crest are only described in global terms, as these phenomena are outside the scope of this research. The emphasis in this research is put on the relation between the plunge characteristics and the rear slope damage.

These five characteristics are determined for every water level inside the reservoir and for all three configurations (see also 4.3.3).

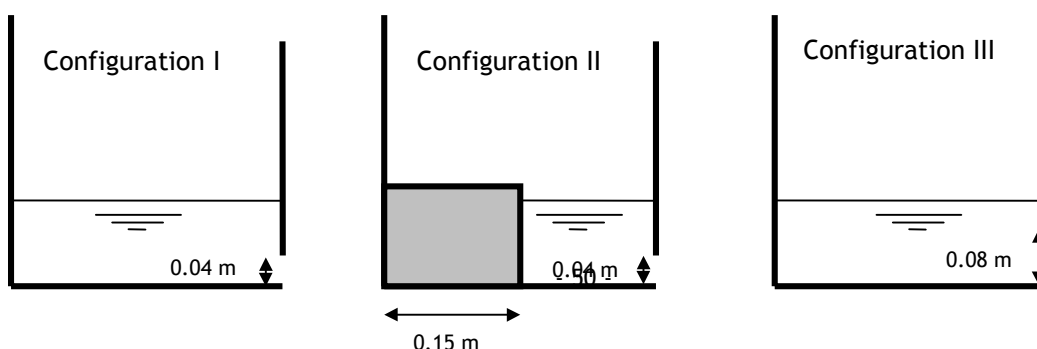


Figure 18: The three configurations of the reservoir (not on scale)

Table 2: Reservoir configurations

	Configuration I	Configuration II	Configuration III
Surface of reservoir A_r (cm ²)	1590	1140	1590
Height of gate opening (cm)	4	4	8

5.2.1 Volume

The volume inside the reservoir depends on the area of the water surface and on the water level inside the reservoir. The area of the water surface remains constant for all three configurations (see Table 2). Therefore, the volume is linearly related to the water level as is visualised in Figure 19. At an arbitrary value of the water level inside the reservoir, the volumes of Configuration I and III are similar, while the volume of Configuration II is about 30% smaller. It is assumed that the spread around the 'theoretical' values due to measuring errors is not significant.

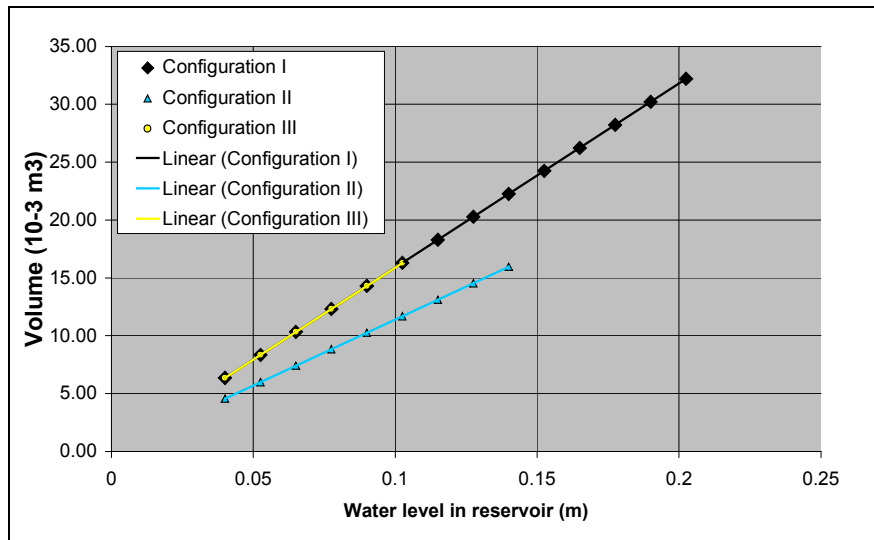


Figure 19: Volume versus the water level inside the reservoir

5.2.2 Maximum discharge

For all three reservoir configurations, the maximum discharge¹⁴ is determined as a function of the water level inside the reservoir, using data from WHM1. The results are presented in Figure 20. In Annex II.B, the calculation method is elaborated.

¹⁴ The maximum values are in fact the average maximum values of six individual tests.

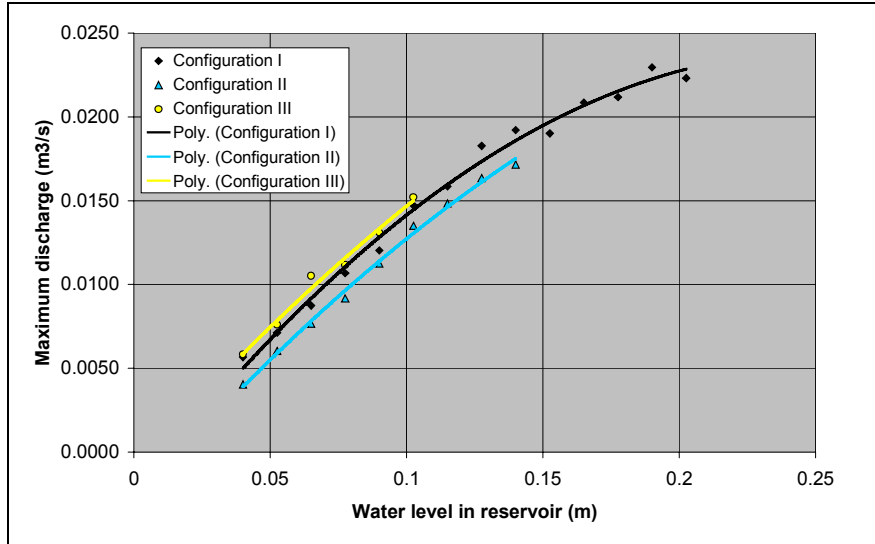


Figure 20: Relation between water level in reservoir and maximum discharge for the three reservoir configurations.

As expected, the maximum discharge increases with increasing water level inside the reservoir. The shape of the graph resembles the theory well. According to Torricelli, the outflow velocity should be proportional to the root of the water level in the reservoir ($U = \sqrt{\Delta h}$). The discharge can be expressed as $Q = \mu A_r \cdot U$, in which the contraction coefficient μ can depend on the water level (the water surface of the reservoir ($= A_r$) remains constant). Theoretically speaking, the maximum discharge plotted against the water level in the reservoir should therefore resemble a square-root-type function. This is clearly the case for Configuration I. The maximum discharges of Configuration II and III show a more linear relation, probably due to the limited number of measuring points.

It can be observed from Figure 20 that, on average, for a particular water level inside the reservoir, the maximum discharges for the three different configurations are related as follows: $Q_{\max,I} : Q_{\max,II} : Q_{\max,III} = 1 : 1.15 : 1.26$

It seems obvious that the maximum discharge of Configuration III is the largest of the three configurations as the opening of Configuration III is larger compared to Configuration I and II (8 cm instead of 4 cm). The difference between Configuration I and Configuration II cannot be easily explained, but are in some way related to the 2 blocks of concrete placed inside the reservoir for Configuration II.

Above data of the maximum discharge as a function of the water level inside the reservoir should be handled with care. The values are average values of six measurements and the spread around these average values is considerable (approximately 10% for configuration I, 5% for configuration II and 15% for configuration III, see Annex II.B). The deviations of the average values are in the same order as the spread. In the analysis of Chapter 6, the spread is visualised by using “blocks” around the average values.

5.2.3 Maximum layer thickness

For all three reservoir configurations, the maximum layer thickness ¹⁵ is determined as a function of the water level inside the reservoir, using data from WHM3. The results are presented in Figure 21. In Annex II.C, the calculation method is elaborated.

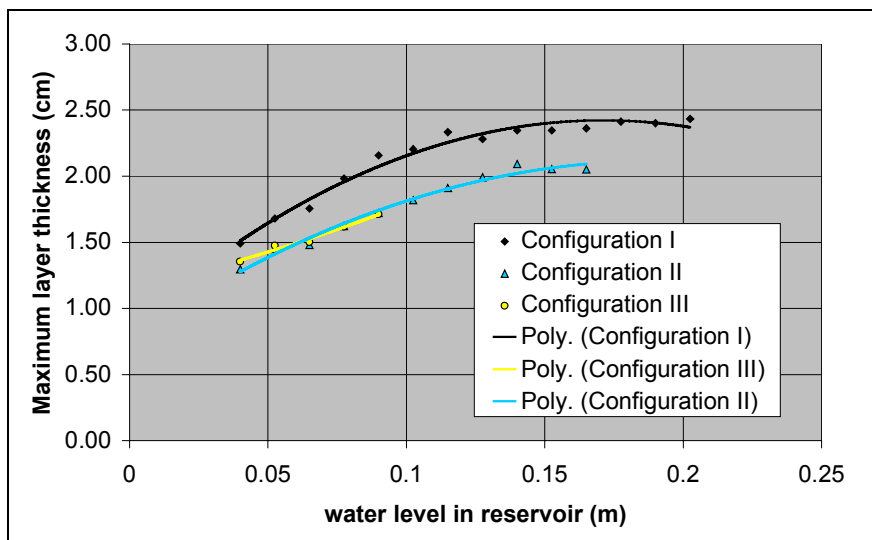


Figure 21: Relation between water level inside the reservoir and maximum layer thickness for the three reservoir configurations.

The maximum layer thickness increases with increasing water level inside the reservoir. The data from Configuration I shows a maximum value of the maximum layer thickness, for large values of the water level inside the reservoir. For Configuration I and III the maximum value of the maximum layer thickness is not yet reached.

It is remarkable that the maximum layer thickness of Configuration III shows lower values than Configuration I. Larger values were expected, due to the larger opening of the reservoir. A simple explanation for this phenomenon cannot be given, due to the complexity of the hydraulic processes involved.

Above data of the maximum layer thickness as a function of the water level inside the reservoir should be handled with care. The values are average values of six measurements and the spread around these average values is considerable (approximately 5% for Configuration I and II and 15% for Configuration III). In this light the maximum layer thicknesses of Configuration II and III are approximately equal for an arbitrary water level inside the reservoir. Even with the spread in mind, the layer thickness of Configuration I is significantly larger than the layer thickness of Configuration II and Configuration III. In the analysis of Chapter 6, the spread is visualised by using “blocks” around the average values.

¹⁵ Also for the layer thickness, the maximum values are in fact the average maximum values of six individual tests.

5.2.4 Front velocity

For all three reservoir configurations, the front velocity ¹⁶ is determined as a function of the water level inside the reservoir, using data from WHM1 and WHM2. The results are presented in Figure 22. In Annex II.D, the calculation method is elaborated.

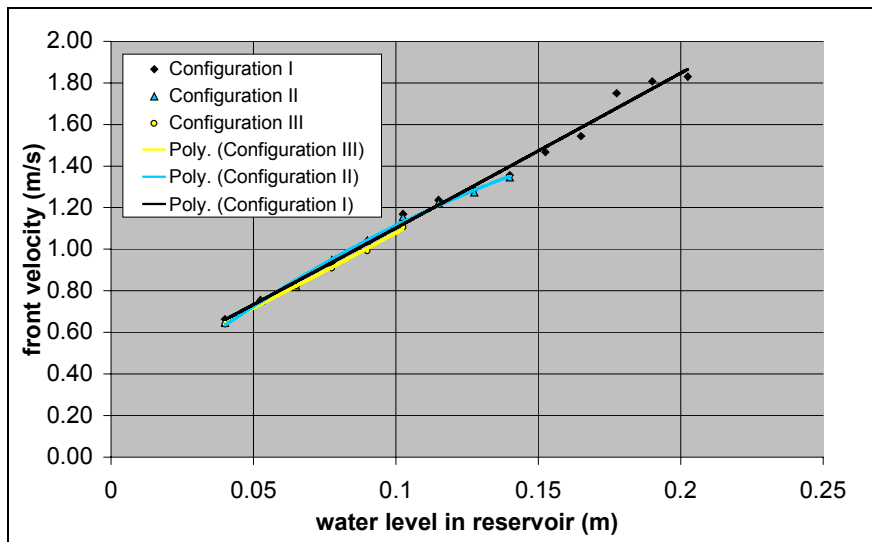


Figure 22: Relation between water level in reservoir and front velocity for the three reservoir configurations.

As expected, the front velocity increases with increasing water level inside the reservoir (due to an increase of the outflow velocity). It is remarkable that at an arbitrary value of the water level inside the reservoir, the respective front velocities are more or less equal for all three configurations. This phenomenon is taken for granted, as it is beyond the scope of this research.

Because of the small deviations between the three configurations, relatively to the spread (10% for all configurations), one single equation is used to describe the relation between 'the' front velocity and the water level in the reservoir. This relation appeared to be nearly linear. In the analysis of Chapter 6, the spread is visualised by using "blocks" around the average values.

5.2.5 Characteristic velocity

For all three reservoir configurations, the characteristic velocity is determined as a function of the water level inside the reservoir, using the information on the maximum discharge and the maximum layer thickness ¹⁷. The results are presented in Figure 23. In Annex II.E, the calculation method is elaborated.

¹⁶ The values are in fact the average values of six individual tests.

¹⁷ These both values are in fact the average values of six individual tests.

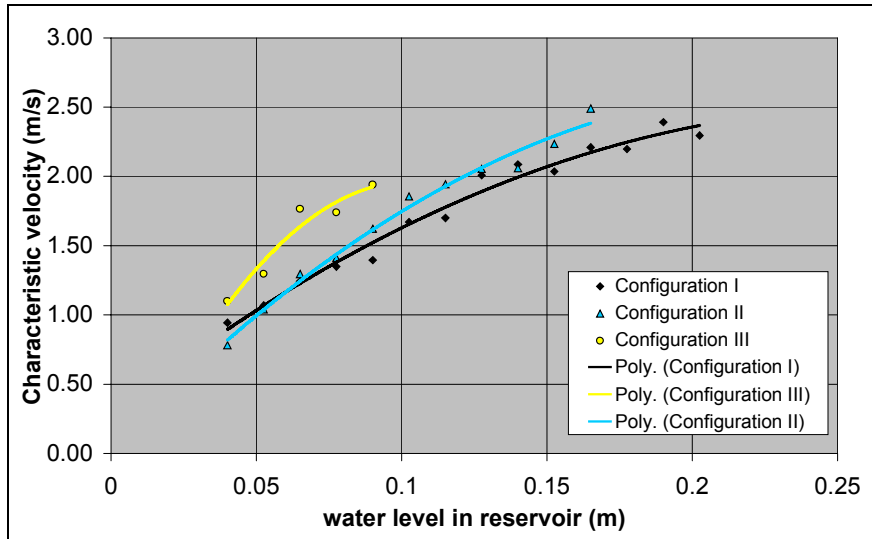


Figure 23: Relation between water level in reservoir and characteristic velocity for the three reservoir configurations.

As expected, the characteristic velocity increases with increasing water level inside the reservoir. The characteristic velocity of Configuration III is obviously the largest for an arbitrary water level inside the reservoir. The difference between the characteristic velocities of Configuration I and II is small for small values of the water level, but for larger values of the water level (> 10 cm), the characteristic velocity of Configuration II exceeds that of Configuration I. This phenomenon is taken for granted in this report. Due to the complexity of the experimental set-up the above derived relation between water level inside the reservoir and the characteristic velocity cannot be easily explained.

Due to the combined spread of the maximum layer thickness and the maximum discharge, the spread for the characteristic velocity is considerable. For Configuration II the spread is approximately 10%, for Configuration I approximately 15% and for Configuration III approximately 20%. In the analysis of Chapter 6, the spread is visualised by using “blocks” around the average values.

5.3 Rear slope damage

In the next sections all data on the rear slope damage is plotted. The results from the experiments can be subdivided into three categories:

- Total cumulative damage (see 5.3.1)
- Damage area (see 5.3.2)
- Damage due to individual plunges (see 5.3.3)

In the graphs, the damage is plotted against the water level inside the reservoir, which is proportional to the hydraulic load. In Chapter 6, the damage development is related to plunge characteristics.

Just as for the data on plunge parameters, a reliability interval is needed for the analysis. Due to the large spread in the results (in the order of 100% and increasing for larger plunges), the difference between the highest damage and the lowest damage at an

arbitrary plunge size is taken as an indication of the reliability. In the analysis of Chapter 6, the spread is visualised by using “blocks” around the average values.

5.3.1 Total cumulative damage

The measuring points of the graphs on cumulative damage development represent the displaced stones that as recorded after three plunges induced by a specific water level inside the reservoir. The number of displaced stones was translated into the damage parameter according to Van der Meer (N_{od}) [2]¹⁸. The cumulative damage was plotted against the water level inside the reservoir.

In the experiments the cumulative damage was measured for three crest freeboards: 10 cm, 7 cm and 3 cm above the waterline in the flume. For the crest freeboard at 10 cm, the damage development was measured for three different configurations of the reservoir. The experiments were repeated five times, except for Configuration I at a crest freeboard of 10 cm. This experiment was repeated nine times (see Table 5)

Table 5: Experiments on cumulative damage

Crest freeboard (cm)	Configuration no.	Repetitions
10	I	9
10	II	5
10	III	5
7	I	5
3	I	5

In Annex II.F and Annex II.G all data on damage development can be found, in different tables.

¹⁸ This damage parameter is defined as the number of displaced stones on the slope per stone width.

5.3.1.1 Crest freeboard = 10 cm

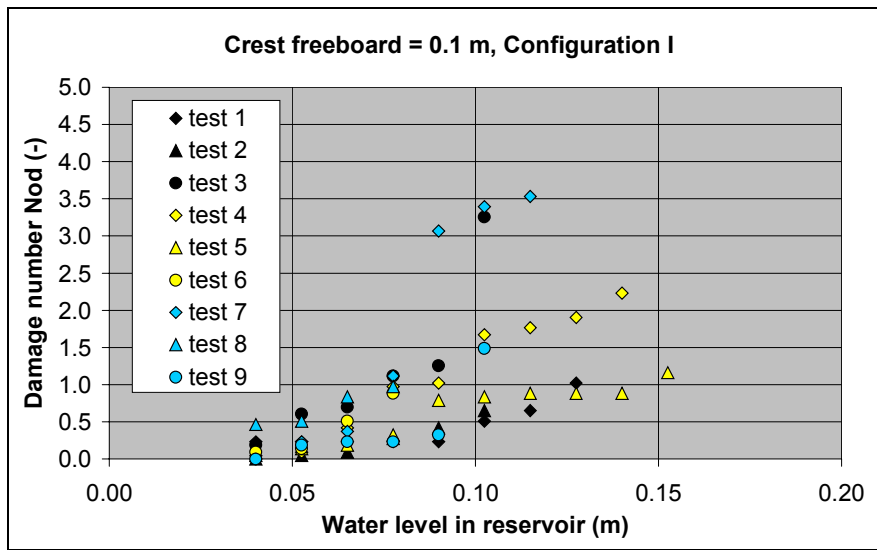


Figure 24: Cumulative damage for Configuration I, crest freeboard = 10 cm

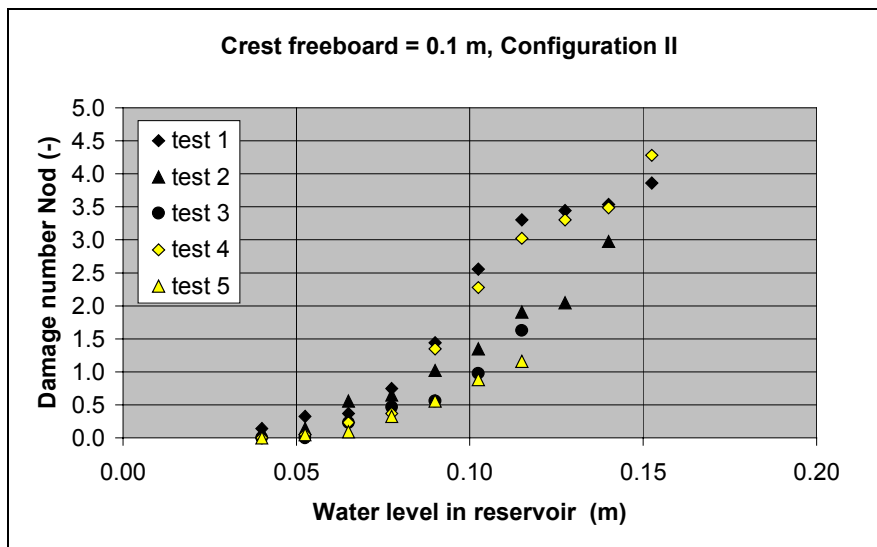


Figure 25: Cumulative damage for Configuration II, crest freeboard = 10 cm

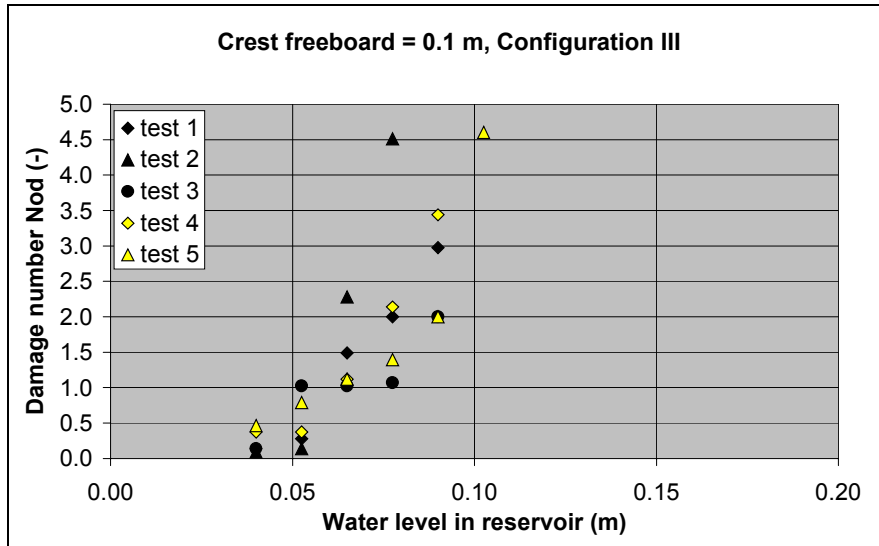


Figure 26: Cumulative damage for Configuration III, crest freeboard = 10 cm

5.3.1.2 Crest freeboard = 7 cm

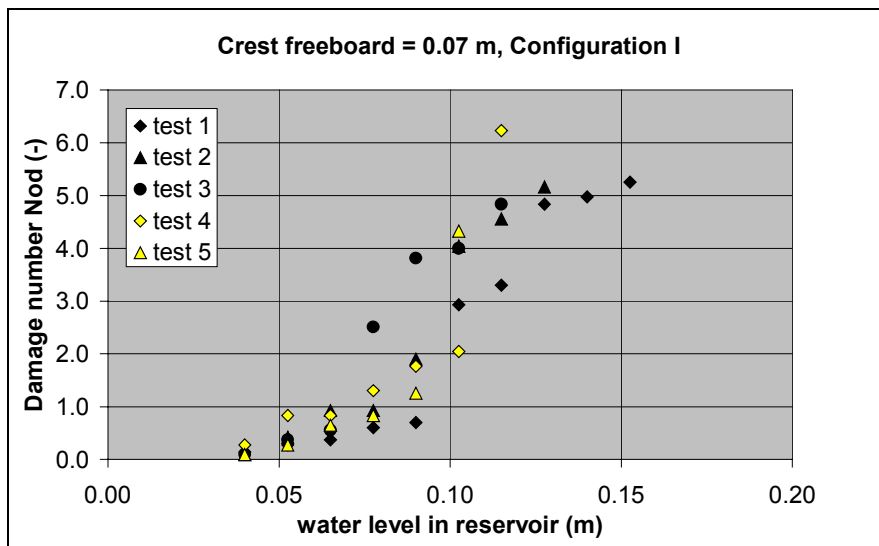


Figure 27: Cumulative damage for Configuration I, crest freeboard = 7 cm

5.3.1.3 Crest freeboard = 3 cm

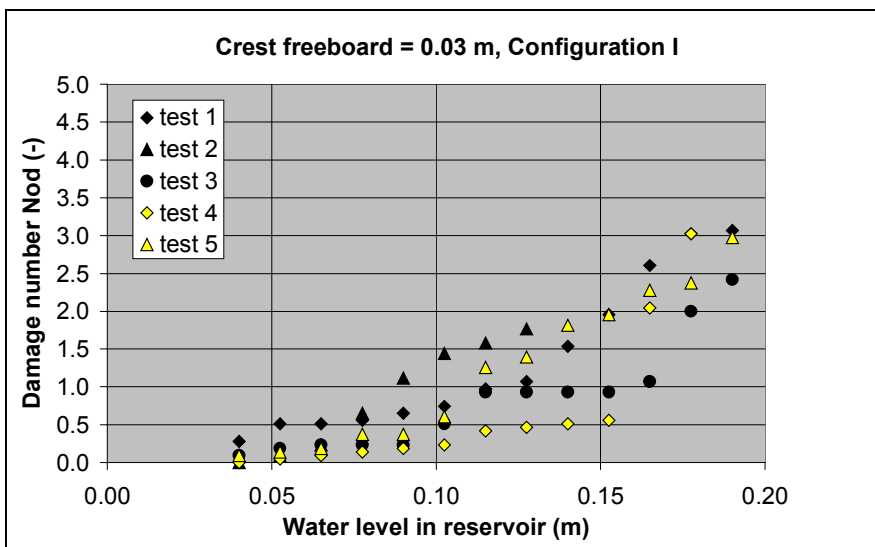


Figure 28: Cumulative damage for Configuration I, crest freeboard = 3 cm

5.3.2 Damage location

Beside the total cumulative damage, also the damage per strip was recorded, which provides information about the damage area and the development of damage along the slope. It was observed that most damage occurred above and around the waterline. Below the waterline, the damage quickly decreased to zero. In Figure 29, Figure 30 and Figure 31 three characteristic examples of the damage per strip are given. These figures represent the following experiments:

- Configuration I Crest freeboard = 10 cm Experiment 3
- Configuration I Crest freeboard = 7 cm Experiment 3
- Configuration I Crest freeboard = 3 cm Experiment 1

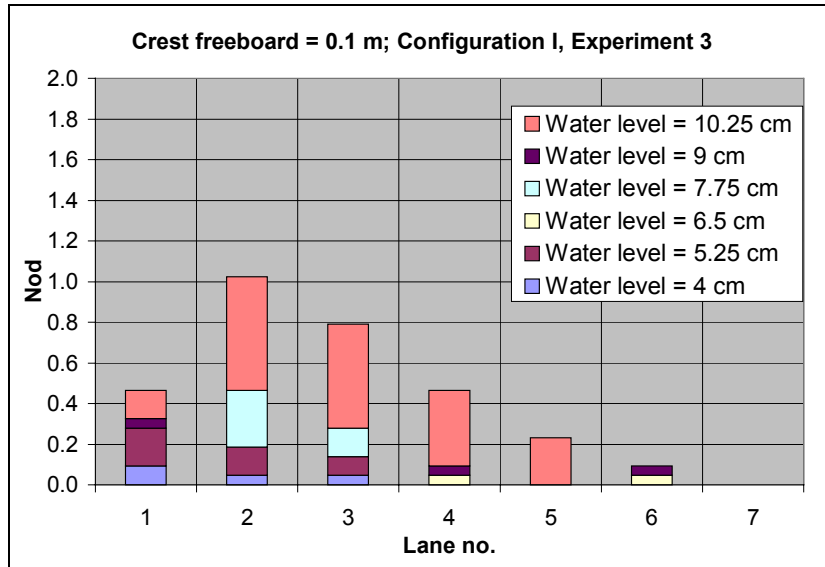


Figure 29: Damage per strip, crest freeboard = 10 cm, experiment 3

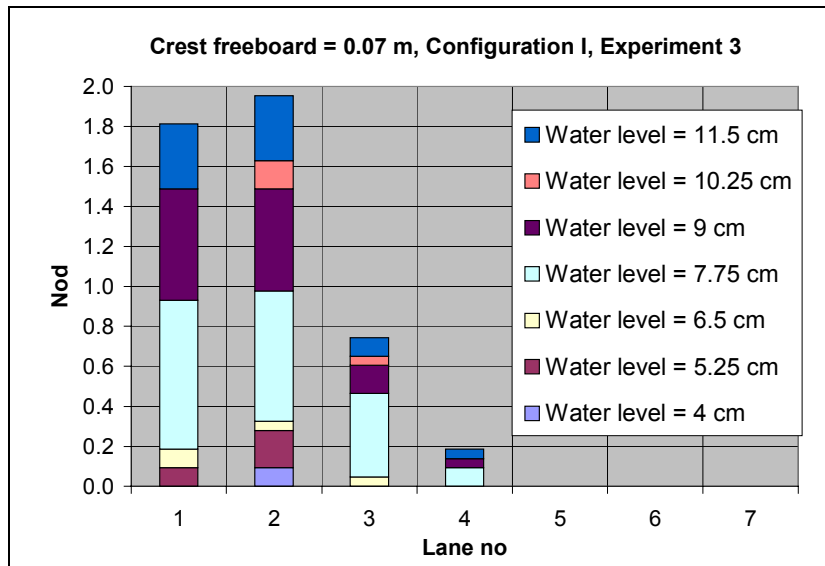


Figure 30: Damage per strip, crest freeboard = 7 cm, experiment 3

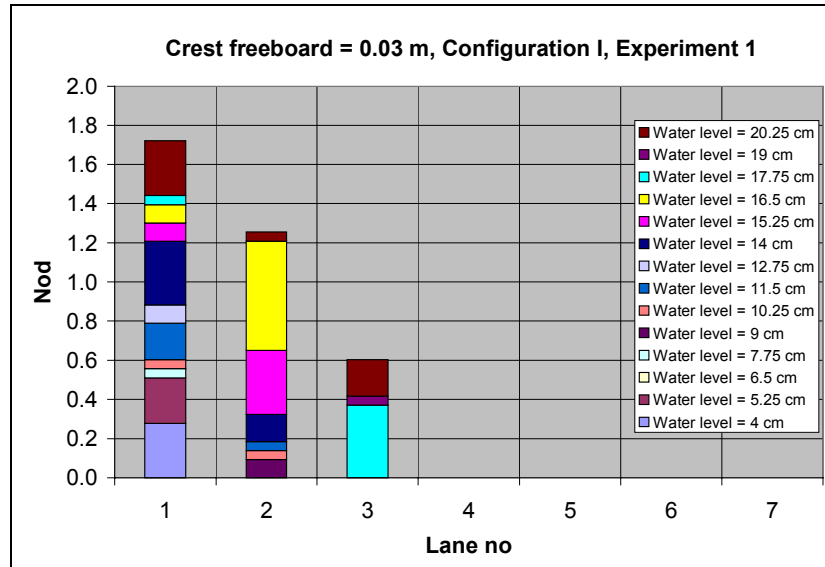


Figure 31: Damage per strip, crest freeboard = 3 cm, experiment 1

In Chapter 6, the results on the damage per strip will be further elaborated.

5.3.3 Damage due to individual plunges

The experiments on damage due to individual plunges were carried out with a crest freeboard of 10 cm and with reservoir configuration I.

The graph on damage due to individual plunges was plotted using the following steps:

- Starting with a minimal water level inside the reservoir the amount of displaced stones were recorded per coloured strip, after one plunge.
- The amount of displaced stones was translated into the damage parameter of Van der Meer (N_{od}).
- The water level inside the reservoir was increased, after repairing the rear slope and again the damage was recorded after one plunge

In total five experiments were carried out per water level inside the reservoir. Four different water levels inside the reservoir were tested, presented in Figure 32. Experiment 19 and 20 are not included, as these experiments lead to rear slope collapse.

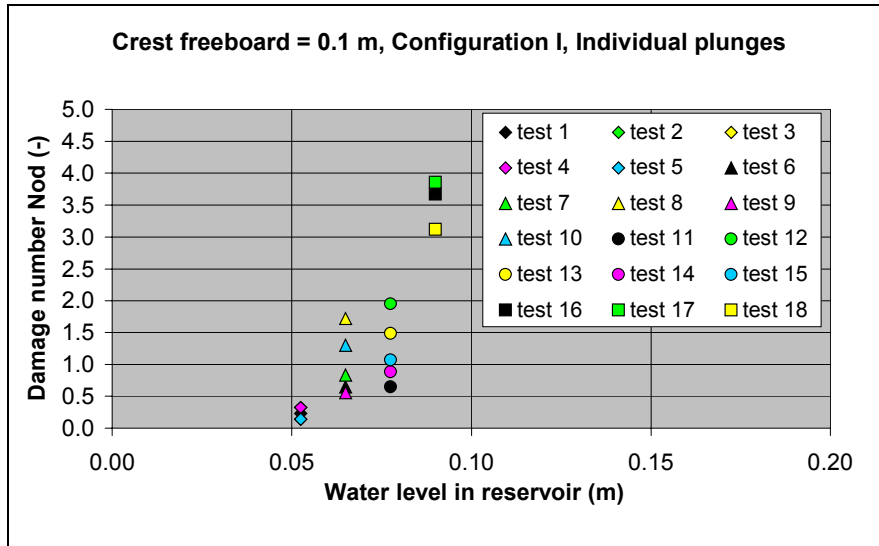


Figure 32: Damage due to individual plunges for Configuration I

6 ANALYSIS OF EXPERIMENTS

6.1 Introduction

In this chapter the analysis of the experiments is dealt with. Five objectives were formulated:

- Isolating the plunge characteristic(s) that determine(s) the total cumulative damage development of the rear slope (dealt with in section 6.3).
- Description of the probability of rear slope collapse (dealt with in section 6.4).
- Determining the influence of the crest freeboard on the total cumulative damage development of the rear slope (dealt with in section 6.5).
- Determining the influence of the crest freeboard on the damage location (dealt with in section 6.6).
- Determining the influence of the crest freeboard on collapse behaviour (dealt with in section 6.7)
- Determining the difference between cumulative damage and damage due to individual plunges (dealt with in section 6.8).

Before dealing with above objectives an important distinction between damage and collapse is discussed.

6.2 Rear slope damage vs rear slope collapse

In this report, 'damage' is defined as the number of displaced stones per stone width (definition of Van der Meer [2]). In this report, 'collapse' is defined as the condition that the filter layer is visible over an area of 3 to 4 times D_{n50} and the armour layer can no longer be expected to function properly (definition of author, see section 4.3.5.2). This collapse criterion is not based on a critical damage number, but on a visual inspection of the condition of the rear slope. Therefore, 'damage' and 'collapse' have to be interpreted as two different phenomena.

As a result, a distinction has to be made between rear slope damage and rear slope collapse. In the experiments the transition between 'damage' and 'collapse' occurred abruptly. Furthermore, for experiments repeated under the same circumstances the rear slope collapsed at different plunge sizes. This difference in collapse behaviour of the experiments is inherent to the experimental set-up in which the rear slope consists of randomly placed, non-cohesive stones. In section 6.4 this collapse behaviour of the rear slope is discussed.

For the analysis of the rear slope damage, a problem occurs due to the unpredictable collapse behaviour of the rear slope. The average rear slope damage at an arbitrary value of the plunge size is easy to determine when none of the experiments resulted in rear slope collapse. However, if this is not the case, this average cannot easily be defined. As it is not possible to express a collapsed slope in terms of damage, two approaches can be followed to calculate the average rear slope damage in the latter case:

- The average damage is calculated using the data of the non-collapsed slopes
- The average damage is not calculated

In the first approach all damage data are taken into account, but the reliability of the average values of the damage decreases for larger plunge sizes. The reason for this is an increasing number of collapsed experiments ¹⁹ and therefore a decreasing number of measuring points for which an average value of the damage is calculated.

The second approach leads to a significant reduction of the actual data that is used in the analysis. The experiment during which collapse of the rear slope appeared at the smallest plunge size, determines the maximum value of the data that can be used. However, the reliability of the average damage, calculated for these data is the greatest.

In this report the second approach is followed in considering the damage development (see section 6.3). This approach results in very reliable values of the average damage up to a certain value of the plunge size. In section 6.4, after describing the probability of collapse, the first approach is used to see whether the results of the second approach can be extrapolated to larger values of the plunge size.

6.3 Relation between cumulative damage and plunge characteristics

6.3.1 Introduction

In Chapter 5, the relation between the plunge characteristics and the water level inside the reservoir is presented for three different configurations of the reservoir. In the same Chapter the relation between the cumulative damage of the rear slope and the water level inside the reservoir is also presented for the three different configurations of the reservoir. With this information, it is possible to relate the cumulative rear slope damage directly to the plunge characteristics.

Above steps are taken to achieve the first objective of this Chapter: isolating the plunge characteristic(s) that determine(s) the cumulative damage development of the rear slope, independent of the configuration of the reservoir. All experiments were done with a crest freeboard of 10 cm.

In the next sections the rear slope damage is related to only two of the five characteristics, discussed in section 5.2, namely to the front velocity and to the maximum discharge. The volume and the maximum layer thickness of the plunge cannot induce a force by itself and can only influence the rear slope damage in combination with any of the other two fundamental parameters. The combinations of parameters that are considered are summed up in Table 6. The combination of the front velocity with the maximum discharge is not considered, as this combination cannot be physically interpreted.

Table 6: Combinations of parameters considered

	Front velocity	Discharge
Front velocity	-	Not considered
Discharge	Not considered	-
Volume	Qualitatively considered (see section 6.3.2)	Qualitatively considered (see section 6.3.3).
Layer thickness	Qualitatively considered (see section 6.3.2)	Quantitatively considered (see section 6.3.4).

6.3.2 Cumulative damage as a function of θ_{u_f}

For the three configurations of the reservoir the average damage development as determined in section 5.3.1 is related to a stability parameter, using the front velocity of the plunge and the average stone size. This leads to the following stability parameter²⁰ :

$$\theta_{u_f} = \frac{u_f^2}{\Delta g D_{n50}} \quad (-)$$

The relation between the damage development and θ_{u_f} is visualised in Figure 33. The dotted line in this figure marks the area for which non of the experiments showed collapse. Left from the dotted line only damage occurred in the experiments, for all three configurations. Right from the dotted line collapse occurred in the experiments. The data point at the right hand side of the dotted line is therefore not used in the analysis although this particular point did not show collapse. In Annex II.H the same figure is presented including reliability intervals.

¹⁹ With the term 'collapsed experiments' the experiments are meant for which the rear slope showed collapse.

²⁰ This method was first introduced by Shields, for stationary flow. Just like Shields, the symbol θ is used for the derived stability parameters.

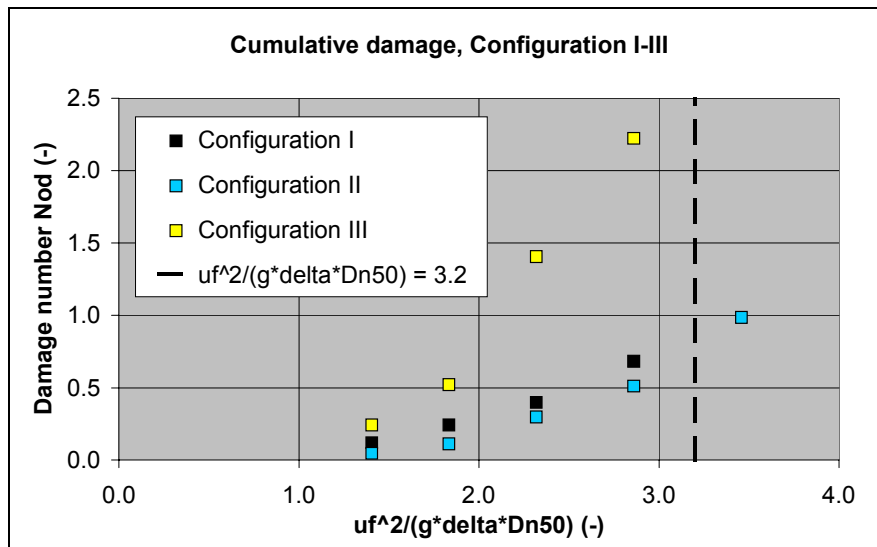


Figure 33: Cumulative damage development plotted against θ_{u_f}

From Figure 33 it can be concluded that the front velocity cannot be seen as the only parameter that determines the rear slope stability. The differences in the damage development between Configuration I en Configuration II could be attributed to the spread in the test results, but the damage development of Configuration III shows a significant different behaviour. For an arbitrary front velocity, the damage is significantly larger for Configuration III, compared to Configuration I and II.

The above analysis can hypothetically be interpreted as follows ²¹:

- either the front velocity is not a good plunge characteristic to determine the rear slope stability,
- or the front velocity in combination with the volume or the maximum layer thickness determines the rear slope stability.

In order to check the second hypothesis, in Table 7 the values of the volume and the layer thickness are compared at an arbitrary value of the front velocity for all three configurations.

Table 7: Values of other plunge characteristics for an arbitrary value of front velocity

Parameter	Configuration I	Configuration II	Configuration III
Volume	Highest	Lowest	Equal to Conf. I
Maximum layer thickness	Highest	Lowest	Equal to Conf. II

It is obvious to assume that *if* the volume influences on the rear slope damage, then the higher the volume, the more the damage. The same applies to the layer thickness. With

²¹ The step size between two consecutive plunges as well as the starting value of the smallest plunge are equal for all configurations and can therefore not be an explanation for the differences in damage development.

these assumptions in mind it can be concluded from the values in Table 7 that the larger damage of Configuration III at an arbitrary value of the front velocity cannot be explained by the difference in volume or layer thickness. For Configuration III, the values of the maximum layer thickness and the volume are not significantly larger than for Configuration I and II.

The conclusion must be that it is not likely that the front velocity is the plunge characteristic that determines the rear slope damage, not by itself and not in combination with other plunge characteristics.

6.3.3 Cumulative damage as a function of θ_q

For the three configurations of the reservoir the average damage development as determined in section 5.3.1 is related to a stability parameter, using the maximum discharge per unit width of the plunge and the average stone size. This leads to the following stability parameter:

$$\theta_q = \frac{q_{\max}^2}{\Delta g D_{n50}^3} \quad (-)$$

The relation between the damage development and θ_q is visualised in Figure 34. In Annex II.H the same figure is presented including reliability intervals.

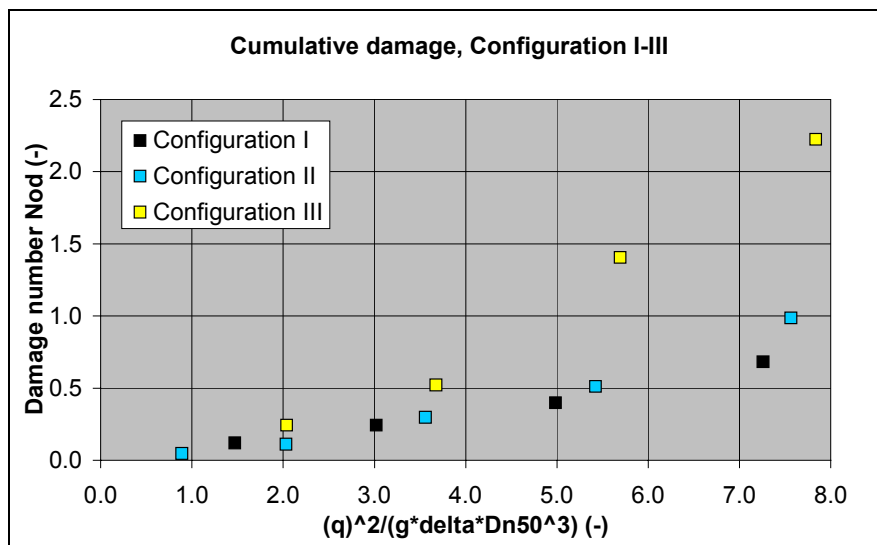


Figure 34: Cumulative damage development plotted against θ_q

From Figure 34 it can be concluded that the maximum discharge cannot be seen as the only parameter determining the rear slope stability. Although the deviations between the different configurations are less than was observed for the front velocity, still a significant difference between Configuration III and Configurations I and II is found.

The above analysis can be interpreted as follows:

- either the maximum discharge is not a good plunge characteristic to determine the rear slope stability,
- or the maximum discharge in combination with the volume or the maximum layer thickness determines the rear slope stability.

In order to check the second hypothesis, in Table 8 the values of the volume and the layer thickness are compared at an arbitrary value of the maximum discharge for all three configurations.

Table 8: Values of other plunge characteristics for arbitrary value of maximum discharge

Parameter	Configuration I	Configuration II	Configuration III
Volume	Highest	Lowest	Intermediate
Maximum layer thickness	Smallest	Intermediate	Highest

From the above Table, it is not expected that the maximum discharge in combination with the volume determines the rear slope stability. However, the combination of the maximum discharge with the maximum layer thickness seems to contribute to the decrease of the deviations between the different configurations. Therefore, a closer look is given to this combination.

At an arbitrary value of the discharge, Configuration III features the largest damage and Configuration I features the smallest damage. Simultaneously, the maximum layer thickness features the largest value for Configuration III and the smallest for Configuration I (see Figure 35). It seems not unlikely that the quotient of the maximum discharge and the maximum layer thickness could reduce the deviations between the three configurations as found in Figure 34.

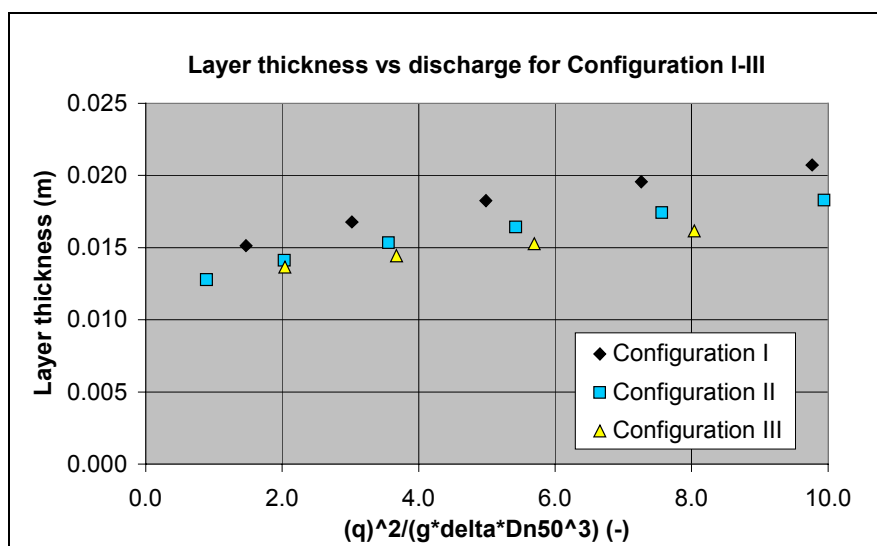


Figure 35: Layer thickness plotted against θ_q

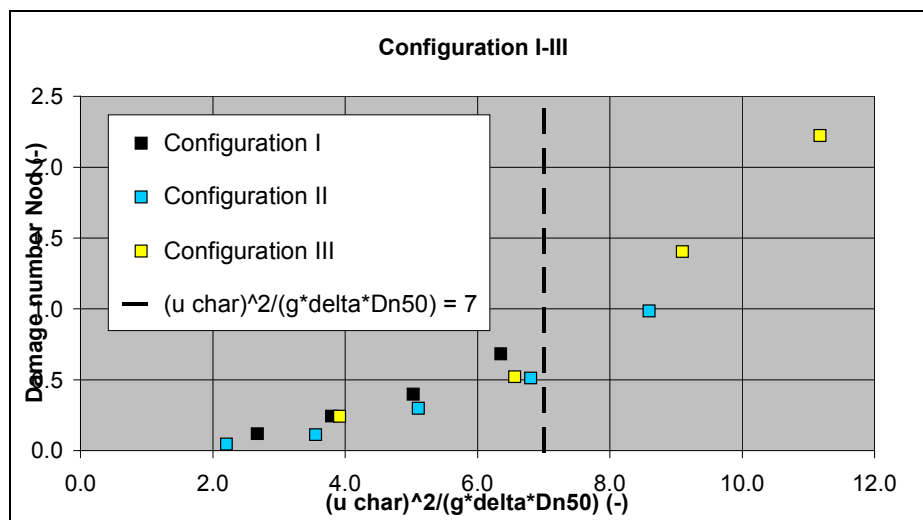
Above considerations lead to the conclusion that it is unlikely that the maximum discharge determines the rear slope stability.²² The quotient of the maximum discharge and the maximum layer thickness, defined as the characteristic velocity, seems to be a better plunge characteristic to determine the rear slope stability. The characteristic velocity is dealt with in the next section.

6.3.4 Cumulative damage as a function of $\theta_{u_{char}}$

For the three configurations of the reservoir the average damage development as determined in 5.3.1 is related to a stability parameter, using the characteristic velocity of the plunge and the average stone size. This leads to the following stability parameter:

$$\theta_{u_{char}} = \frac{u_{char}^2}{\Delta g D_{n50}} \quad (-)$$

The relation between the damage development and $\theta_{u_{char}}$ is visualised in Figure 36. The dotted line in this figure marks the area for which non of the experiments showed collapse. Left from the dotted line only damage occurred in the experiments, for all three configurations. Right from the dotted line collapse occurred in the experiments. The data points at the right hand side of the dotted line are therefore not used in the analysis although these particular points did not show collapse. In Annex II.H the same figure is presented including reliability intervals.



²²A reservation should be made to this conclusion. The difference in damage could also be attributed to the step size of the successive plunges. For Configuration III this step size is larger than for Configuration I and II. Furthermore, the first plunge of Configuration III is larger than the first plunges of Configurations I and II. More research into the influence of the step size is needed.

Figure 36: Cumulative damage development plotted against $\theta_{u_{char}}$

From Figure 36 it can be concluded that it is not unlikely that the characteristic velocity, defined by the quotient of maximum discharge and maximum layer thickness, can be considered as the primary factor that determines the rear slope stability. Other parameters such as the volume of the plunge or the front velocity play at the utmost a secondary role.

However, due to the limited amount of data and the large spread of this data, this conclusion must be handled with care. More measurements are needed to confirm the conclusion (for instance with larger differences between the layer thicknesses). Also the influence of the step size between two consecutive plunges should be better examined.

6.4 Probability of collapse

In section 6.2 a distinction between the rear slope damage and the rear slope collapse is made. It was observed that in some experiments collapse occurred at relatively small values of the plunge size, while in other experiments the rear slope could resist fairly large values of the plunge size. This justifies a closer look at the collapse behaviour of the rear slope, besides the investigation of the damage in section 6.3.

In order to get an idea of the probability of collapse, the values of the plunge sizes at which collapse occurred (expressed as a function of $\frac{u_{char}^2}{\Delta g D_{n50}}$) were recorded for all 19 experiments of section 6.3. No distinction was made between the three configurations. With this information the probability of collapse was plotted against $\frac{u_{char}^2}{\Delta g D_{n50}}$ in Figure 37²³.

²³ The probability of collapse is calculated as follows: $F(\text{collapse}) = \frac{N_{\text{collapsed}}}{N + 1}$, in which N_{collapse} = the number of collapsed slopes in the experiments at a certain value of $\frac{u_{char}^2}{\Delta g D_{n50}}$ and N = the total number of experiments.

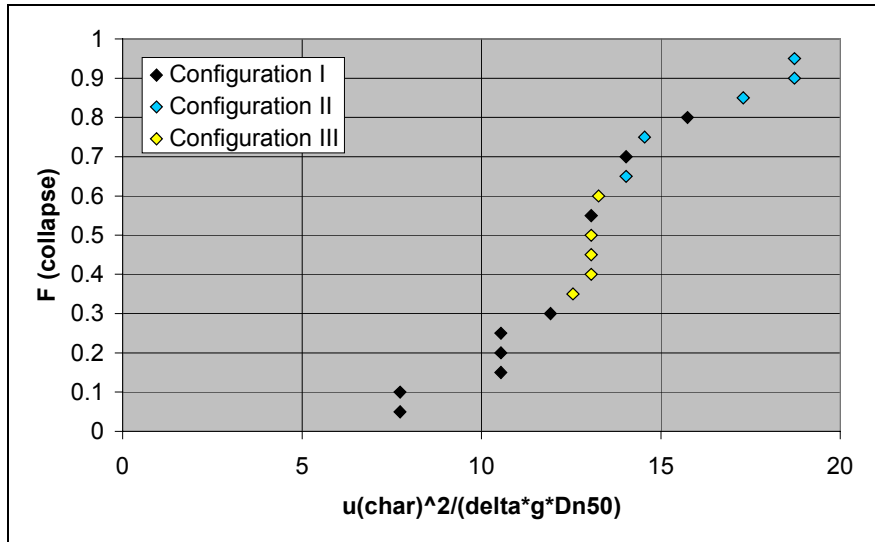


Figure 37: Probability of collapse

From Figure 37 it can be concluded that even with the limited number of experiments, the probability of collapse resembles a Gaussian-type curve. Theoretically it could be concluded that the rear slope collapse can occur at any load. Naturally, the probability of collapse increases with increasing plunge size.

This leads to the assumption that both phenomena, damage and collapse, have to be accounted for. At an arbitrary plunge size there is a probability of collapse and when collapse does not occur, a certain (average) damage is inflicted by the plunge. Both damage and probability of collapse increases with increasing plunge sizes.

Two remarkable features of Figure 37 have to be mentioned:

- Experiment 6 from Configuration I was carried out with ten plunges instead of three plunges per plunge size. It turns out that in this experiment a collapse occurred at the lowest plunge size of all nineteen experiments (together with experiment 8 from Configuration I). This could implicate an effect of the number of plunges on the collapse behaviour. However, more measurements have to be carried out to investigate this.
- The values of $\frac{u_{char}^2}{\Delta g D_{n50}}$ at which the experiments with Configuration II showed collapse, are relatively high. More measurements are needed to investigate whether this is accidental, or not.

In section 6.3, the average damage was calculated using only data for which none of the experiments showed rear slope collapse. From Figure 37 it can be concluded that this approach corresponds to a probability of collapse of approximately 5% ($\frac{u_{char}^2}{\Delta g D_{n50}} = 7$).

It is now checked whether the second approach (see section 6.2) leads to reliable values of the average damage for larger plunge sizes. In this approach the average damage is

calculated for the non-collapsed experiments and all data is used. This is presented in Figure 38.

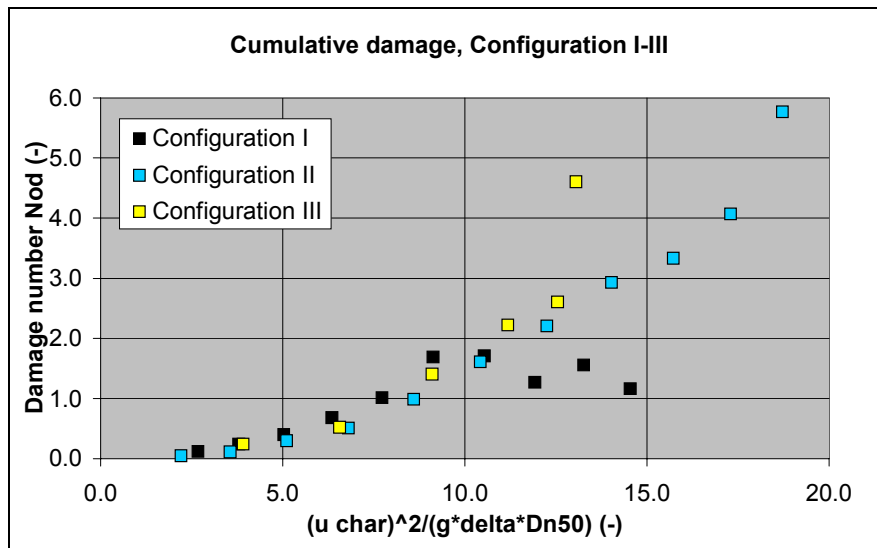


Figure 38: Average damage development for all data (second approach)

The conclusion is that with the current number of experiments, the reliability of the graph quickly decreases with increasing plunge size. This is obvious as the number of data used to calculate the average damage decreases with increasing plunge size. Up to a value of

$$\frac{u_{char}^2}{\Delta g D_{n50}} = 10,$$

the reliability of the graph seems to be reasonable. This is not surprising as

the number of collapsed experiments is only two out of nineteen for this value of $\frac{u_{char}^2}{\Delta g D_{n50}}$

(see Figure 37). For larger values of $\frac{u_{char}^2}{\Delta g D_{n50}}$, no reliable value of the expected damage can

be given. More experiments are needed to acquire reliable values of the average damage

for these values of $\frac{u_{char}^2}{\Delta g D_{n50}}$. It is however questionable whether this part of the graph is

interesting for design purpose, as the probability of collapse is larger than 15%.

In this report preference is given to the first approach for the analysis of the damage, as

was used in section 6.3. The maximum value of $\frac{u_{char}^2}{\Delta g D_{n50}}$ with this approach equals 7.

6.5 Influence crest freeboard on rear slope damage

The influence of the position of the waterline was investigated for three different water levels inside the flume (see Figure 39). For all three crest freeboards, the configuration of the reservoir was taken equal (Configuration I) and the testing procedure was also taken equal. In other words: the rear slope was subjected to the same size of the plunges for all three crest freeboards.

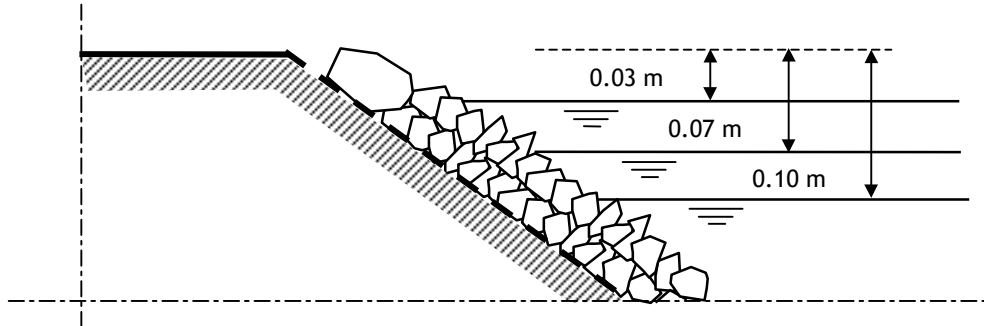


Figure 39: Three different water levels (not on scale)

In Figure 40 the average damage development at the three different water levels, as determined in 5.3.1 is plotted against the dimensionless characteristic velocity.

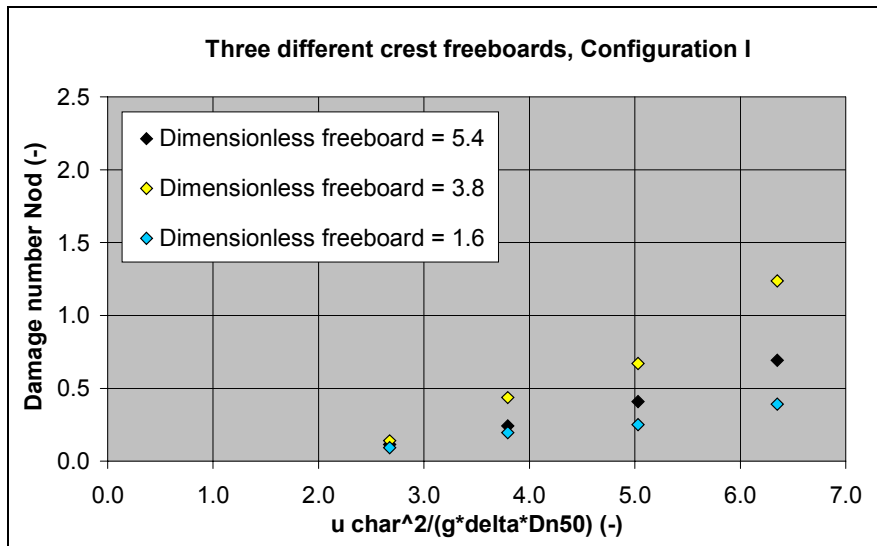


Figure 40: Influence of crest freeboard on cumulative damage development.

From Figure 40 it can be observed that for an arbitrary value of the plunge characteristic the rear slope damage is highest for the experiment with a dimensionless crest freeboard

$\frac{R_c}{D_{n50}} = 3.8$ and lowest for the experiment with a dimensionless crest freeboard of 1.6. The experiment with a dimensionless crest freeboard of 5.4 featured an intermediate damage development. These differences in stability are significant.

In order to explain the above results, the stability of a single stone on a rubble slope has to be considered. The stability of a single stone on a rubble slope depends on numerous parameters (e.g. position relative to the crest, stone shape, stone size, slope angle) but in the experiments only the waterline was varied. It is assumed that all other influencing parameters are equal for the three waterlines.

The waterline has a twofold effect on the stability of a single stone:

- Stones under the water level have a virtually smaller density due to the uplifting force of the surrounding water (Archimedes) and therefore a smaller stabilising force
- The destabilising force of the plunge is damped for a stone under water and the force is spread over a larger surface

The damping effect depends on the height of the water above the stone and therefore on the position of the stone relative to the waterline. The uplift effect is maximal if the stone is fully positioned under the waterline and zero if the stone is positioned above the waterline. The least favourable position for a stone is therefore around the waterline. This was also observed in the experiments: most damage occurred just below the waterline and as a consequence also above the waterline (see section 6.6).

Above-mentioned effects of the waterline on the stability of single stones obviously determine the total rear slope stability. The total rear slope stability is more complex than the stability of a single stone, due to mutual dependencies of the stability of single stones. With the results from the experiments only remarks about the average effect of the waterline can be given. It can be stated that for an arbitrary plunge size the following applies:

- The more stones under water, the larger the total damping effect for the rear slope (positive contribution to the stability)
- The more stones under water, the larger the total uplifting effect for the rear slope (negative contribution to the stability)

When comparing the results of the experiments with a dimensionless freeboard of 3.8 with those at a dimensionless freeboard of 1.6, one can state that for the latter experiments the total damping effect and the total uplifting effect are larger. According to the damage results, the increased damping effect is more dominant than the increased uplifting effect.

When comparing the results of the experiments with a dimensionless crest freeboard of 3.8 with those at a dimensionless crest freeboard of 5.4, one can state that for the latter experiments the total damping effect and the total uplifting effect are smaller. According to the damage results, the decreased damping effect is less dominant than the decreased uplifting effect.

To better understand the effect of the waterline on the rear slope, further research should be carried out. It is recommended that such research concentrates on individual plunges on individual stones on a rubble slope.

6.6 Influence crest freeboard on damage location

During the experiments the damage per strip was recorded after every plunge. With this information the damage location was examined. In Figure 41, Figure 42 and Figure 43 the average damage per strip is presented for three crest freeboards (all for reservoir

configuration I). Just like in the other sections on damage, the data was restricted to those plunge sizes for which none of the experiments showed collapse. In these figures the width of a strip is equal to $2 \cdot D_{n50}$.

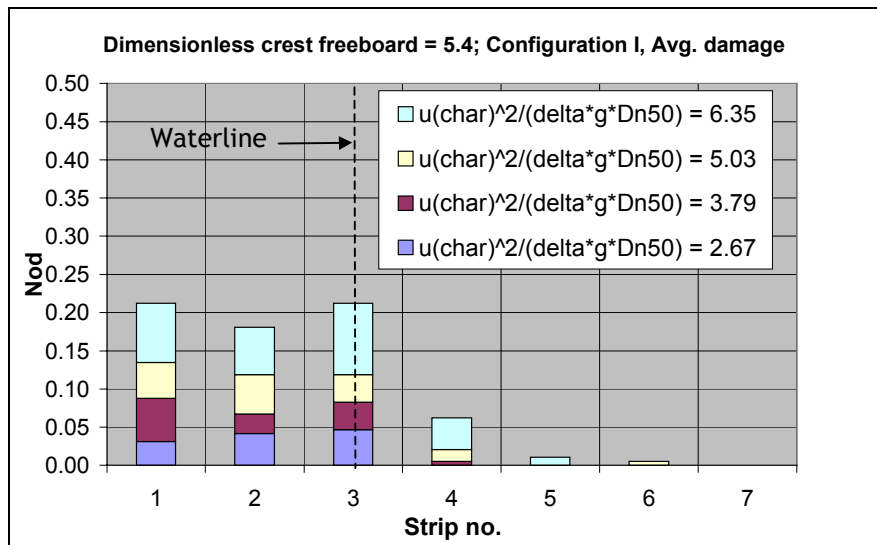


Figure 41: Damage per strip for Configuration I and crest freeboard of 10 cm

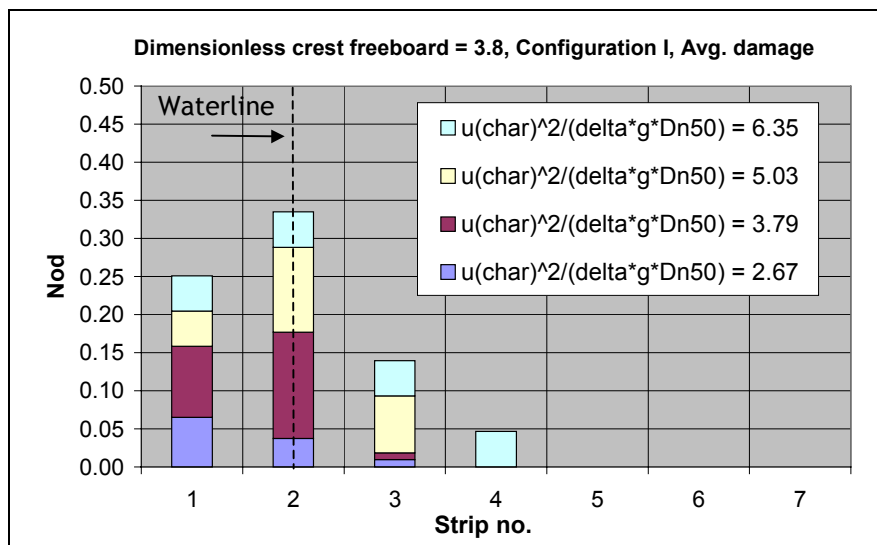


Figure 42: Damage per strip for Configuration I and crest freeboard of 7 cm

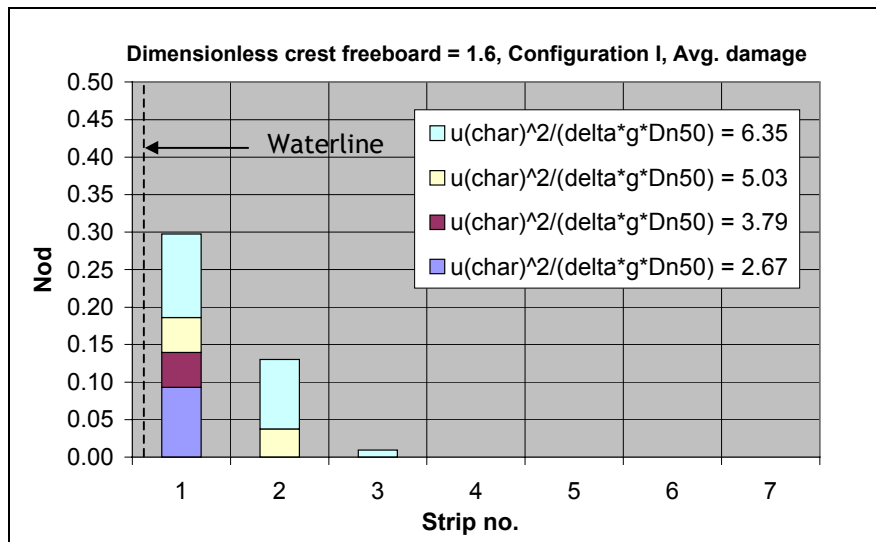


Figure 43: Damage per strip for Configuration I and crest freeboard of 3 cm

From the above figures and the observations during the experiments the following general conclusions can be drawn:

- Most damage occurred just below the waterline.
- Because of damage just below the waterline, damage above the waterline was inflicted (displaced stones around the waterline caused stones above to move).
- Beneath the water level the damage decreases to zero (at a distance more than about four stones below the water level, the damage is insignificant, for above-considered plunge sizes).

Also, differences between the results attained at the different water levels can be summed up:

- The spread in damage over the different strips is largest for a dimensionless crest freeboard of 5.4 (probably due to the large number of stones above the waterline).
- Most damage occurred at a dimensionless crest freeboard of 3.8 (probably due to the impact of the plunges around the waterline).
- The damage at a dimensionless crest freeboard of 1.6 is restricted to the first 2 strips (probably due to the damping effect of the water).

Above conclusions confirm the assumptions from section 6.5.

6.7 Influence crest freeboard on collapse behaviour

In Figure 44 the probability of collapse of the rear slope is presented for all three crest freeboards.

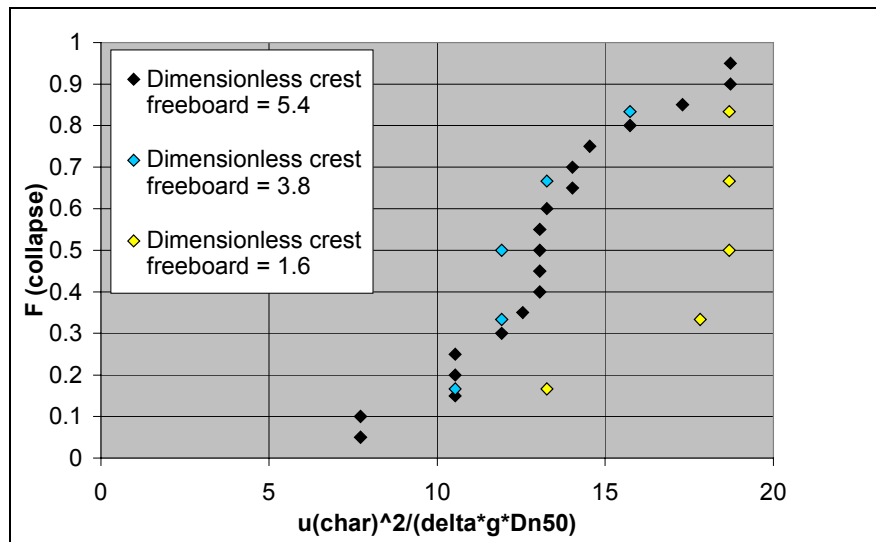


Figure 44: Comparison of collapse behaviour of three dimensionless crest freeboards

It is remarkable that, according to the measurements, the collapse behaviour of the experiments with a dimensionless crest freeboard of 3.8 is similar to the collapse behaviour of the experiments with a dimensionless crest freeboard of 5.4. This is remarkable as the damage development of the experiments with a dimensionless crest freeboard of 3.8 is more progressive than that of the experiments with a dimensionless crest freeboard of 5.4.

Also remarkable is that the probability of collapse for the experiments with a dimensionless crest freeboard of 1.6 is significantly lower than for those with the other two crest freeboards at an arbitrary value of the dimensionless characteristic velocity.

However, above considerations have to be handled with great care. Due to the limited number of experiments, especially at dimensionless crest freeboards of 1.6 and 3.8, the derived probability of collapse is highly questionable. More experiments have to be carried out to see whether the differences and the similarities in collapse behaviour exist or are accidental.

6.8 Damage due to individual plunges

In this section the damage due to individual plunges is compared with the cumulative damage development discussed in section 6.3. For this comparison Configuration I of the reservoir is used. Again, the data is restricted to the plunge size under which no collapse occurred in the experiments.

Before a comparison between the data on cumulative damage and damage due to individual plunges could be made, an adaptation to the data on cumulative damage was needed. During the experiments with individual plunges the damage was determined after each single plunge. During the experiments with cumulative plunges, the damage was determined after every three plunges of the same size. In this section, the damage of the cumulative plunges after the first of the three plunges was taken and compared with the damage due to individual plunges. The damage due to individual plunges was determined in 5.3.2. In Figure 45 the comparison is presented.

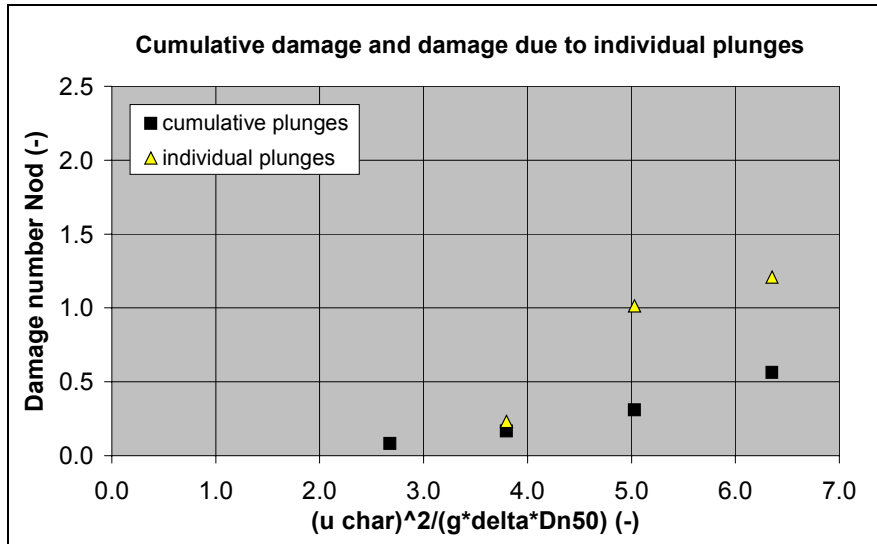


Figure 45: Comparison between cumulative damage and damage due to individual plunges

As can be concluded from Figure 45, the damage due to an individual plunge of arbitrary size is larger than the damage due to a plunge of the same size preceded by smaller plunges. It is clear that a sort of 're-arrangement' of the stones on the rear slope due to small plunges helps to increase the rear slope stability for larger plunges. The difference between cumulative damage and damage due to an individual plunge increases with increasing plunge size.

When the measurements of damage due to individual plunges are considered beyond the value of 7 for the dimensionless characteristic velocity, it seems that the damage has an exponential character (see Figure 46). However, the extra point in this figure is the average damage of three out of five experiments. The other two experiments showed collapse for this value of the plunge size. More experiments are needed to confirm the potential exponential damage character for individual plunges. Also the collapse behaviour of the rear slope due to individual plunges is an interesting field for more research.

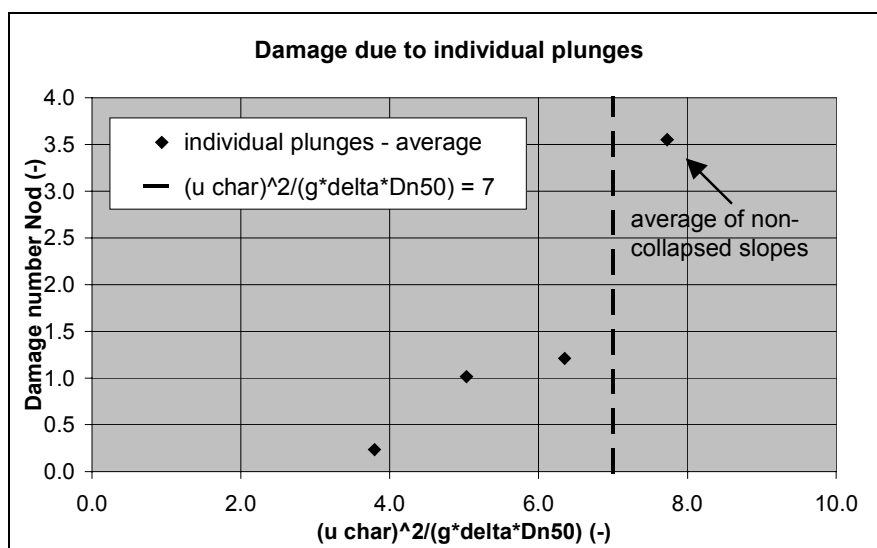


Figure 46: 'Exponential' character of damage due to individual plunges

6.9 Comparison damage results with former research

6.9.1 Introduction

From the analysis in section 6.3 it can be concluded that the rear slope stability can be expressed using the parameter $\frac{u_{char}^2}{\Delta g D_{n50}}$. For a *fixed shape of the breakwater* this stability

parameter can be rewritten into the stability parameter $\frac{H_s}{\Delta D_{n50}}$, using the equations of Van

Gent [9]. In this way the results described in this report can be verified with the results of Burger [1] who expressed the stability of the rear slope with the stability parameter

$$\frac{H_s}{\Delta D_{n50}}$$

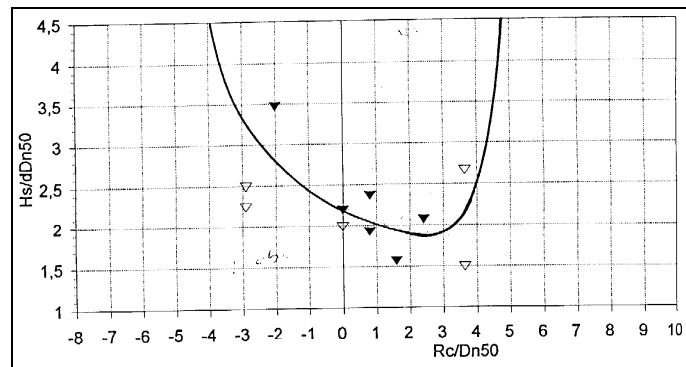


Figure 47: Burger's relation between significant wave height and rear slope stability ($S=0.5$)

It must be emphasised that the comparison of the results in this report with the results of Burger are carried out to see whether they are in the same order of magnitude. It is physically not correct to describe the rear slope stability in terms of the significant wave height alone, as the shape of the breakwater influences the overtopping velocity (as well as the wave period). The resulting graph can therefore not be seen as a design graph for the rear slope.

On the other hand, the ultimate goal of the research on rear slope stability is to find a reliable relationship between the wave parameters and the rear slope stability, taking also into account the breakwater parameters. With this in mind, in the next sections a first attempt is made to establish this relation, for a given shape of the breakwater, and this relation is compared to the findings of Burger.

6.9.2 Relation between significant wave height and overtopping velocity

One of the equations of Van Gent [9], derived for (impermeable) dikes, translates the significant wave height into the overtopping velocity, exceeded only by 2% of the incoming waves ²⁴:

$$\frac{u_{2\%}}{\sqrt{g \cdot H_s}} = c'_u (\gamma_{f-c})^{0.5} \left(\frac{z_{2\%} - R_c}{\gamma_f \cdot H_s} \right)^{0.5} \quad (48)$$

in which:

$u_{2\%}$	maximum overtopping velocity at the rear side of the crest, exceeded by 2% of the incident waves	[m/s]
g	gravitational acceleration	[m/s ²]
H_s	significant wave height	[m]
c'_u	constant (= 0.95)	[-]
γ_{f-c}	crest roughness reduction factor	[-]
γ_f	front slope roughness reduction factor	[-]
$z_{2\%}$	maximum run-up, exceeded by 2% of the incident waves	[m]
R_c	Crest freeboard	[m]

With this equation a relation between the overtopping velocity and the significant wave height can be found, for a fixed shape and roughness of the breakwater's front slope and crest. As a first approximation the characteristic velocity is taken equal to the overtopping velocity, exceeded by 2% of the incoming waves: $u_{char} = u_{2\%}$. With this assumption $\theta_{u_{char}}$, from section 6.3.4 equals:

$$\theta_{u_{char}} = \frac{u_{2\%}^2}{\Delta g D_{n50}}$$

This can be rewritten into:

$$u_{2\%} = \sqrt{\Delta g D_{n50} \cdot \theta_{u_{char}}}$$

The equation of Van Gent now becomes:

$$\frac{\sqrt{\Delta g D_{n50} \cdot \theta_{u_{char}}}}{\sqrt{g \cdot H_s}} = c'_u (\gamma_{f-c})^{0.5} \left(\frac{z_{2\%} - R_c}{\gamma_f \cdot H_s} \right)^{0.5}$$

²⁴ See Annex I.F.

or:

$$\frac{\Delta g D_{n50} \cdot \theta_{u_{char}}}{g \cdot H_s} = (c'_u)^2 (\gamma_{f-c}) \left(\frac{z_{2\%} - R_c}{\gamma_f \cdot H_s} \right)$$

or:

$$\frac{H_s}{\Delta D_{n50}} \cdot \frac{1}{\theta_{u_{char}}} = \frac{1}{(c'_u)^2 (\gamma_{f-c})} \left(\frac{\gamma_f \cdot H_s}{z_{2\%} - R_c} \right)$$

or:

$$\frac{H_s}{\Delta D_{n50}} = \left[\frac{1}{(c'_u)^2 (\gamma_{f-c})} \left(\frac{\gamma_f \cdot H_s}{z_{2\%} - R_c} \right) \right] \cdot \theta_{u_{char}}$$

The above equation represents the relation between the stability parameter $\theta_{u_{char}}$ and the stability parameter $\left(\frac{H_s}{\Delta D_{n50}} \right)$. For fixed values of $z_{2\%}$, c'_u , γ_f and γ_{f-c} , the relation between the dimensionless overtopping velocity and the stability parameter can be determined for different values of the crest freeboard R_c . This is visualised in Figure 48. The following fixed values were used in the calculation:

- $z_{2\%} = C_0 \cdot \gamma_f \cdot \xi_{s,-1} \cdot H_s$
- $C_0 = 1.35$
- $\gamma_f = 0.5$ (recommended value for rubble slope, see Pilarczyk [11])
- $\xi_{s,-1} = 3$ (arbitrary value, see Van Gent [9])
- $c'_u = 0.95$ (determined by Van Gent [9])
- $\gamma_{f-c} = 0.5$ (recommended value for rubble slope, see Pilarczyk [11])

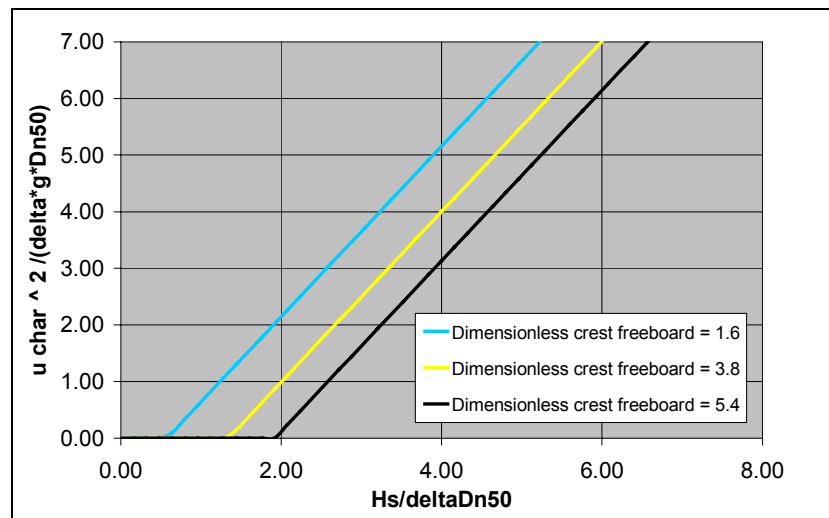


Figure 48: Relation between overtopping velocity and significant wave height for different crest freeboards

According to the equation of Van Gent a linear relation exists between $\theta_{U_{char}}$ and $\frac{H_s}{\Delta D_{n50}}$.

At an arbitrary significant wave height the overtopping velocity is larger for low crest freeboards, according to Figure 48. This seems obvious.

6.9.3 Relation between significant wave height and damage number

With Figure 48 and the results of section 6.5, for a fixed shape of front slope and crest, the rear slope damage can be expressed as a function of the stability parameter $\frac{H_s}{\Delta D_{n50}}$ for different crest freeboards. This is visualised in Figure 49.

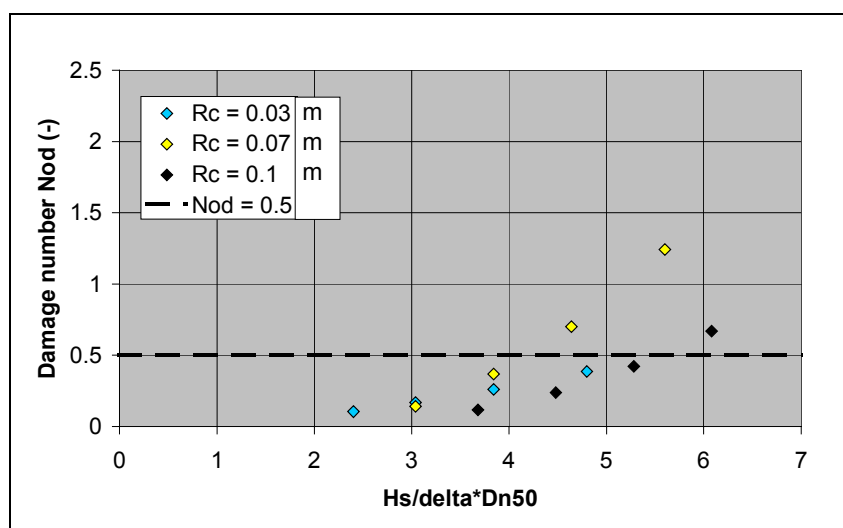


Figure 49: Dimensionless overtopping velocity vs dimensionless significant wave height

It is now possible to compare the experimental results from this report with the results of Burger. This is presented in Figure 50 for a damage level N_{od} of 0.5 (by interpolation of the graph in Figure 49).

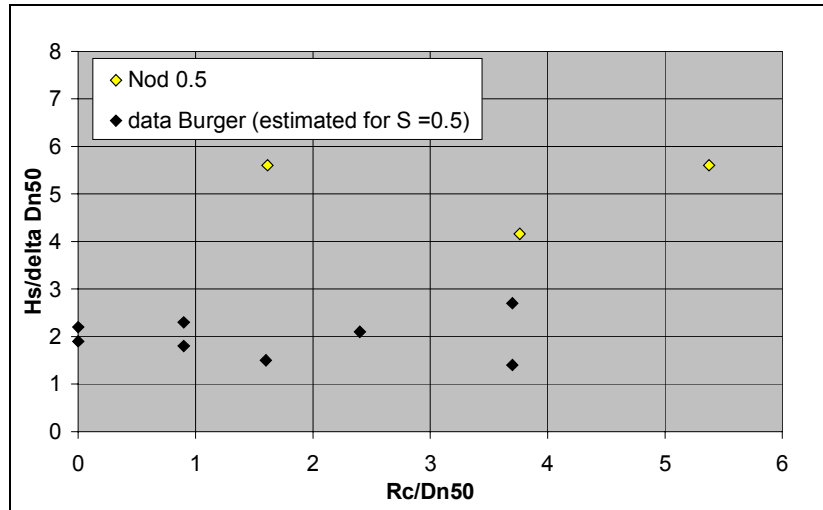


Figure 50: Comparison of experimental data with Burger's data

From Figure 50 two conclusions can be drawn:

- Quantitatively, the rear slope stability as found in the current experiments is (much) better than found by Burger
- Qualitatively, the trend of the graph is similar to the one found by Burger, with a minimum somewhere between $\frac{R_c}{D_{n50}} = 1.6$ and 5.4.

Some reasons that could explain the quantitative difference between the experiments described in this report and the research of Burger are:

- The simplification of the overtopping wave in the current experiments (Burger used random waves). In the experimental set-up some characteristics of an overtopping wave were not taken into account:
 - The inclusions of air of overtopping waves
 - The extreme turbulence of overtopping waves
 - The orbital movement of water in the overtopping wave.
- Discarding the effect of seepage in the current research.
- The sequence and number of plunges the rear slope is subjected to in the current research.
- Differences between the characteristic velocity and the overtopping velocity, exceeded by only 2% of the incoming waves, used in the formula of Van Gent.
- The equation of Van Gent that is used to translate the significant wave height into the overtopping velocity exceeded by 2% of the incident waves, may not be suitable for breakwaters.
- Burger uses the damage number S instead of the damage number N_{od} as used in the current research.

7 CONCLUSIONS / RECOMMENDATIONS

7.1 Conclusions

1. In describing the rear slope response to plunges, both the damage and the collapse behaviour should be considered.

7.1.1 Rear slope damage

2. The rear slope damage is related to the characteristic velocity of the plunge, which is defined as the quotient of the maximum instantaneous discharge of the plunge per unit width and the maximum layer thickness of the plunge.
3. The rear slope damage increases progressively with increasing plunge size.
4. The experimental set-up requires a relative high amount of repeated experiments (at least five) because of the great spread in the damage measurements (in the order of 100%). The spread increases with increasing plunge size.
5. The waterline relative to the crest influences the rear slope damage considerably. The stability is least at a dimensionless crest freeboard between 1.6 and 5.4. This is in accordance with former research on low-crested breakwaters subjected to random waves.
6. Most damage occurs just below the waterline. Due to the loss of support, stones above the waterline are moved in a later stage. Under water the damage decreases. At a distance of more than 4 times D_{n50} under water, the damage is insignificant.
7. At an arbitrary plunge size, the damage due to an individual plunge is larger than the damage due to a plunge preceded by several smaller plunges. This difference quickly increases with increasing plunge size.

7.1.2 Collapse behaviour

8. The collapse behaviour of the rear slope features a Gaussian-like curve.
9. The rear slope seems less sensitive to collapse in the case of a very low crest freeboard.

7.2 Recommendations

For future research it is recommended that:

1. The development of the plunge velocity is measured.
2. The method of measuring the layer thickness is improved.
3. A standard experiment is repeated many times (approximately a hundred times) in order to
 - better investigate the spread in the damage development
 - better investigate the collapse behaviour of the rear slope.
4. All experiments are repeated at least five times in order to obtain a minimum reliability in the results.
5. The influence of the crest freeboard on the rear slope damage is investigated with more values of the dimensionless crest freeboard. Especially the dimensionless crest freeboard for which the rear slope stability is the least is important to determine.
6. The influence of the following breakwater characteristics on the damage development and the collapse behaviour are investigated (in order of priority):
 - the rear slope angle
 - the average stone size
 - the stone shape
 - the roughness of the filter layer.
7. The influence of the following plunge characteristics on the damage development and the collapse behaviour are investigated (in order of priority):
 - the step size between two consecutive plunges
 - the number of plunges per step (only on the collapse behaviour).
8. The influence of the crest freeboard on the collapse behaviour is investigated.
9. The stability of single stones on a rubble slope is investigated.
10. The (possible) influence of the reservoir configuration on the collapse behaviour is investigated.

8 REFERENCES

- [1] Burger, G., "Stabiliteit golfbrekers met lage kruin", M.Sc. thesis, Faculty of Civil Engineering and Geosciences, Delft University of Technology, 1995
- [2] Meer, J.W. van der, "Rock slopes and gravel beaches under wave attack", Publication Delft Hydraulics no. 396, 1988
- [3] Walker, J.R., Palmer, R.Q. and Dunham, J.W., "Breakwater Back slope Stability", Proc. Civil Engineering in the Oceans, 1976
- [4] Vidal, C., Losada, M.A., Medina, R., Mansard, R., Gomez-Pina, G., "A Universal Analysis for the Stability of both Low-crested and Submerged Breakwaters", Proc. Coastal Engineering Conference, 1990
- [5] Jong de, R.J., "Wave transmission at low-crested structures, Stability of Tetrapods at Front, Crest and Rear of a low-crested Breakwater", M.Sc. thesis, Faculty of Civil Engineering and Geosciences, Delft University of Technology, 1996
- [6] Gent van, M.R.A., "Wave run-up on dikes with shallow foreshores", Proceedings ICCE, 2000
- [7] Hunt, I.A., "Design of seawalls and breakwaters, Proceedings ASCE, 85, WW3, 1959
- [8] Battjes, J.A., "Computation of set-up, longshore currents, run-up and overtopping due to wind-generated waves", Ph.D. thesis, Faculty of Civil Engineering and Geosciences, Delft University of Technology, 1974
- [9] Gent van, M.R.A., "Low-exceedence wave overtopping events", Delft Cluster report OCO30202/H3803, March 2001
- [10] Meer van der, J.W., "Wave run-up and wave overtopping at dikes and revetments", publication number 485, Delft Hydraulics, 1994
- [11] Pilarczyk, K.W., "Manual on the use of Rock in Hydraulic Engineering", CUR Report 169, 1994
- [12] Andersen, O.H., Juhl, J., Sloth, P., "Rear Side Stability of Berm Breakwaters", Proceedings ICCE, 1992
- [13] Perdijk, H.W.R., "Golfoverslag bij dijken", H181/M1258, Delft Hydraulics Laboratory, 1987
- [14] Meer, van der, J.W., "Erosiebestendigheid van gras op klei taluds", M1930, Delft Hydraulics Laboratory, 1984
- [15] Waal, de, J.P., Meer, van der, J.W., "Wave run-up and overtopping on coastal structures", Proceedings ICCE, 1994
- [16] Owen, M.W., "Design of seawalls allowing for wave overtopping", Hydraulic Research Station, Wallingford, England, 1980
- [17] Hebsgaard, H., Sloth P., Juhl, J., "Wave overtopping of rubble mound breakwaters", Proceedings ICCE, 1998
- [18] Meer, van der, J.W., Veldman, J.J., "Singular points at berm breakwaters: scale effects, rear, round head and longshore transport", Proceedings ICCE, 1992
- [19] Kobayashi, N, Kudale, M.D., "Hydraulic stability analysis of leeside slopes of overtopped breakwaters", Proceedings ICCE, 1996

ANNEX I - LITERATURE

Annex I.A Van Gent's equations for wave run-up

With the use of numerical modelling and physical model investigations, Van Gent investigated the run-up of random waves on impermeable dikes with shallow foreshores.

Due to a combination of wind waves and swell, wave energy spectra at the toe of coastal structures are often double-peaked. Next to this, a shallow foreshore may influence the wave height distribution considerably and therefore also the wave run-up. Van Gent tried to find a characteristic wave period²⁵ to be used in the Irribarren number to take the effects of wave energy spectra on the run-up into account.

Van Gent found that the wave run-up is best described with the use of another wave period than the peak period or the average wave period, namely the spectral wave period $T_{m-1,0}$. He recommends the use of the following equation for $R_{u2\%}$, for both deep water situations and situations with shallow foreshores:

$$\frac{R_{u2\%}}{(\gamma \cdot H_s)} = c_0 \cdot \xi_{s,-1} \quad \text{for } \xi_{s,-1} \leq \rho \quad (14)$$

$$\frac{R_{u2\%}}{(\gamma \cdot H_s)} = c_1 - \frac{c_2}{\xi_{s,-1}} \quad \text{for } \xi_{s,-1} \geq \rho \quad (15)$$

in which

$$\xi_{s,-1} = \frac{\tan \alpha}{\sqrt{\frac{2\pi}{g} \cdot \frac{H_s}{T_{m-1,0}^2}}} \quad \text{Irribarren parameter, using the spectral wave period} \quad [-]$$

$$T_{m-1,0} \quad \text{spectral wave period at the toe of the structure, using the spectral moments } m_{-1} \text{ and } m_0 \quad [s]$$

$$m_n = \int_0^{\infty} f^n \cdot S(f) df \quad \text{spectral moment } n \quad [s^{-n}]$$

$$\gamma = \gamma_f \cdot \gamma_\beta \quad \text{reduction factor, which takes into account the effects of friction } \gamma_f \text{ and angular wave attack } \gamma_\beta \quad [-]$$

²⁵ The wave height that is used by Van Gent in the calculations is arbitrarily set at the significant wave height

c_0, c_1	constants, depending on which characteristic wave height is applied (H_s or H_{m0}) and whether long waves are taken into account in the wave parameters.	[-]
$c_2 = \frac{1}{4} \cdot \frac{c_1^2}{c_0}$	constant	[-]
$p = \frac{1}{2} \cdot \frac{c_1}{c_2}$	constant	[-]

The equations of Van Gent are visualised in *Figure 51*.

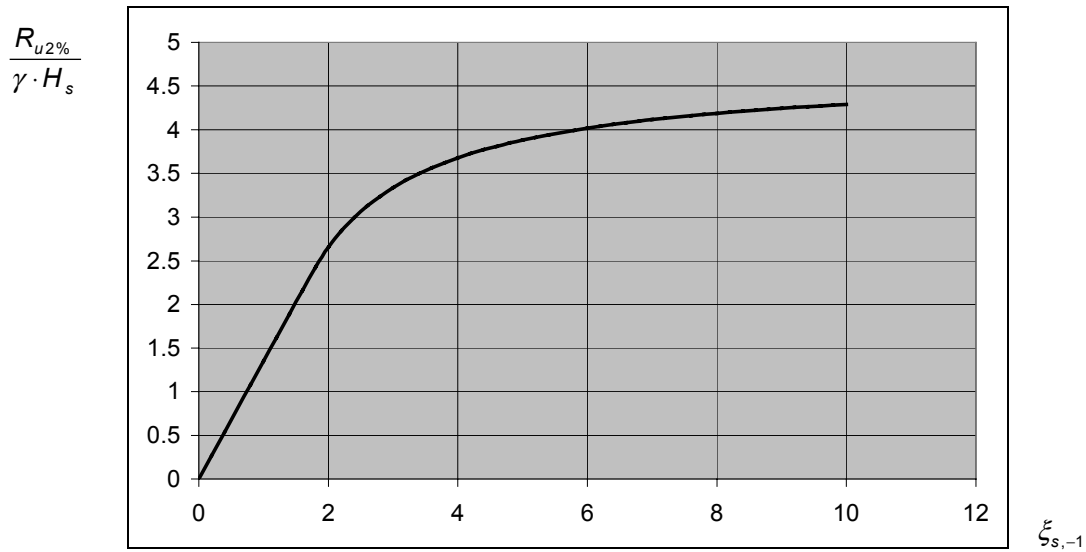


Figure 51: Wave run-up according to Van Gent

Annex I.B Periodic wave overtopping - Battjes

Battjes [8] states that the overtopping quantities can be expressed in terms of the run-up parameters. The run-up volume V_{Ru} , which is defined as the water volume above a point at a distance x from the still-water line, can be expressed as the run-up length L_{Ru} along the slope times the layer thickness d_{Ru} of the up rushing wave:

$$V_{Ru} = L_{Ru} \cdot d_{Ru} \quad (16)$$

The layer thickness as well as the run-up length is proportional to $\sqrt{HL_0}$ (for gentle slopes), which leads to the expectation that V_{Ru} is proportional to HL_0 . An analysis of data confirmed this proportionality, but makes clear that V_{Ru} is also proportional to $\sqrt{\tan \alpha}$. The normalised volume v_m^{χ} is defined by:

$$v_m^{\chi} = \frac{V_{Ru}}{HL_0 \sqrt{\tan \alpha}} \quad (17)$$

Battjes found that the normalised volume depends only on the fractional distance χ along the slope:

$$\chi = \frac{x}{L_{Ru}} \quad (18)$$

in which

x distance along the slope [m]

Experiment results showed that v_m^{χ} is roughly proportional to $(1 - \chi)^2$.

Battjes states that the overtopping volume V_{over} equals the run-up volume V_{Ru} above the crest. The overtopping volume V_{over} can therefore be normalised the same way as the run-up volume V_{Ru} :

$$\frac{V_{over}}{HL_0 \sqrt{\tan \alpha}} = b \quad (19)$$

in which

b normalised overtopping volume [-]

The normalised overtopping volume equals the normalised run-up volume at the crest. The fractional distance along the slope χ can also be expressed as the quotient of crest freeboard and run-up:

$$\chi = \frac{x}{L_{RU}} = \frac{R_c}{R_u} \quad (20)$$

Test results have shown that the normalised wave overtopping b can be expressed as follows:

$$b = 0.1 \cdot (1 - R_c)^2 \quad (21)$$

It is now possible to give the expression of the overtopping volume as function of the hydraulic and breakwater parameters:

$$V_{over} = HL_0 \cdot \sqrt{\tan \alpha} \cdot 0.1 \cdot (1 - R_c)^2 \quad (22)$$

The influence of roughness and oblique waves is not taken into account in above equation.

Annex I.C Periodic wave overtopping - Perdijk

Perdijk [13] performed physical tests to describe the overtopping parameters of periodic overtopping waves as well as random overtopping waves over dikes. In this report only Perdijk's findings on periodic overtopping waves will be discussed. Tests were performed on a smooth, gentle slope and with perpendicular wave attack. Perdijk measured the overtopping parameters (maximum layer thickness d , maximum overtopping velocity u , overtopping time τ and overtopping volume V_{over}) at only one fixed point on the dike crest.

Perdijk used mathematical expressions of previous research found by Roos and Battjes, which is not discussed in this report. Perdijk found the following expression for the overtopping volume V_{over} :

$$V_{over} = 0.075 \cdot H \cdot L_0 \cdot \frac{1}{\sqrt{\cot \alpha}} \left(1 - \frac{R_c}{R_u}\right)^{1.67} \quad (23)$$

This expression features great resemblance to the expression derived by Battjes [8]. Apart from the differences in constants only one parameter is added to the expression of Battjes, namely the run-up height R_u . This result can be seen as a confirmation of Battjes' findings.

Perdijk also derived an expression for the maximum layer thickness d , the maximum overtopping velocity u and the overtopping time τ as a function of hydraulic and breakwater parameters. Previous research stated that these (dependent) parameters can be made dimensionless as follows:

- $\frac{d}{\sqrt{HL_0}}$
- $\frac{v}{\sqrt{gH}}$
- $\frac{\tau}{T}$

Perdijk states that these parameters are determined by three dimensionless parameters:

- $\frac{x}{\sqrt{HL_0}}$ the dimensionless distance along the slope
 (for overtopping waves $x = \frac{R_c}{\sin \alpha}$ and $\frac{x}{\sqrt{HL_0}}$ can be formulated as $\frac{R_c}{R_u \cdot \cos \alpha}$).
- $\frac{H}{L_0}$ wave steepness
- α front slope angle

Perdijk found that the maximum overtopping layer thickness in dimensionless form only depends on $\frac{R_c}{R_u \cdot \cos \alpha}$. He derived the following equation for the maximum overtopping layer thickness:

$$d = 0.08 \cdot \sqrt{H \cdot L_0} \cdot \left(1 - \frac{R_c}{R_u \cdot \cos \alpha} \right) \quad (24)$$

For fixed points located low on the front slope Perdijk found that the maximum run-up velocity depends only on $\frac{H}{L_0}$ and α and therefore on the Irribarren parameter ξ . For low-crested structures this expression for the maximum run-up velocity can be used as an approximation of the maximum overtopping velocity:

$$v = 0.60 \cdot \xi \cdot \sqrt{g \cdot H} \quad (25)$$

Perdijk defined the overtopping time τ as the duration of time of water running over the crest. Using the expression of Roos and Battjes of total (fictitious) run-up time and subtracting the time needed for the wave to reach the crest yields the overtopping time. However, the time for the wave to reach the crest depends on the crest height, the wave steepness and the front slope angle. Perdijk did not investigate these dependencies thoroughly. Therefore, in this report the time for the wave to reach the crest is neglected and the expression of Roos and Battjes is used as a first approximation of the overtopping time:

$$\tau = \frac{0.7 \cdot T}{\sqrt{\xi}} \quad (26)$$

Despite the periodic waves, Perdijk found a lot of scatter around above equations.

Annex I.D Comparison avg. overtopping equations

Experimental studies into overtopping of dikes and breakwaters in the past have led to a number of empirical equations that predict the average overtopping discharge during a storm. Many of them relate a dimensionless average discharge to a dimensionless crest freeboard. Examples of these models are presented in this annex.

Owen

Owen [16] related a dimensionless discharge parameter (Q), to a dimensionless crest freeboard parameter (R) by an exponential equation of the form

$$Q = a \cdot e^{\frac{bR}{\gamma}} \quad (27)$$

in which

γ	front slope roughness	[-]	
$Q = \frac{\bar{q}}{\sqrt{gH_s^3}} \sqrt{\frac{s_{om}}{2\pi}}$	dimensionless discharge parameter	[-]	(28)

\bar{q}	average discharge	[m ³ /s]	
-----------	-------------------	---------------------	--

s_{om}	average wave steepness at deep water	[-]	
----------	--------------------------------------	-----	--

$R = \frac{R_c}{H_s} \sqrt{\frac{s_{om}}{2\pi}}$	dimensionless crest freeboard parameter	[-]	(29)
--	---	-----	------

a	dimensionless parameter	[-]	
-----	-------------------------	-----	--

b	dimensionless parameter	[-]	
-----	-------------------------	-----	--

The values for the coefficients a and b were derived from test results and depend on the steepness of the front side slope. Important to notice is that Owen only studied smooth slopes, for which γ equals 1.

De Waal and Van der Meer

De Waal and Van der Meer [15] made a distinction between overtopping due to breaking waves and overtopping due to non-breaking waves. De Waal and Van der Meer used the same form of the equation of Owen and found:

$$Q_b = 0.06 \cdot e^{-5.2R_b} \quad (30)$$

$$Q_n = 0.2 \cdot e^{-2.6R_n} \quad (31)$$

in which:

$Q_b = \frac{\bar{q}}{\sqrt{gH_s^3}} \sqrt{\frac{s_{op}}{\tan \alpha}}$	dimensionless discharge parameter breaking waves	[-]	(32)
---	--	-----	------

$Q_n = \frac{\bar{q}}{\sqrt{gH_s^3}}$	dimensionless discharge parameter non-breaking waves	[-]	(33)
---------------------------------------	--	-----	------

$$s_{op} \quad \text{wave steepness at deep water using the peak period} \quad [-]$$

$$R_b = \frac{R_c}{H_s} \frac{\sqrt{s_{op}}}{\tan \alpha} \frac{1}{\gamma} \quad \text{dimensionless crest freeboard parameter breaking waves} \quad [-] \quad (34)$$

$$R_n = \frac{R_c}{H_s} \frac{1}{\gamma} \quad \text{dimensionless crest freeboard parameter non-breaking waves} \quad (35)$$

As can be concluded from above, De Waal and Van der Meer used other dimensionless parameters than Owen.

The total reduction factor γ is equal to:

$$\gamma = \gamma_b \gamma_f \gamma_\beta \quad (36)$$

in which:

$\gamma_b =$ reduction factor accounting for the influence of a berm on front side slope

$\gamma_f =$ reduction factor accounting for the influence of a rough front side slope

$\gamma_\beta =$ reduction factor accounting for the influence of oblique wave attack

Both the equation of Owen and the equations of De Waal and Van der Meer were derived for dike design. As dikes are usually relatively higher than breakwaters, it could be questioned whether these equations can be used in breakwater design.

Bradbury et al

Bradbury et al investigated the overtopping performance of rock armoured sea walls without crown walls. The following empirical equation was derived:

$$Q = a \cdot R^b \quad (37)$$

in which:

$$Q = \frac{\bar{q}}{\sqrt{gH_s^3}} \sqrt{\frac{s_{om}}{2\pi}} \quad \text{dimensionless discharge parameter} \quad [-] \quad (38)$$

$$R = \frac{R_c^2}{H_s^2} \sqrt{\frac{s_{om}}{2\pi}} \quad \text{dimensionless crest freeboard parameter} \quad [-] \quad (39)$$

a dimensionless parameter [-]

b dimensionless parameter [-]

Values of a and b have been calculated from the results of tests with the steepness of the front slope at 1:2 and with two different crest details.

Hebsgaard, Sloth and Juhl

Hebsgaard, Sloth and Juhl (referred to as 'Hebsgaard et al') [17] have carried out a series of model tests with the aim of studying overtopping discharges of rubble mound breakwaters. The dimensionless crest height was chosen between 0.45 and 2. Hebsgaard et al used the following parameter to describe the influence of the geometry of the profile:

$$C = \left(\frac{1}{\tan \alpha} \right)^{0.3} (2R_c + 0.35 \cdot B_c) \quad (40)$$

Subsequently, they derived the following expression for the dimensionless overtopping discharge:

$$Q = k_1 \cdot \ln(s_{op}) \cdot e^{\left(\frac{k_2 \cdot C}{\gamma \cdot H_s} \right)} \quad (41)$$

in which $k_1 = -0.3$ and $k_2 = -2.9$; the roughness factor $\gamma = 0.55$.

The actual overtopping discharge equals:

$$q = Q \cdot \sqrt{g} \cdot H_s^3 \quad (42)$$

Comparison overtopping equations

The choice of the most promising overtopping equation is based on a comparison between the four equations. As all of the equations have different appearances, it is hard to compare them. Van der Meer uses the peak wave steepness, while the others use the average wave steepness. Furthermore, Bradbury only conducted experiments for $\tan \alpha = \frac{1}{2}$ and Hebsgaard et al assumes that the width of the breakwater crest influences the average overtopping discharge. Finally, Owen and Bradbury et al both use parameters a and b , but with different meanings. Nevertheless it is tried to compare the four equations. The numerical values of the different variables used in the comparison are given in *Table 9*. All of the equations are taken a closer look at.

Table 9: Variables used in the comparison

	Owen	De Waal / Van der Meer	Bradbury et al	Hebsgaard et al
g [m ² /s]	9.81	9.81	9.81	9.81
π	3.1415	3.1415	3.1415	3.1415
T_m [s]	10	-	10	10
T_p [s]	-	$10 * 1.15 = 11.5$	-	-
H_s [m]	8	8	8	8
L_m [m]	156	-	156	156
L_p [m]	-	$156 * 1.15^2 = 206$	-	-
s_{om} [-]	$8 / 156 = 0.05$	-	0.05	0.05
s_{op} [-]	-	$8 / 206 = 0.04$	-	-
$\tan \alpha$ [-]	0.5	0.5	0.5	0.5
γ	0.55	0.55	-	0.55
a	0.0125	-	$1 * e^{-9}$	-
b	22.06	-	3	-
B_c	-	-	-	12

De Waal and van der Meer used Owen’s data to formulate their equations. Owen’s equation is only validated on smooth surfaces ($\gamma = 1$). For these two reasons the equation of Owen is not discussed: it is assumed that the equation of De Waal and Van der Meer can be seen as the ‘improved’ equation of Owen.

De Waal and Van der Meer validated their equations for a relative crest freeboard $R > 0.5$. For smaller values of R the average overtopping discharge rapidly increases.

The overtopping discharge calculated with the equation of Bradbury et al produces fairly high values in the range of $0 < R < 0.25$, and even becomes infinite at $R = 0$. This is highly unlikely. For $R > 0.5$, the overtopping discharges according to Bradbury et al are low compared to De Waal and Van der Meer.

Three remarks on the equation of Bradbury should be mentioned. Firstly, only experiments were executed with $\tan \alpha = 0.5$. The equation is not validated for other angles of the front slope.

Secondly, the constant b in the equation is doubtful. The average overtopping discharge is very sensitive to changes in the value of b . According to Bradbury et al, the value of b lies between 3.0 and 3.8. The average overtopping discharge calculated with $b = 3.8$ is 16 times the calculated average overtopping discharge with $b = 3.0$ ($R = 0.5$; $H_s = 8$ m ; $s_{op} = 5\%$). It is not clear what value for b should be used in calculations.

Finally, the equation produces high values of overtopping discharge for waves with a low steepness. The overtopping discharge for waves with an average steepness of 1% reaches $1.8 \text{ m}^3/\text{ms}$ (b equal to 3). This is more than 25 times the calculated overtopping discharge with waves with an average wave steepness of 5%.

When it is assumed that the wave steepness does not become less than 2%, the maximum average overtopping discharge is in the order of $0.5 \text{ m}^3/\text{ms}$ according to Bradbury et al, for $R > 0.5$. For waves with a lower steepness, or a lower crest height, the equation of Bradbury et al seems unreliable.

In the equation of Hebsgaard et al a parameter C describes the influence of the geometry of the profile. This parameter contains the width B_c of the breakwater crest, a variable that is not used in the other equations. In the comparison the crest width is arbitrarily taken equal to 12 m. According to Hebsgaard et al a larger crest width reduces the average overtopping discharge. A smaller crest width increases the average overtopping discharge.

Comparison of equations - Conclusions

In *Figure 52* the above-mentioned equations are compared to each other. It can be concluded that the average overtopping discharge calculated by the four different equations differ a lot for the 'same' situation. The average overtopping discharge according to Van der Meer is 35 times the average overtopping discharge according to Bradbury et al for $R = 0.5$ and $H_s = 8 \text{ m}$). None of the equations are validated for $0 < R < 0.5$. Therefore, the values in this region could be questioned.

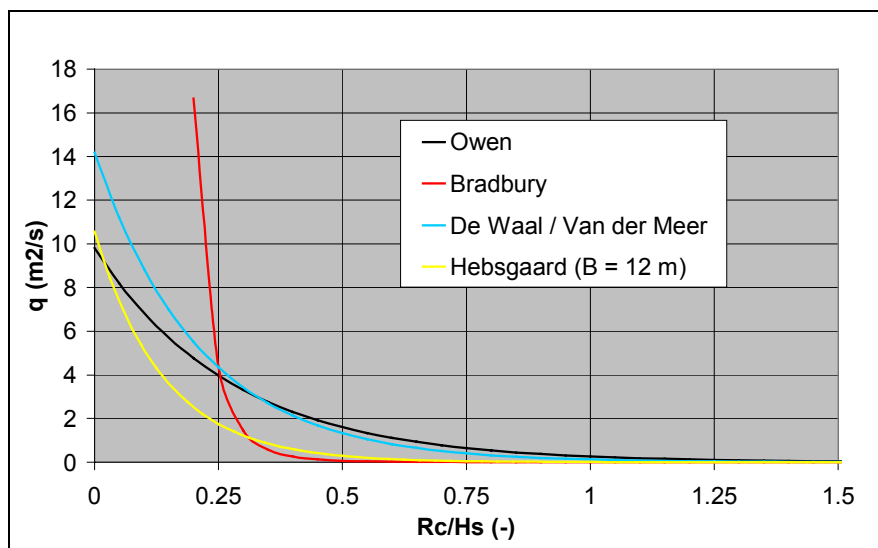


Figure 52: Comparison of equations that predict overtopping ($H_s = 8 \text{ m}$)

The field of interest in this report is low-crested breakwaters with a crest freeboard lower than 1.5 times the significant wave. It is unclear to the author which equation is the most appropriate for this subject. Therefore, it is decided not to use any of these equations. Besides this it should be questioned whether it is the right approach to describe the rear slope stability using the average discharge. It is more likely that the (largest) momentary values of overtopping volumes or overtopping velocities determine the rear slope stability of low-crested breakwaters.

Annex I.E Distribution of overtopping waves

Van der Meer [10] states that the average discharge can be used to compute the probability distribution function of the overtopping volumes per wave. The probability distribution function follows the Weibull distribution with a form factor of 0.75 and a scale factor 'a' depending on the average overtopping discharge per wave and the overtopping probability. The probability distribution function is given by:

$$R_V = P(\underline{V} < V) = 1 - \exp\left(-\left(\frac{V}{a}\right)^{0.75}\right) \quad (43)$$

in which:

R_V	Probability of the overtopping volume per wave \underline{V} being less than or similar to V	[-]
V	Overtopping volume per wave	[m ³ /m]
$a = 0.84 \cdot \frac{T_m \cdot q}{P_{ow}}$	Scale factor	[m ³]
T_m	Average wave period	[s]
q	Average overtopping discharge	[m ³ /ms]
$P_{ow} = \frac{N_{ow}}{N_w}$	Probability of overtopping per wave	[-]
N_{ow}	Number of overtopping waves	[-]
N_w	Number of incoming waves	[-]

The probability of overtopping can be computed by:

$$P_{ow} = \exp\left(-\left(\frac{R_c}{c \cdot H_s}\right)^2\right) \quad (44)$$

This is in fact the Rayleigh distribution as is also observed for wave heights. It is assumed that the probability of overtopping has the same form. The coefficient c can be seen as the run-up height divided by H_s and is therefore expressed in the same way as $R_{u2\%}$:

$$c = 0.81 \cdot \gamma_h \cdot \gamma_f \cdot \gamma_\beta \cdot \zeta_{eq} \quad \text{with a maximum of} \quad c = 1.62 \cdot \gamma_h \cdot \gamma_f \cdot \gamma_\beta \quad (45)$$

The probability of overtopping is therefore completely determined by the quotient of the crest freeboard R_c and the run-up height $R_{u2\%}$. Other authors also use this expression.

Annex I.F Wave overtopping - Van Gent

Van Gent [9] investigated the overtopping of random waves with the use of a numerical model and existing physical model tests. These tests were performed with impermeable slopes. Instead of concentrating on finding an expression for the average value of the overtopping discharge, like was done by previous authors (see 3.4.2.2), Van Gent tried to provide more information on individual wave overtopping events. In order to describe an overtopping wave, Van Gent considered four parameters. It is assumed that these parameters characterise an overtopping wave. The parameters can be summed up as follows:

- $d_{2\%}$ maximum layer thickness of overtopping volume at the rear side of the crest ²⁶, exceeded by 2% of the incident waves [m]
- $u_{2\%}$ maximum overtopping velocity at the rear side of the crest, exceeded by 2% of the incident waves [m/s]
- $q_{2\%}$ maximum overtopping discharge at the rear side of the crest, exceeded by 2% of the incident waves [m^3/ms]
- $V_{2\%}$ overtopping volume exceeded by 2% of the incident waves [m^3/m]

These overtopping parameters are made non-dimensional using the significant wave height H_s and the gravitational acceleration g :

- $\frac{h_{2\%}}{H_s}$
- $\frac{u_{2\%}}{\sqrt{g \cdot H_s}}$
- $\frac{q_{2\%}}{\sqrt{g \cdot H_s^3}}$
- $\frac{V_{2\%}}{H_s^2}$

Van Gent related above-mentioned non-dimensional overtopping parameters to three breakwater parameters:

- The crest level R_c
- The crest width B_c
- The reduction factor because of crest roughness $\gamma_{f,c}$

The crest level R_c relative to the fictitious wave run-up $R_{u2\%}$ ²⁷ was taken as a measure to predict overtopping. It was assumed that the overtopping volume of water behaves

²⁶ As Van Gent performed his research for wave overtopping of sea dikes he uses the expression 'land side' instead of 'rear side'. Although the appearance of a breakwater is different from dikes, it is assumed that the rather generic equations of Van Gent also apply for low-crested breakwaters.

according to Bernoulli's equation. With this assumption the height difference between $R_{u2\%}$ and R_c can be expressed in terms of layer thickness $d_{2\%}$ and overtopping velocity $u_{2\%}$ as follows²⁸:

$$R_{u2\%} - R_c = d_{2\%} + \frac{(u_{2\%})^2}{2g} \quad (46)$$

The height difference ($R_{u2\%} - R_c$) was made non-dimensional using the significant wave height H_s . Furthermore, the roughness factor of the front slope γ_f occurs in the equations. This is necessary as in the computation of the fictitious run-up $R_{u2\%}$ it is assumed that the crest freeboard is high enough to prevent overtopping. If the fictitious run-up $R_{u2\%}$ is higher than the crest freeboard, the roughness of the front slope γ_f is only affective up to the crest freeboard and not up to the fictitious run-up $R_{u2\%}$. Therefore, the effect of roughness above the crest freeboard ($R_{u2\%} - R_c$) needs to be corrected for. This results in the following 'crest freeboard parameter' to be accounted for in the equations:

$$c \cdot \left(\frac{R_{u2\%} - R_c}{\gamma_f \cdot H_s} \right)^n$$

For every overtopping parameter the value of c and n is calculated. It

was found that the overtopping volume $V_{2\%}$ was most sensitive to changes in the crest freeboard, as for this parameter the value of n was determined at 2.

The crest width B_c is much less influential than the crest freeboard. The maximum overtopping volume $V_{2\%}$ and the maximum overtopping velocity $u_{2\%}$ are not influenced at all. This seems reasonable for the overtopping volume $V_{2\%}$, as it is assumed that the motion on the crest is supercritical. This implicates that all water reaching the crest also overtops the crest, no matter how long the crest extends. It is less reasonable that the crest width does not influence the maximum overtopping velocity, as a longer crest implicates more resistance and therefore deceleration of the overtopping wave. However, this was not observed by Van Gent. The influence of the crest width on the maximum layer thickness $d_{2\%}$ and the maximum discharge $q_{2\%}$ is very small. Only for large crest widths, in the order of 10 m, the influence becomes significant. This is probably due to the limitation to non-permeable structures. For permeable breakwaters, the influence of the crest width could be considerable higher. Van Gent made the crest width B_c non-dimensional by dividing it with the significant wave height H_s . This results in the following 'crest width parameter'

to be accounted for in the equations: $\frac{c_1}{\left(c_2 + \frac{B_c}{H_s} \right)}$.

An increased crest roughness (and therefore a *decreased* reduction factor γ_{f-c}) reduces the maximum overtopping velocities $u_{2\%}$, the maximum overtopping discharge $q_{2\%}$ and the maximum overtopping volume $V_{2\%}$. No influence was found on the maximum overtopping

²⁷ $R_{u2\%}$ is calculated with the equation of Van Gent (see Annex I.A)

²⁸ This approach was also followed by Andersen [12] and others.

layer thickness $d_{2\%}$. This results in the following ‘crest roughness parameter’ to be accounted for in the equations: $c(\gamma_{f-c})^n$.

Combining above influences on the overtopping parameters leads to the following equations:

$$\frac{d_{2\%}}{H_s} = c_d' \cdot \left(\frac{z_{2\%} - R_c}{\gamma_f \cdot H_s} \right) \cdot \left(c_d'' + \frac{B_c}{H_s} \right)^{-1} \quad (47)$$

$$\frac{u_{2\%}}{\sqrt{g \cdot H_s}} = c_u' \cdot (\gamma_{f-c})^{0.5} \cdot \left(\frac{z_{2\%} - R_c}{\gamma_f \cdot H_s} \right)^{0.5} \quad (48)$$

$$\frac{q_{2\%}}{\sqrt{g \cdot H_s^3}} = c_q' \cdot (\gamma_{f-c})^{0.5} \cdot \left(\frac{z_{2\%} - R_c}{\gamma_f \cdot H_s} \right)^{1.5} \cdot \left(c_q'' + \frac{B_c}{H_s} \right)^{-1} \quad (49)$$

$$\frac{V_{2\%}}{H_s^2} = c_v' \cdot (\gamma_{f-c})^{0.5} \cdot \left(\frac{z_{2\%} - R_c}{\gamma_f \cdot H_s} \right)^2 \quad (50)$$

in which

Parameter	c'	c''	σ (standard deviation)
$d_{2\%}$	2.7	10	0.026
$u_{2\%}$	0.95	-	0.086
$q_{2\%}$	2.3	10	0.046
$V_{2\%}$	0.8	-	0.417

Van Gent also produces equations for the layer thickness and the overtopping velocity at the rear slope. In these equations Van Gent assumes stationary flow and uses the one-dimensional shallow-water equations to express the development of the layer thickness and the velocity. No physical model tests are yet performed to validate these assumptions of quasi-steady flow. Numerical model tests with unsteady flow however showed good resemblance.

Annex I.G Rear slope stability - Walker

Walker [3] investigated the rear slope stability of low-crested breakwaters subjected to periodic overtopping waves. Walker was motivated by preceding model studies on low-crested breakwaters which showed that in some cases failure of the rear slope occurred prior to failure of the front slope. In these tests the stone size on front slope and rear slope were taken equal. Next to this “underdesign” of the rear slope stone size, Walker considered the risk of “overdesign” of the rear slope. In both cases the economic optimum is not reached.

Walker realised that the stability of the rear slope is determined by other hydraulic processes than the stability of the front slope. Therefore, other means of failure of the rear slope must be looked upon. He distinguished three different failure mechanisms for the rear slope:

- Failure due to pore pressures caused by waves impinging on the front slope and crest
- Failure due to jet impingement on rear slope toe protection (only in shallow water)
- Failure due to jet impingement on rear slope

Walker performed several tests in which he varied two dimensionless parameters:

- $\frac{R_c}{H}$ (crest freeboard divided by the wave height)
- $\frac{W_f}{W_b}$ (front slope stone weight divided by the rear slope stone weight)

The structure was characterised as ‘failed’ if after 6 hours of wave attack more than 5 percent of the stones was displaced. Some other model and prototype measurements were added to his test results. In Figure 53 Walker’s results are plotted.

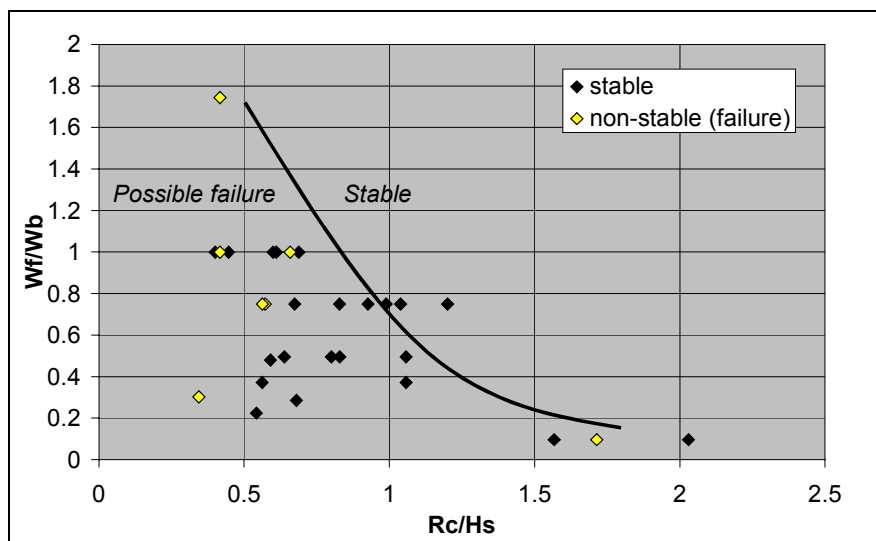


Figure 53: Rear slope stability results of Walker

According to Walker, the data appear to indicate that when $\frac{R_c}{H}$ exceeds approximately 0.7, the armour units on the rear slope may be reduced relative to those on the front slope.

When $\frac{R_c}{H}$ is less than 0.7, larger units or better placement may be required on the rear slope. When $\frac{R_c}{H}$ exceeds approximately 1.5, only minor protection may be required on the rear slope. Walker realised that far more variables play a role in the stability of the rear slope. He therefore emphasises that this relation should only be used as a first approximation in rear slope design.

Walker also discussed some measures to increase the rear slope stability:

- Strengthening of the rear slope (larger stones, better placement etc.)
- Increasing the crest width in order to reduce the pore pressures on rear slope
- Steepening the rear slope

Strengthening of the rear slope seems the most obvious measure. Failure of the rear slope due to high pore pressures is outside the scope of this report. Therefore, only the last measure will be further discussed. In contrary to the front slope, the rear slope stability is increased when its slope is steepened. This is explained by the interaction of the overtopping wave, which has a greater area on which to impinge on a flatter rear slope.

Some of Walker's conclusions can be summed up as follows:

- The rear slope of low-crested breakwaters may be subjected to more damage than the front slope
- More research on rear slope design may lead to more economic breakwater designs in the future
- The design wave for the rear slope is not necessarily equal to the design wave for the front slope
- Waves that have the highest rate of overtopping and break just at the structure appear to damage the rear slope more severely.

Interesting detail is the lack of information about the wave period used in the different tests. Walker probably didn't think this parameter would have much effect. This could be one of the causes of the experienced scatter in Walker's test results.

Annex I.H Rear slope stability - Vidal

Vidal investigated the front slope, crest and rear slope of detached rubble mound breakwaters using a three-dimensional physical model and a random wave field. Vidal tried to prove that the different sections of the breakwater trunk have a very diverse stability response to sea state conditions. He therefore divided the breakwater up into four different sections:

- Front slope
- Rear slope
- Crest
- Total slope

In his tests the stone size of the front slope, the crest and the rear slope were taken equal.

Vidal supposed that the damage level (S) of all four sections depends on two dimensionless parameters:

- $N_s = \frac{H_s}{\Delta \cdot D_{n50}}$ stability parameter
- $R_d = \frac{R_c}{D_{n50}}$ crest freeboard parameter

in which

N_s	the stability number	[-]
H_s	the significant wave height	[m]
$\Delta = \frac{\rho_s - \rho_w}{\rho_w}$	Relative buoyant density of the stones	[-]
ρ_s	stone density	[kg/m ³]
ρ_w	density of water	[kg/m ³]
D_{n50}	nominal stone diameter	[m]
R_d	the dimensionless freeboard, relative to stone size	[-]
R_c	the crest freeboard	[m]

The damage level was determined by counting the displaced stones and by taking a profile measurement before and after the one-hour tests. After each test run the breakwater was rebuilt.

The results can be summarised as follows:

- The front slope stability is minimal for non-overtopped breakwaters
- The front slope stability increases when the crest is lowered
- The crest stability is at its minimum slightly below the zero freeboard
- The crest stability decreases when the crest is lowered for low-crested structures (positive freeboard)
- The rear slope stability was much higher than the crest stability and front slope stability
- The damage on the rear slope is concentrated on smaller areas than on front slope and crest
- The rear slope stability increases when the crest is lowered

Annex I.1 Rear slope stability - Van der Meer

Among other things, Van der Meer [2] investigated the stability of low-crested breakwaters subjected to random waves. He performed several physical tests in which the stone size of the front slope, the crest and the rear slope was taken equal. Van der Meer investigated the influence of the crest freeboard R_c , the significant wave height H_s , the peak period T_p and the number of waves N on the stability of the front slope, the crest and the rear slope. In this report only Van der Meer's findings on the rear slope are discussed.

Van der Meer's main purpose was to establish a reduction factor for the front slope's stability equation. Consequently, the data on the rear slope stability was quite limited. However, some conclusions can be drawn after studying the test results of Van der Meer.

First, it was found that the rear slope stability is least for a dimensionless crest freeboard $\frac{R_c}{H_s}$ of 0.8. For $\frac{R_c}{H_s} < 0.8$, the rear slope stability increases and for $\frac{R_c}{H_s} < -0.5$ hardly any damage was reported. For $\frac{R_c}{H_s} > 0.8$ the rear slope stability increases and for $\frac{R_c}{H_s} > 1.5$ hardly any damage was reported. The number of waves has only a minor influence on the rear slope stability. It was furthermore observed that a longer peak period T_p causes more damage, probably due to more overtopping.

Van der Meer concluded that for most low-crested breakwaters the front slope stability was normative for the total stability. Only for negative freeboards and a large damage number, the crest stability is normative. The rear slope stability was never normative for the total breakwater stability.

Annex I.J Rear slope stability - De Jong

De Jong analysed data from physical model tests performed by Delft Hydraulics on the stability of tetrapods at low-crested structures (H2061). Some of the parameters that were investigated can be summed up as follows:

- R_c the crest freeboard
- H_s significant wave height
- h the water level
- T_m average wave period
- N number of waves

In all tests, the size of the tetrapods on the rear slope were taken equal to the tetrapods on the front slope and on the crest.

Among other things, De Jong investigated the influence of the relative crest freeboard $\frac{R_c}{H_s}$, the influence of the peak period T_p and the influence of the storm duration N on the armour layer stability. He developed stability equations for the front slope, crest and rear slope. In this report only the findings concerning the rear slope are considered.

According to De Jong, the rear slope is most stable for negative relative freeboards. In other words: the rear slope is most stable when the crest is below the SWL. In this situation the rear slope is protected from the overtopping waves by the tailwater. The rear slope stability decreased when the relative crest freeboard was increased. For $\frac{R_c}{H_s} = 0$ the rear slope showed hardly any damage, but for larger values of $\frac{R_c}{H_s}$ the damage quickly increased. The maximum damage occurred at $\frac{R_c}{H_s} = 0.75$. For even higher crest freeboards, the damage decreased again and for $\frac{R_c}{H_s} > 1.75$ hardly any damage occurred. For this situation few waves overtop the breakwater, which results in only little wave attack on the rear slope.

De Jong investigated the influence of the wave period using the average wave steepness s_{om} . It was found that a decreasing s_{om} leads to an increasing damage number N_{od} . This can be explained by the fact that a decreasing wave steepness could lead to both a higher percentage of overtopping waves and to larger overtopping waves.

The influence of the storm duration is quite clear according to De Jong. A longer storm duration causes more damage to front slope, crest and rear slope. It is unclear however, if this increase in damage is induced by more overtopping waves, or by larger overtopping waves.

According to the tests analysed by De Jong, the rear slope was never the normative segment. In other words: damage started always on the front slope and the crest. For a crest freeboard below or at SWL, the stability of the crest was normative for the breakwater stability. For higher crests, the front slope stability became normative. This implies that the tetrapods on the rear slope could have been taken smaller in these tests. The rear slope was 'overdesigned'.

De Jong derived a equation which describes the rear slope stability. In this equation the same stability number for the rear slope is used as the stability number for the front slope

derived by Van der Meer: $N = \frac{H_s}{\Delta D_{n50}}$. De Jong states that this stability parameter depends

on the average wave steepness, the rear slope damage, the number of incident waves, the placing density and the quotient of crest height and nominal stone size.

Annex I.K Rear slope stability - Andersen

Andersen, Juhl and Sloth investigated the rear slope stability of berm breakwaters subjected to random waves. They performed several model tests, varying three wave parameters and four breakwater parameters:

▪	h	water depth at the toe	[m]	}	Wave parameters
▪	H_{m0}	average wave height at deep water	[m]		
▪	T_{02}	wave period	[s]		
▪	B_c	crest width	[m]	}	Breakwater parameters
▪	R_c	crest freeboard	[m]		
▪	B_b	berm width	[m]		
▪	R_b	berm height	[m]		

All other parameters were taken constant: the armour stone size ($D_{n50} = 0.034$ m), the armour stone grading ($\frac{D_{n85}}{D_{n15}} = 1.35$), the relative density ($\Delta = 1.68$), the armour layer thickness ($2 \cdot D_{n50}$), the stone size of the core ($D_{50} = 0.011$ m) and the wave steepness ($s_{02} = \frac{2\pi H_{m0}}{g T_{02}^2} = 0.030$ and 0.044).

Andersen defined the rear slope damage as a settlement of the rear slope armour layer, which in some cases was followed by exposure of the core. A typical damage development started with displacement of a few stones just above still water level, followed by a settlement of the rear slope armour layer after some severe wave overtoppings. Sometimes, rear slope damage was observed prior to front slope damage.

Andersen assumes that the velocity of the overtopping water is the governing factor in determining the rear slope stability. The velocity at the crest u_c is taken as a reference velocity. Andersen further assumed that u_c can be calculated using the Bernoulli equation for stationary water movement, in which the height difference between the fictitious run-up and the crest level determines the overtopping velocity u_c . A similar approach was followed by Van Gent [9].

In this way, the overtopping velocity can be expressed as follows:

$$u_c^2 = 2g \cdot (R_{u2\%} - R_c) \tag{51}$$

Andersen expresses the stability of a single stone at still water level by a force balance parallel to the rear slope, see Figure 54.

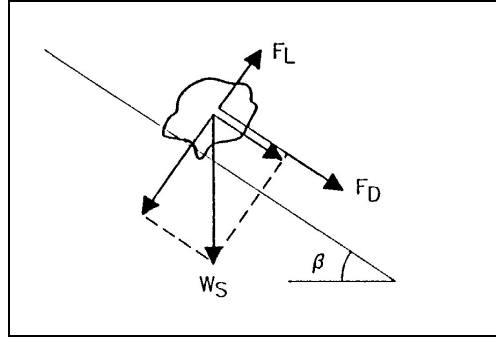


Figure 54: Forces acting on a single stone, according to Andersen

Stability is assured when

$$F_D + \mu \cdot F_L < W_s (\mu \cos \beta - \sin \beta) \quad (52)$$

in which

F_D	drag force
F_L	lift force
$\mu = \tan \phi$	friction factor
ϕ	natural angle of repose
$W_s = \Delta \rho g \cdot D_{n50}^2$	submerged weight
β	rear slope angle

The wave force can be expressed as follows:

$$F_D + \mu \cdot F_L = (C_D + \mu \cdot C_L) \frac{1}{2} \rho \cdot u_c^2 \cdot D_{n50}^2 \quad (53)$$

while the fictitious run-up $R_{u2\%}$ is expressed as a function of the Iribarren parameter:

$$R_{u2\%} = \xi_{02} \cdot H_{mo} = \frac{\tan \alpha}{\sqrt{s_{02}}} \cdot H_{mo} \quad (54)$$

Combining above equations and made dimensionless by dividing it by $\frac{H_{mo}}{\sqrt{s_{02}}}$ gives:

$$\frac{R_c}{H_{mo}} \sqrt{s_{02}} > \tan \alpha - \left(\frac{H_{mo}}{\Delta D_{n50}} - \frac{1}{\sqrt{s_{02}}} \right)^{-1} \frac{\mu \cos \beta - \sin \beta}{C_D + \mu C_L} \quad (55)$$

A fairly good agreement between the measurements and the stability expression was obtained.

From the above equation Andersen concludes that the rear slope stability depends on the crest freeboard relative to the average wave height, the wave steepness, the front slope angle, the rear slope angle, the stone size and the stone density. The friction between the stones is included in the friction factor μ and the drag and lift forces are represented by the factors C_d (drag) and C_L (lift). In the tests it was observed that the crest width B_c did not influence the stability. More research on this parameter is currently taking place.

Andersen states that the rear slope stability can be increased in several ways:

- increase of the crest freeboard
- increase of the stone diameter
- increase of relative density
- decrease of rear slope angle

The last statement is completely the opposite of Walker's [3] conclusions. However, it should be noted that in Andersen's tests, the stone diameter as well as the relative density and the rear slope angle were kept constant. Therefore, statements about these parameters could be questioned.

Annex I.L Rear slope stability - Kobayashi

Kobayashi [19] investigated the rear slope stability using numerical model tests, calibrated with physical tests performed by Vidal [4]. Kobayashi used a numerical flow model that predicts the flow characteristics on rough slopes. This numerical model was extended to predict the overtopping velocity and layer thickness on the crest. The velocity and layer thickness of the overtopping jet ²⁹ at the landward edge of the crest were the input of the stability analysis of the rear slope armour layer.

Kobayashi considered only impermeable breakwaters and the static stability of the rear slope under attack of an impinging jet. This jet may directly hit the rear slope above SWL or plunges into the tailwater and then attack the rear slope. These two situations are visualised in *Figure 55*. Kobayashi assumes that the destabilising force is primarily determined by the jet velocity.

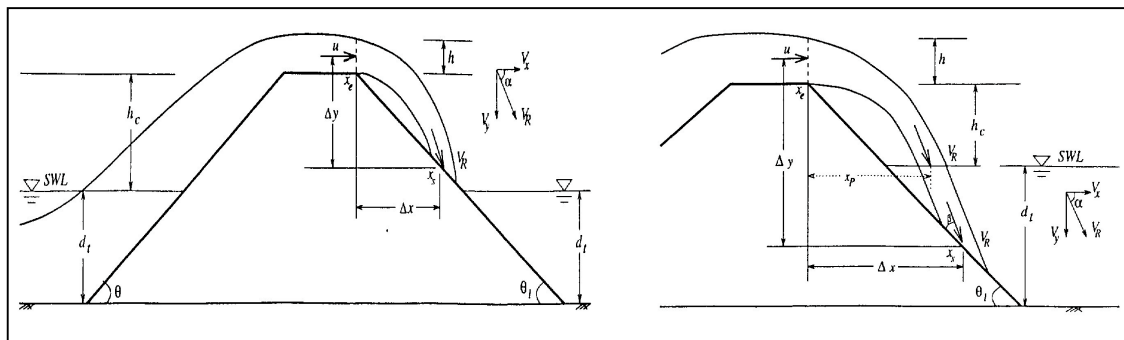


Figure 55: Overtopping wave according to Kobayashi

Kobayashi assumed that after reaching the rear end of the crest, the jet falls freely due to gravity. The jet's horizontal velocity remains constant during this fall and the vertical acceleration is assumed to be equal to the gravitational acceleration g , until it reaches the rear slope or enters the tailwater. When a jet enters the tailwater before reaching the rear slope, it is assumed that the jet penetrates this tailwater in a straight line with the same velocity as the jet velocity at the free surface (no accelerations).

The forces on the rear slope due to the impinging jet are translated into a drag force F_D , a lift force F_L and an inertia force F_I . It is assumed that under water no inertia force is present (due to the absence of accelerations). These forces can be resolved in the directions parallel and normal to the slope. Also the submerged weight of the armour stone can be resolved parallel and normal to the slope. This is visualised in *Figure 56*.

²⁹ Kobayashi uses the term 'jet' for the overtopping wave. In this section the same equationation as Kobayashi is used.

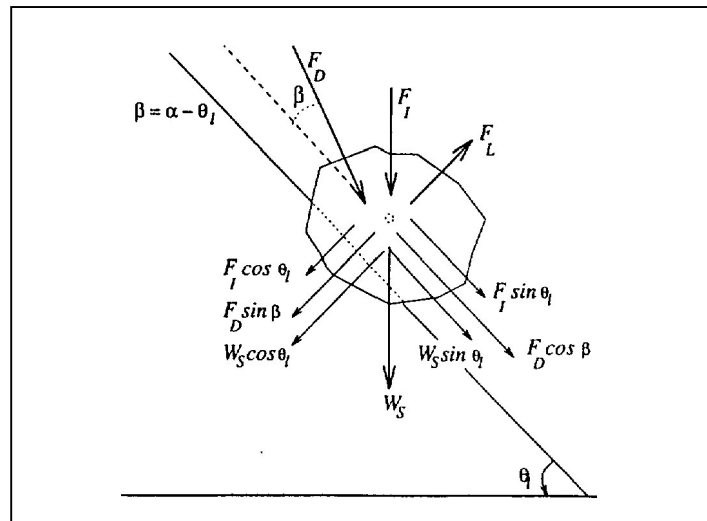


Figure 56: Forces on stone according to Kobayashi

Kobayashi expresses the stability of the armour units using Van der Meer's the stability number $N_s = \frac{H_s}{\Delta D_{n50}}$. With the expressions of all forces, a static stability relation is formulated. The non-dimensional force coefficients in this relation are calibrated using (only four!) physical tests performed by Vidal. The coefficients appeared to be small compared to the force coefficients derived earlier for the front slope.

With above calibrated stability equation, the influence of several parameters on the rear slope stability was determined. Kobayashi's conclusions can be summarised as follows:

- *Influence of rear slope angle β* : for steeper slopes, the stability decreases. Furthermore, the relative crest freeboard for which the rear slope is least stable shifts towards 0 for gentler slopes than 1:1.5.
- *Influence of front slope angle α* : a flatter front slope improves the rear slope stability.
- *Influence of water level*: the rear slope stability generally increases with an increasing water level. For the same $\frac{R_c}{H_s}$ ratio, the stability of the breakwater in deeper water is larger. Kobayashi does not give a clear explanation for this observation. In the case of a very low relative crest freeboard ($0 < \frac{R_c}{H_s} < 0.25$) the rear slope is more stable in shallow water than in deep water. This is explained as the jet then impinges beyond the toe of the rear slope.
- *Influence of crest width*: an increased crest width increases the rear slope stability. This is explained by the fact that an increased crest width implies more resistance and therefore a smaller jet velocity.
- *The influence of wave period T* : an increased peak period T_p causes more damage to the rear slope. Other authors also came to this conclusion.

ANNEX II - EXPERIMENTS

Annex II.A Reservoir outflow

A mathematical expression of the hydraulic processes on the crest of the experimental set-up can be found applying the equation of continuity and the equation of motion for open watercourses (first derived by De Saint-Venant). If the resistance term as well as the local accelerations are neglected in these equations (stationary flow), the equation of motion reduces to the equation of Bernoulli (along a streamline):

$$\frac{dH}{ds} = 0 \quad (56)$$

in which:

$$H = h + \frac{U^2}{2g} \quad \text{Energy head} \quad (m) \quad (m)$$

Torricelli used the equation of Bernoulli to predict the outflow velocity of a relatively large reservoir with a relatively small opening. When the energy head of a water particle in the opening is taken equal to the energy head of a water particle in the surface of the water inside the reservoir, the outflow velocity can be approximated by:

$$U = \sqrt{2g(\Delta z)} \quad (57)$$

The discharge becomes:

$$Q = \mu \cdot A_{hole} \cdot U \quad (58)$$

in which

μ	contraction coefficient
A_{hole}	area of outflow opening
B	width of opening
U	outflow velocity
g	acceleration due to gravity
Δz	head difference

In these equations the outflow velocity depends only on the head difference between the respective water levels in the reservoir and the outflow opening. The discharge depends on the head difference as well as on the contraction coefficient, which in turn could depend on the head difference.

In reality the outflow of a reservoir is never a stationary process. Due to the decrease of the water level inside the reservoir in time, the outflow velocity is not independent of time $\left(\frac{du}{dt} \neq 0\right)$. However, when the opening is relatively small, the local accelerations are

relatively small compared to the advective accelerations and the local accelerations can be neglected. Strictly spoken, the outflow is not steady, but for the calculation of the outflow velocity it is assumed that the flow is steady at any moment. This is called the quasi-steady approach.

In the experimental set-up, the area of the opening of the reservoir is not small compared to the reservoir volume and the quasi-steady approach is not valid. Next to advective accelerations also local accelerations as well as resistance will play a role in the hydraulic processes. Therefore, the real occurring outflow velocity and the real occurring discharge in the experimental set-up will probably not behave according the above described theoretically derived equations.

Annex II.B Derivation of maximum discharge

Calculation method

The discharge from the reservoir in the experimental set-up was calculated with use of the data from a Wave Height Meter inside the reservoir (WHM1). During a test, WHM1 produced data about the position of the water level inside the reservoir as a function of time. The development of the discharge as a function of time was calculated with use of the following equation:

$$Q = -A \cdot \frac{dh}{dt}$$

in which

Q	Discharge	(m ³ /s)
A	Free surface area of water in reservoir	(m ²)
h	Water level inside reservoir	(m)
t	Time	(s)

WHM1 produced data on the water level every 0.02 s. Therefore, dt in above equation is equal to 0.02 s. Theoretically spoken, the calculated discharge equals the average discharge over 0.02 s.

The data from WHM1 is not reliable anymore when the water level inside the reservoir is less than 3 cm. Therefore, data below this water level is not used in the calculation of the discharge.

Characteristic development of discharge in time

For an arbitrary water level inside the reservoir and an arbitrary configuration of the reservoir, the discharge qualitatively showed a similar development in time. This development in time can be characterised as follows:

- A swift increase of the discharge up to a maximum value, during tenths of seconds
- A slower decrease of the discharge from the maximum value to zero, during several seconds

In Figure 57 the development of the discharge in time is presented for two different water levels inside the reservoir for Configuration II, including the schematised development of the layer thickness ³⁰.

³⁰ In all figures the 'water level in the reservoir' is in fact the 'initial water level in the reservoir'. Furthermore, the time axis is relative to the moment at which the gate is lifted.

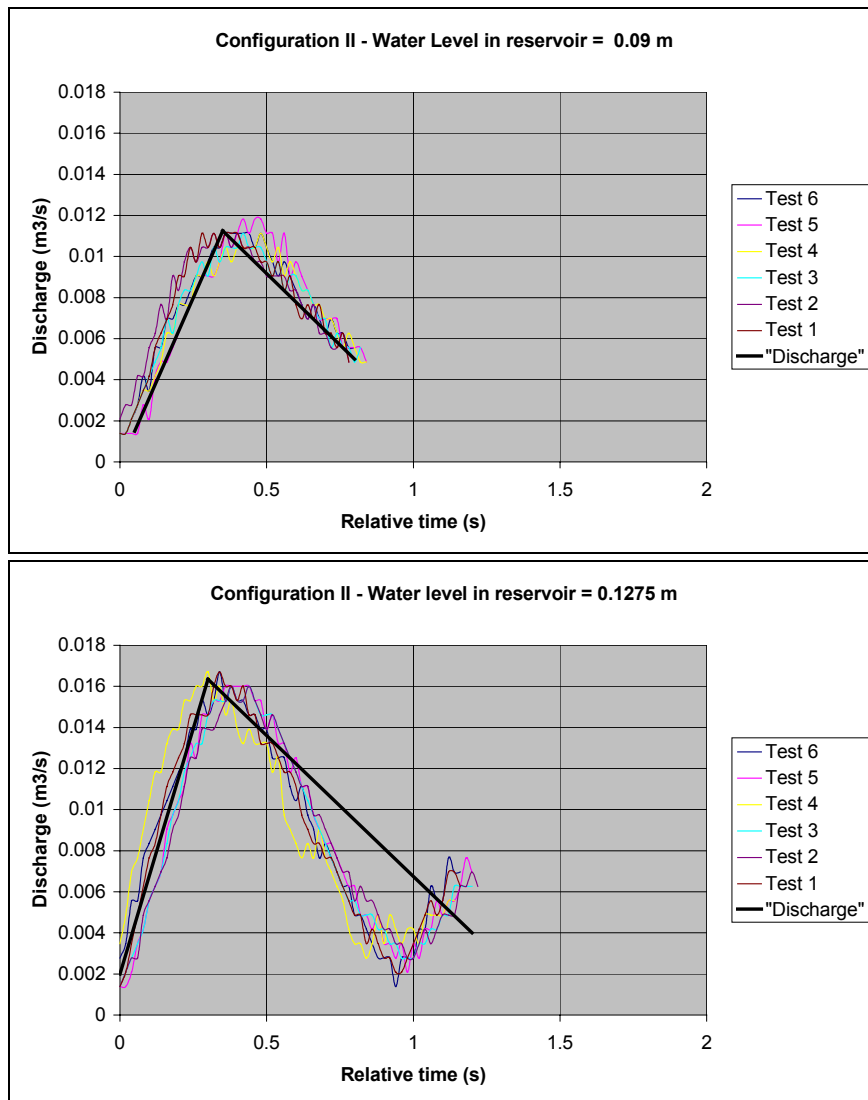


Figure 57: Examples of data on discharge

Due to oscillations inside the reservoir during the experiment, the discharge shows fluctuations. This is probably the reason for the increase of discharge after one second in Figure 57³¹. This hypothesis is confirmed by Figure 58 that displays the development of the discharge for a water level inside the reservoir of 17.75 cm for Configuration I. The 'translation wave' in the reservoir is clearly visible in this figure.

³¹ In this region the measurement data of WHM1 are still reliable, as the water level is above 3 cm.

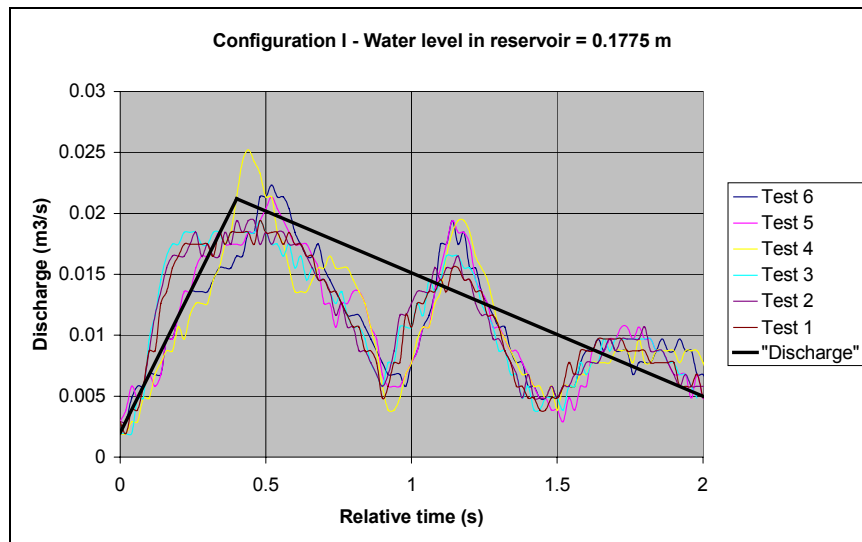


Figure 58: 'Translation wave' in reservoir

The development of the discharge is in agreement with the theory. In the first few tenths of seconds the local accelerations are not negligible due to the relatively large opening. Therefore, the discharge is not instantly equal to its maximum (a large part of the water in the reservoir first has to accelerate). When the discharge has reached its maximum and the water inside the reservoir is put into motion, the development of the discharge resembles the theoretical development from the quasi-steady approach quite well, apart from the reservoir oscillations.

The development of the discharge is characterised by a single parameter, the maximum discharge (Q_{max}). This characteristic of the discharge is further considered.

Maximum discharge vs. water level in reservoir

For each initial water level inside the reservoir, six measurements of the discharge were carried out. With these measurements the average value of the maximum discharge as well as the spread around this average value is determined.

In Figure 59 all measurements of the maximum discharge are plotted for all three configurations. In the same graph the average values of the maximum discharge per water level are plotted as well as the best-fit line through these averages. Finally, a reliability interval is added.

The reliability interval is based on a rough approximation of the spread in the results of the measurements. Figure 60 is used in this approximation. This figure presents per measurement the deviation from the average value. All deviations of the measurements together give an insight in the spread of the measuring results. Due to the limited number of measurements carried out, it is not possible to give an accurate value of the spread. An approximation of the spread (and therefore of the reliability interval) is therefore done visually in such a way that the deviations of nearly all measurements are within this spread.

For all three configurations the spread (in %) is independent of the water level inside the reservoir. However, per configuration the spread differs. Configuration II features the least

spread ($\pm 5\%$), followed by Configuration I ($\pm 10\%$) and Configuration III ($\pm 15\%$). The difference in spread between Configuration I en Configuration III can be caused by the larger opening of Configuration III. The larger the opening the more time it takes to open the gate. Therefore, Configuration III is more sensitive to the way the reservoir is opened, which leads to more spread. The difference between Configuration I en II cannot be easily explained.

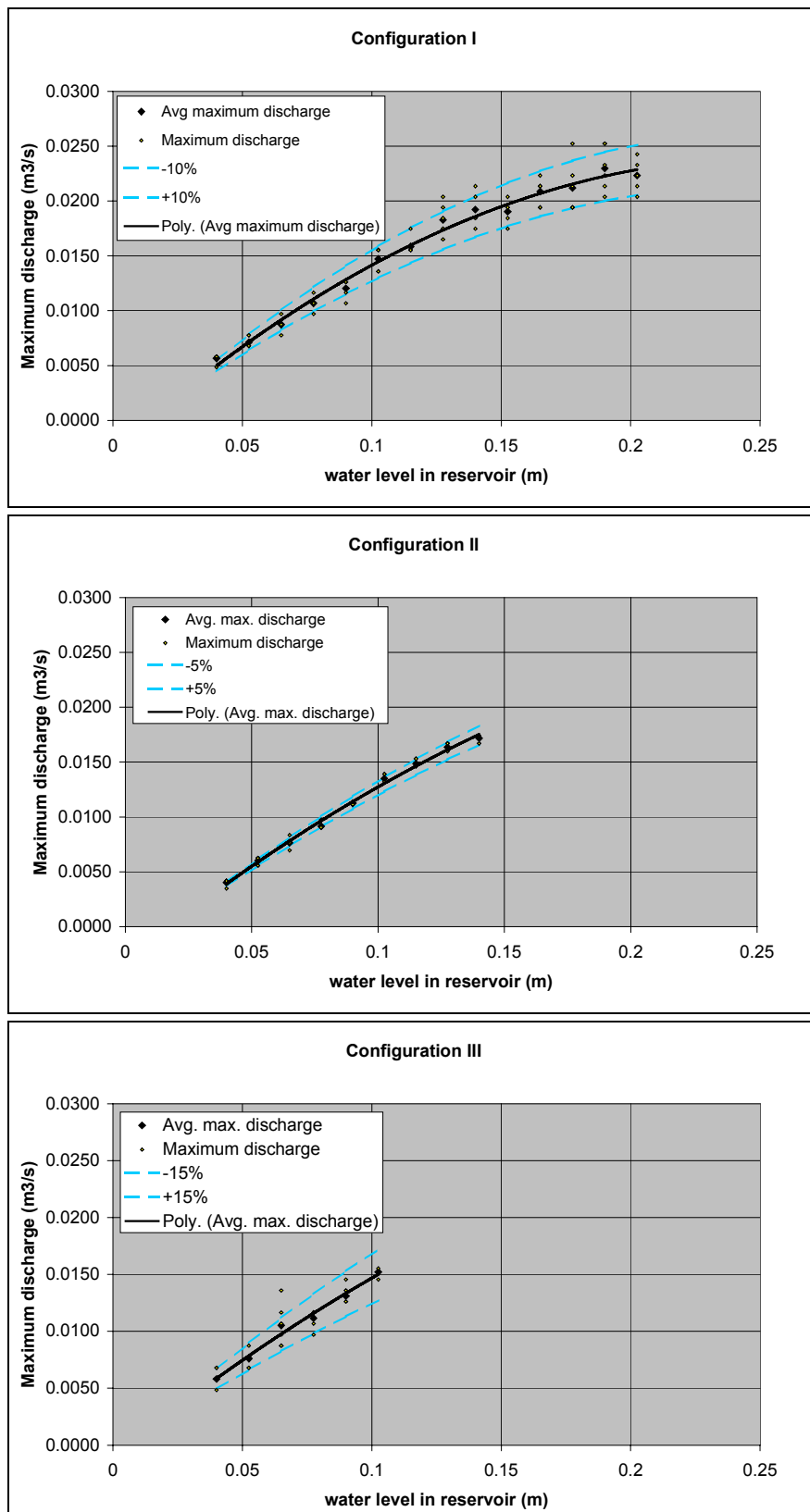


Figure 59: Average maximum discharge vs initial water level in reservoir

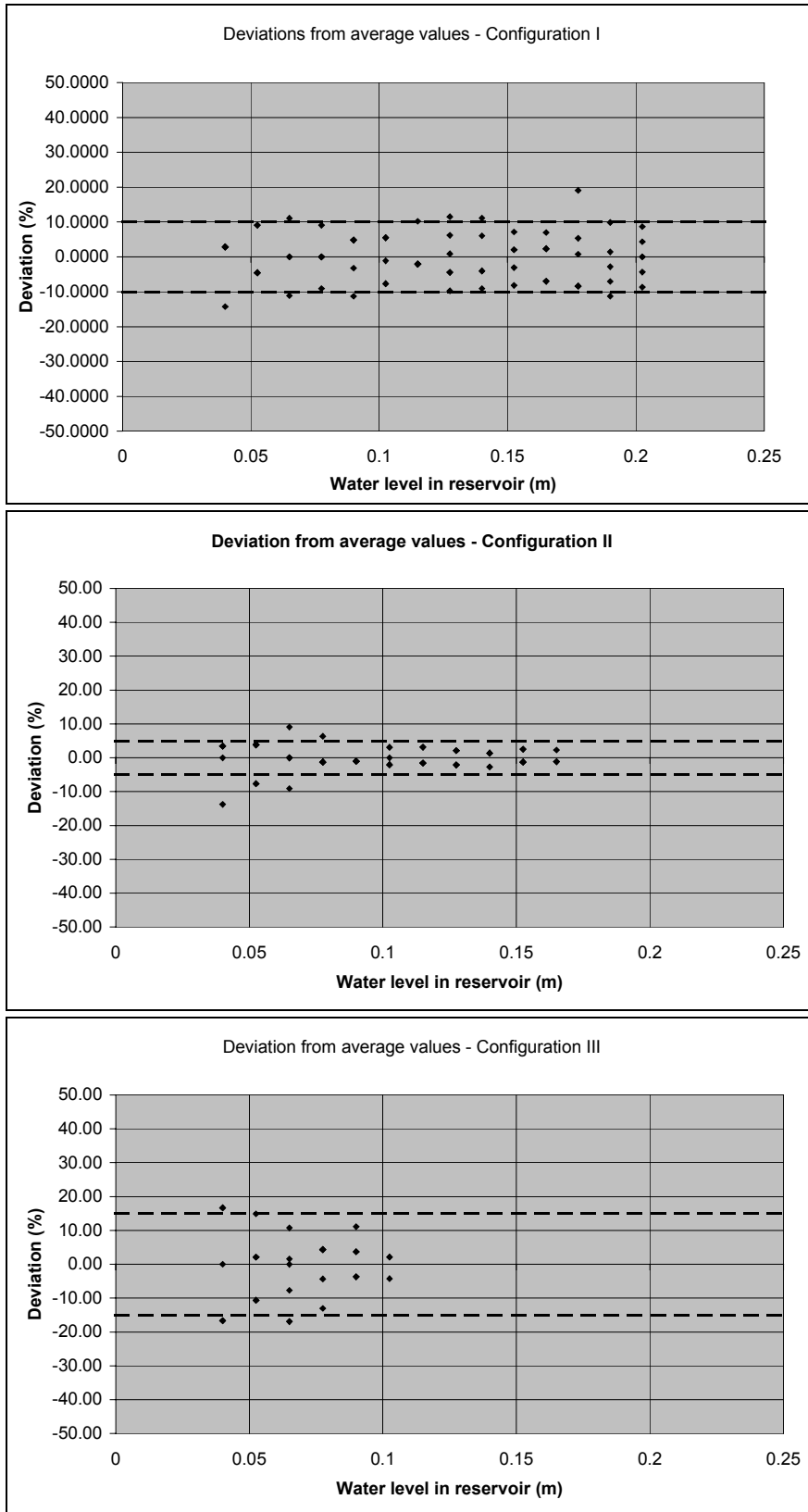


Figure 60: Reliability of data

Annex II.C Derivation of max. layer thickness

Calculation method

The development of the layer thickness was calculated using data from the Wave Height Meter on the crest, situated 92 cm from the opening of the reservoir and 8 cm from the rear slope (WHM3, see section 4.3). During a test, WHM3 produced data about the development of the water level as a function of time and accordingly data about the layer thickness. No additional calculations were needed.

Characteristic development of layer thickness in time

It was expected that for an arbitrary initial water level inside the reservoir and an arbitrary configuration of the experimental set-up the layer thickness would feature a qualitatively similar development in time as the discharge:

- A swift increase of the layer thickness up to a maximum value, during tenths of seconds
- A slower decrease of the layer thickness from the maximum value to zero, during several seconds

Above expected development of the layer thickness did occur. However, around the maximum value of the layer thickness, the data from WHM3 seems unreliable (see Chapter 4), especially for larger values of the water level inside the reservoir. Figure 61 features a typical example of the development of the layer thickness as measured by WHM3. According to the data, the layer thickness first increases to a maximum value, then drops to a lower value and then increases again. After this last increase, the layer thickness decreases slowly to zero.

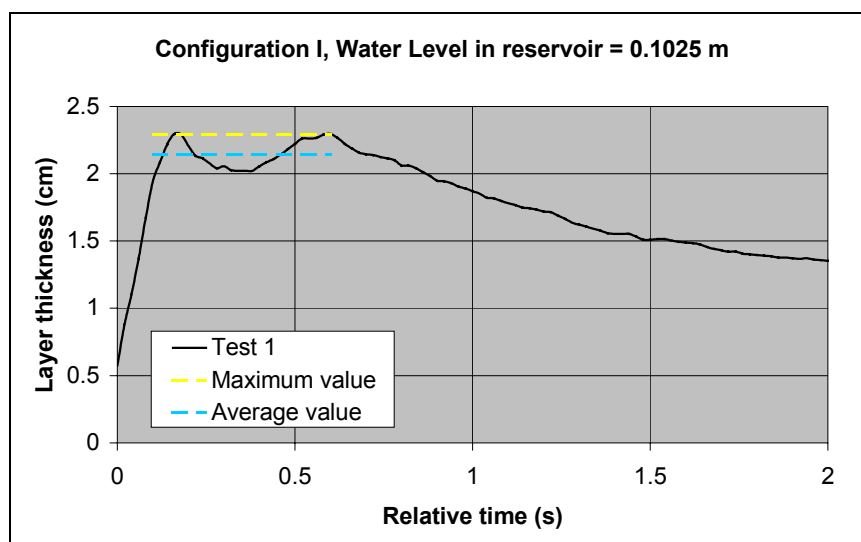


Figure 61: Typical example of data

In order to approximate the maximum value of the layer thickness two methods can be followed (see also Figure 61)

- The maximum value of the layer thickness is taken equal to the maximum value of the data.
- The maximum value of the layer thickness is taken equal to the average value of the data over a short period of time.

Both methods were carried out and compared to each other. In Figure 62 this comparison is plotted for Configuration I.

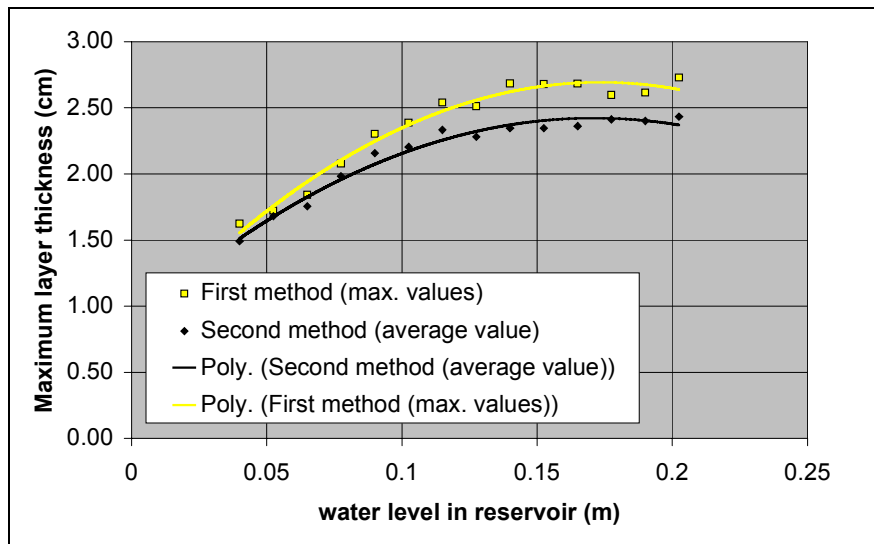


Figure 62: Comparison of the two methods to determine maximum layer thickness

As expected, the first method produces higher values for the maximum layer thickness. The relative deviation between both methods (around 10%) is independent of the initial water level inside the reservoir. The other two configurations showed the same results. With this in mind and also with consideration of the spread in the results (see next section) it is quite arbitrary which of the two methods is used to approximate the maximum layer thickness. In this report the second method is chosen, for one important reason: the approximation of the maximum layer thickness according to this method is structurally just as dubious as the first method, however, the second method is less vulnerable for deviations in the maximum value of the data. In Figure 63 the development of the layer thickness in time is presented for two different water levels inside the reservoir for Configuration II, including the schematised development of the layer thickness.

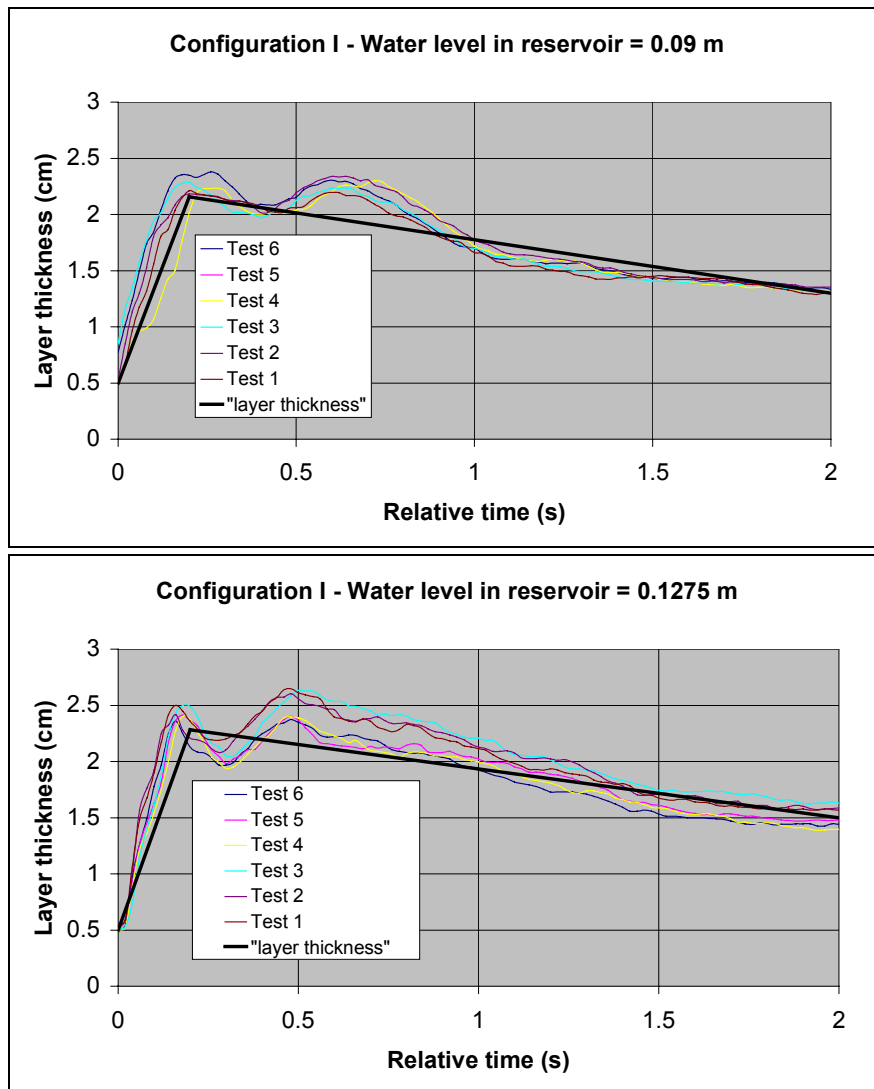


Figure 63: Examples of data on layer thickness

The development of the layer thickness is characterised by a single parameter, the maximum layer thickness (d_{max}). This characteristic of the layer thickness is further considered.

Maximum layer thickness vs. water level in reservoir

For each initial water level inside the reservoir, six measurements of the layer thickness were carried out. With these measurements the average value of the maximum layer thickness as well as the spread around this average value is determined.

In Figure 64 all measurements of the maximum layer thickness are plotted for all three configurations. In the same graph the average values of the maximum layer thickness per water level are plotted as well as the best-fit line through these averages. Finally, a reliability interval is added. This reliability interval is determined in the same way as for the discharge.

In Figure 65 the spread around the average values of the layer thickness is plotted. For all three configurations the spread (in %) is independent of the water level inside the reservoir. However, per configuration the spread differs. Configuration III features a spread of 15%, while Configuration I and II feature only a spread of 5%. This difference can be attributed to the larger opening of Configuration III (8 cm instead of 4 cm). This was also observed for the discharge.

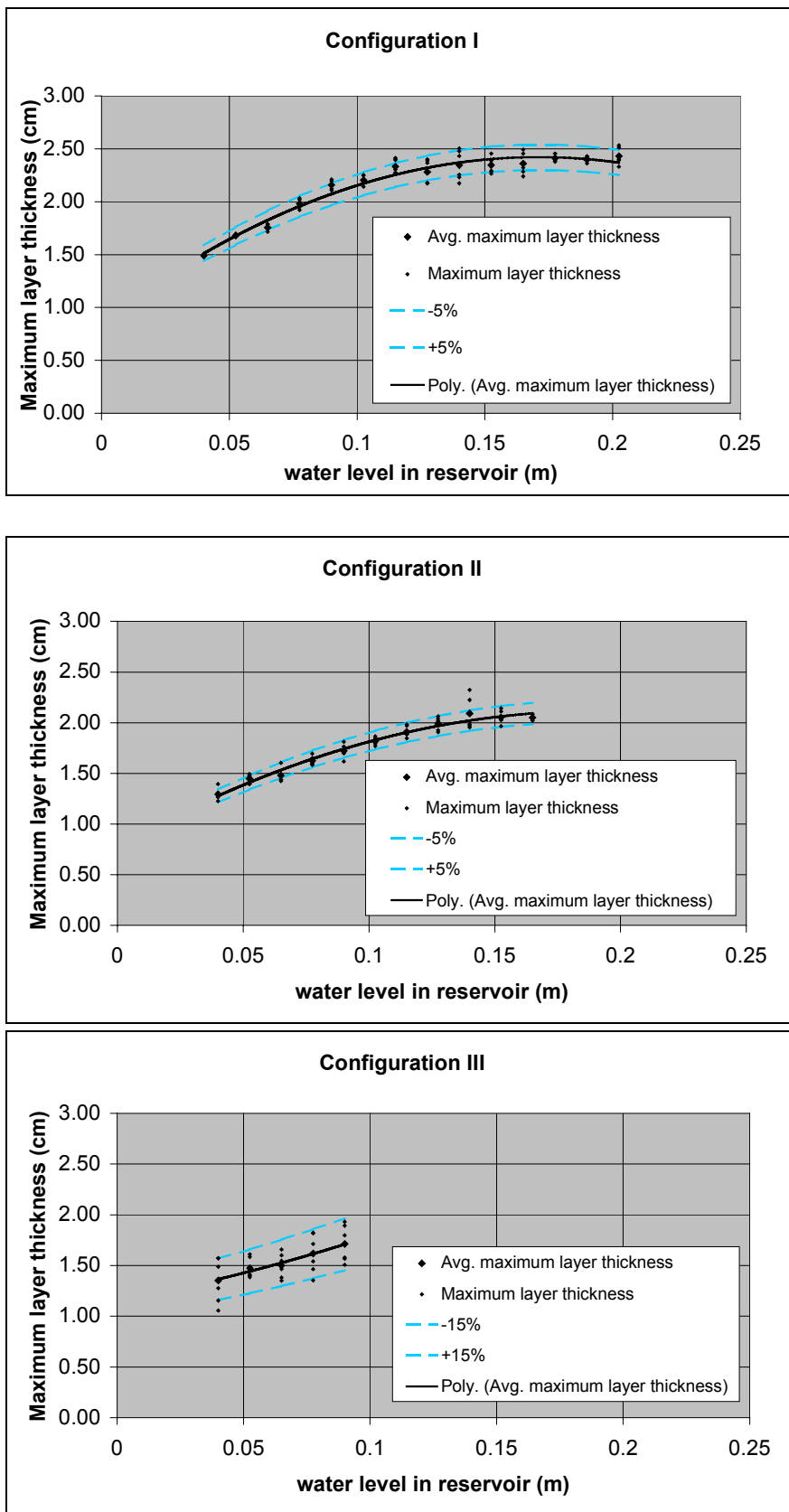


Figure 64: Maximum layer thickness vs initial water level in reservoir

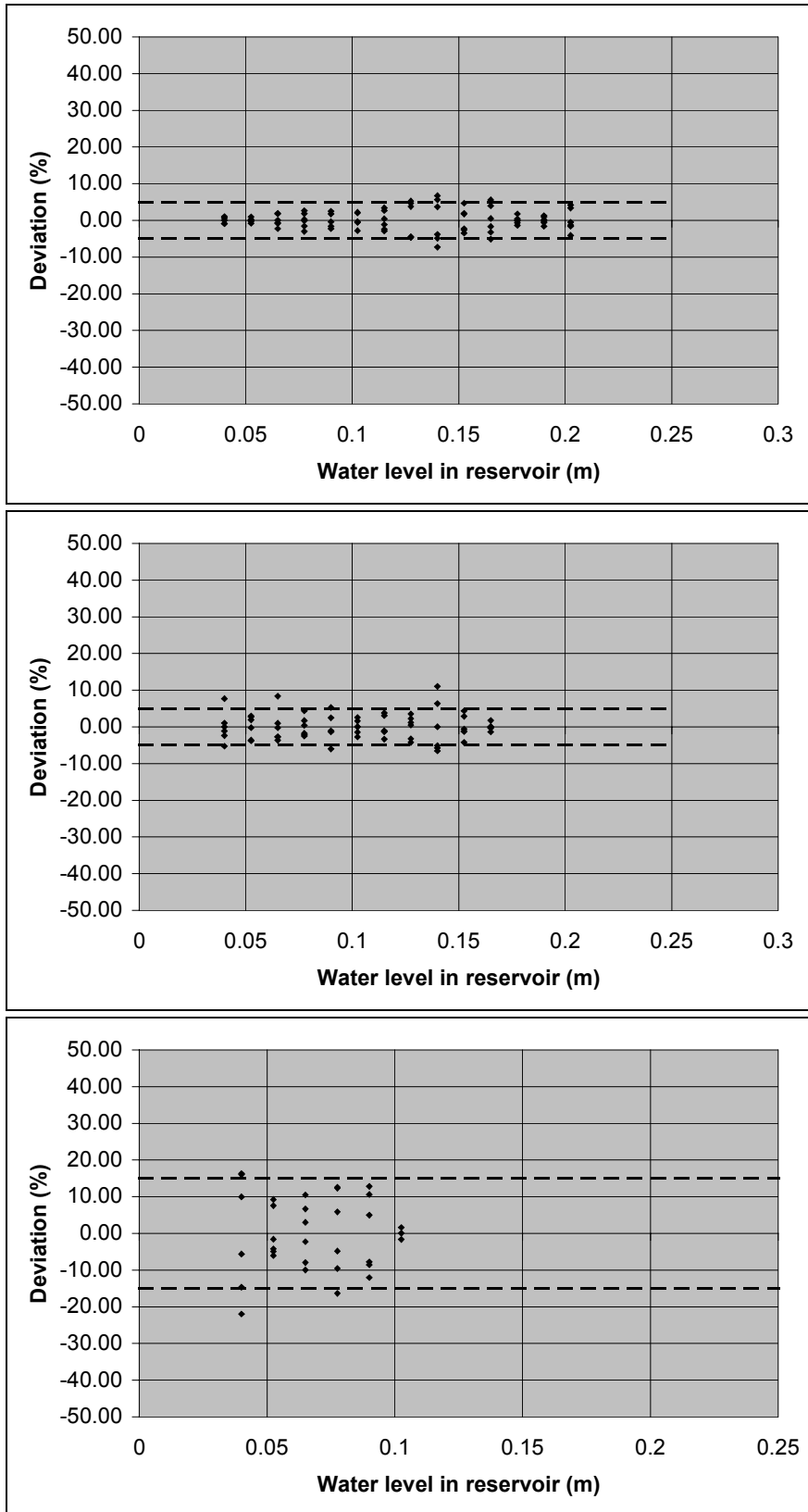


Figure 65: Reliability of data

Annex II.D Derivation of front velocity

Calculation method

The front velocity was calculated using of data from the Wave Height Meters on the crest, WHM2 and WHM3, situated 50 cm and 92 cm from the opening of the reservoir, respectively (see section 4.3). During a test, WHM2 as well as WHM3 produced data about the development of the water level as a function of time. The front velocity was calculated using the following equation:

$$u_f = \frac{\Delta s}{\Delta t_{d=0.01}}$$

in which

Δs	distance between WHM2 and WHM3 (= 0.42 m)
$\Delta t_{d=0.01}$	time difference between the moment that WHM2 measures a layer thickness of 0.01 m and the moment that WHM3 measures a layer thickness of 0.01 m ³² .

Two remarks about the above equation should be made. First, the equation does not take into account the distortion of the front of the plunge between WHM2 and WHM3. From the measurements however, it appeared that this distortion is insignificant. Second, the front velocity decreases as it moves along the crest, due to friction. Therefore, the calculated front velocity overestimates the real occurring front velocity at the rear slope. However, as the front velocity is overestimated for every water level, it is expected that this does not significantly influence the results.

Front velocity vs water level in reservoir

For each initial water level inside the reservoir, six calculations of the front velocity were carried out. With these calculations the average value of the front velocity as well as the spread around this average value is determined. In Figure 66 all calculations of the front velocity are plotted for all three configurations. In the same graph the average values of the front velocity per water level are plotted as well as the best-fit line through these averages. Finally, a reliability interval is added. This reliability interval is determined in the same way as for the discharge and the layer thickness. For all three configurations the spread (in %) is independent of the water level inside the reservoir and similar for all three configuration. The spread is about 10%.

³² The maximum value of the layer thickness was always higher than 0.01 m, therefore this value was chosen to calculate the front velocity.

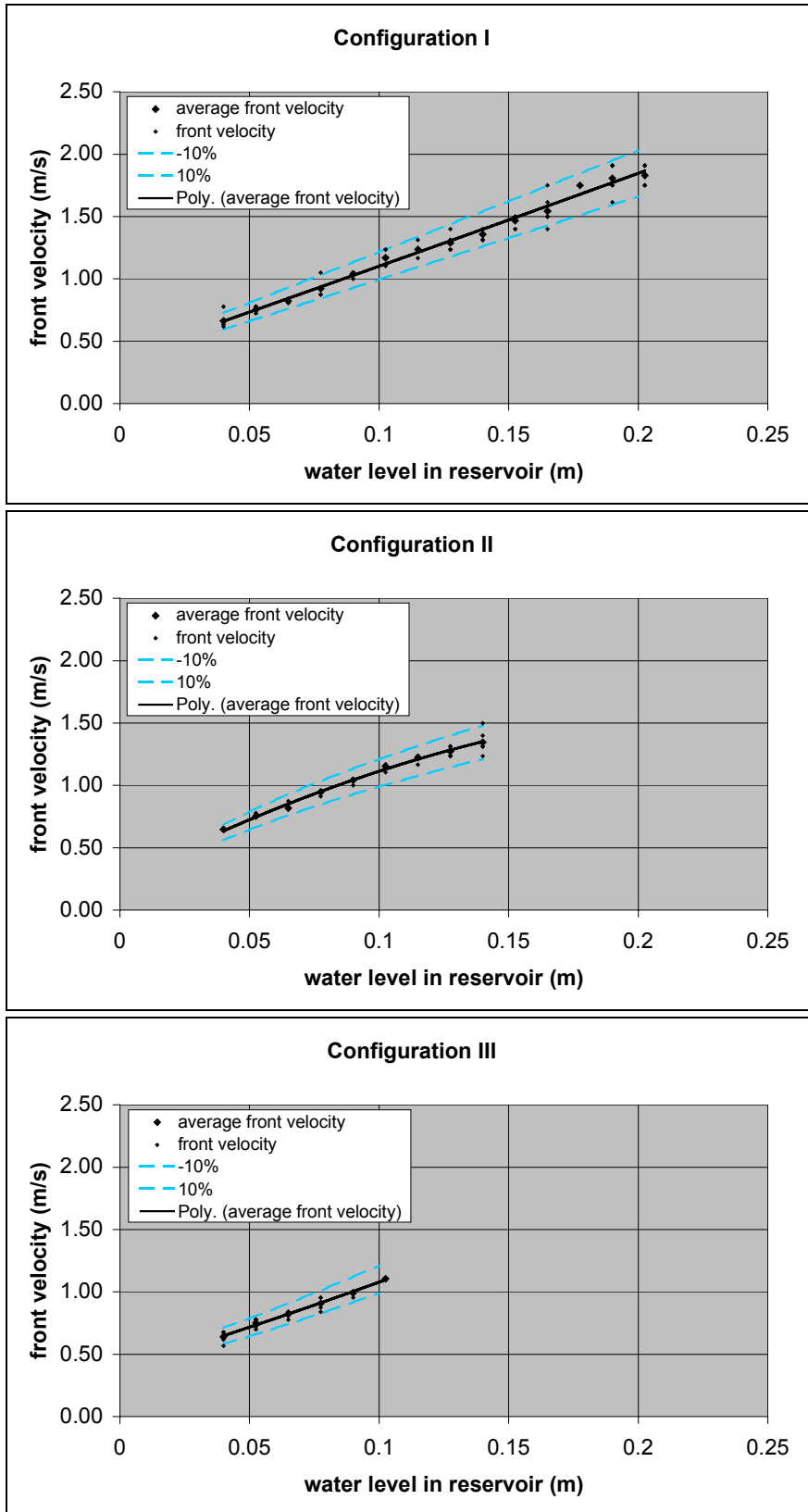


Figure 66: Front velocity vs initial water level in reservoir

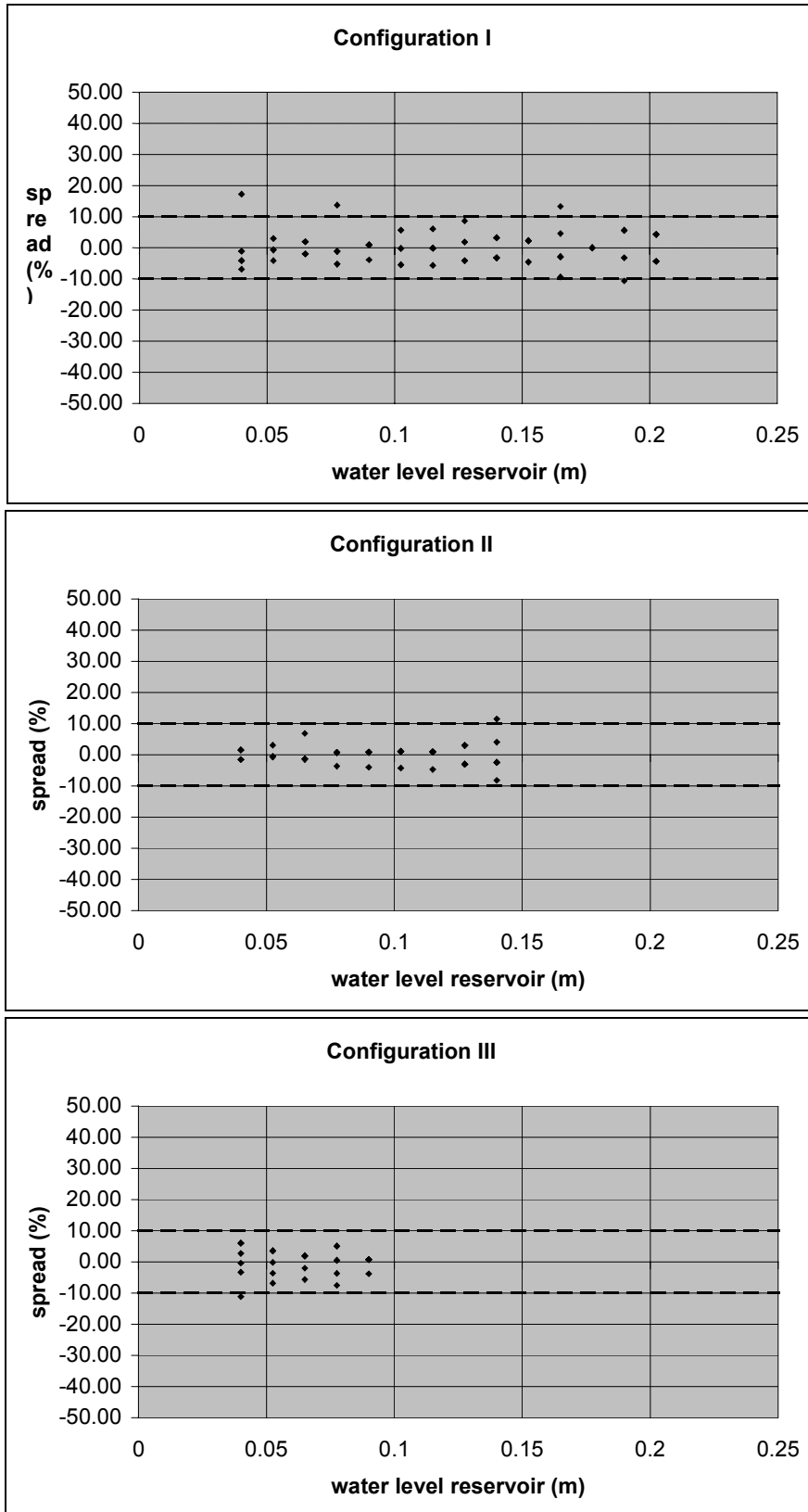


Figure 67: Reliability of data

Annex II.E Derivation of characteristic velocity

Calculation method

The characteristic velocity was calculated using the measurements of the maximum discharge and the maximum layer thickness as follows:

$$u_{char} = \frac{Q_{max}}{B \cdot d_{max}}$$

in which

- Q_{max} Maximum discharge, measured with WHM1
- B Width of the crest at WHM3 (=0.4 m)
- d_{max} Maximum layer thickness, measured with WHM3

It is assumed that the maximum discharge measured with WHM1 also occurs at WHM3. Due to the transient character of the hydraulic processes on the crest, the storage of water can be neglected and this assumption is permissible.

Characteristic velocity vs. water level in reservoir

For each initial water level inside the reservoir, six calculations of the characteristic velocity were carried out. With these calculations the average value of the characteristic velocity as well as the spread around this average value is determined.

In Figure 68 all calculations of the characteristic velocity are plotted for all three configurations. In the same graph the average values of the characteristic velocity per water level are plotted as well as the best-fit line through these averages. Finally, a reliability interval is added. This reliability interval is determined in the same way as the other plunge characteristics.

For all three configurations the spread (in %) is independent of the water level inside the reservoir. However, per configuration the spread differs. Configuration III features a spread of 20%, while the spread of Configuration II is only 10%. The spread of Configuration I is 15%. The large spread is due to the combined spread of the layer thickness and the discharge. Because of this large spread, conclusions based on the average values of the characteristic velocity should be handled with care.

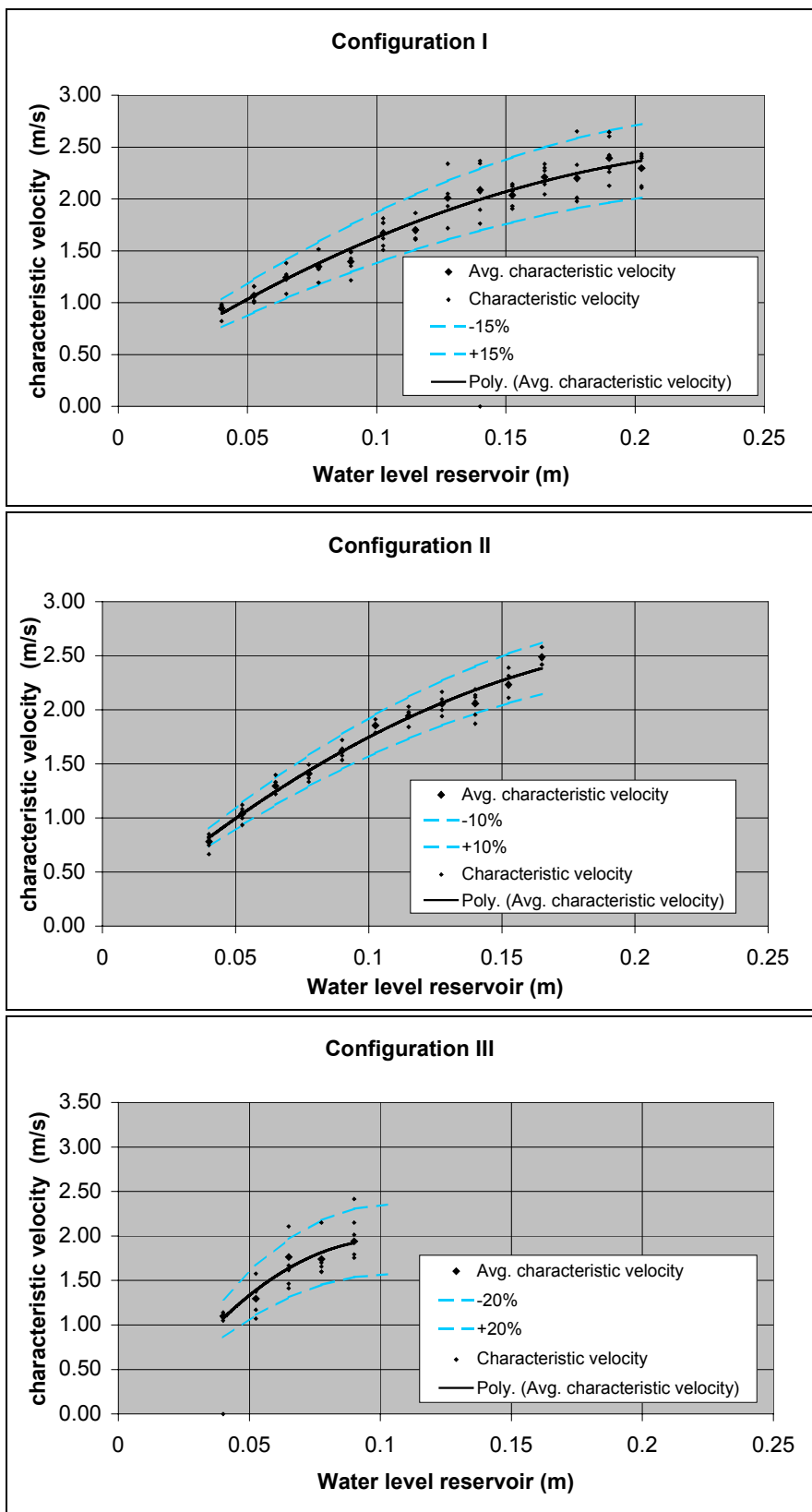


Figure 68: Characteristic velocity vs initial water level in the reservoir

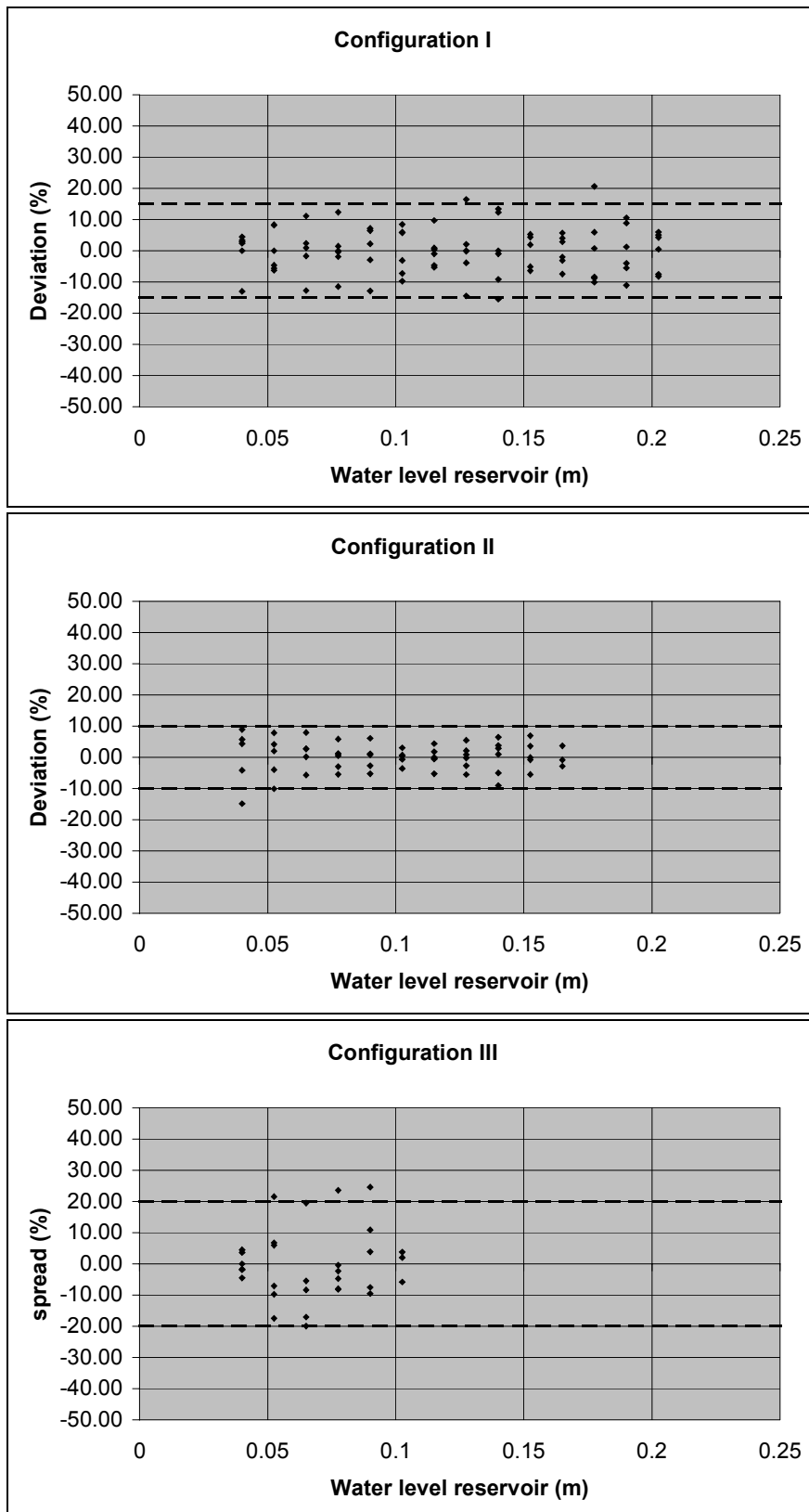


Figure 69: Reliability of data

Annex II.F Data on cum. damage development

C = Collapse
 WL = Initial water level inside reservoir

Table 10: Damage vs. water level; $R_c = 10$ cm; Configuration I

WL (cm)	Nod Exp. 1	Nod Exp. 2	Nod Exp. 3	Nod Exp. 4	Nod Exp. 5	Nod Exp. 6	Nod Exp. 7	Nod Exp. 8	Nod Exp. 9
4	0.233	0.000	0.186	0.047	0.047	0.093	0.000	0.465	0.000
5.25	0.233	0.047	0.605	0.093	0.140	0.1395	0.2325	0.512	0.186
6.5	0.233	0.093	0.698	0.419	0.186	0.5115	0.372	0.837	0.233
7.75	0.233	0.279	1.116	0.977	0.326	0.8835	1.116	0.977	0.233
9	0.233	0.419	1.256	1.023	0.791	C	3.069	C	0.326
10.25	0.512	0.651	3.255	1.674	0.837		3.3945		1.488
11.5	0.651	C	C	1.767	0.884		3.534		C
12.75	1.023			1.907	0.884		C		
14	C			2.232	0.884				
15.25				C	1.163				
16.5					C				

Table 11: Damage vs water level; $R_c = 10$ cm; Configuration II

WL (cm)	Nod Exp. 1	Nod Exp. 2	Nod Exp. 3	Nod Exp. 4	Nod Exp. 5
4	0.1395	0.093	0	0	0
5.25	0.3255	0.1395	0	0.0465	0.0465
6.5	0.372	0.558	0.2325	0.2325	0.093
7.75	0.744	0.651	0.465	0.372	0.3255
9	1.4415	1.023	0.558	1.3485	0.558
10.25	2.558	1.3485	0.9765	2.2785	0.8835
11.5	3.3015	1.9065	1.6275	3.023	1.1625
12.75	3.441	2.046	C	3.302	C
14	3.534	2.976		3.4875	
15.25	3.8595	C		4.278	
16.5	5.766			C	
17.75	C				

Table 12: Damage vs water level; $R_c = 10$ cm; Configuration III

WL (cm)	Nod Exp. 1	Nod Exp. 2	Nod Exp. 3	Nod Exp. 4	Nod Exp. 5
4	0.140	0.093	0.140	0.372	0.465
5.25	0.279	0.140	1.023	0.372	0.791
6.5	1.488	2.2785	1.023	1.116	1.116
7.75	2.000	4.5105	1.070	2.139	1.395
9	2.976	C	1.9995	3.441	2.000
10.25	C		C	C	4.604
11.5					C
12.75					
14					
15.25					
16.5					

Table 13: Damage vs water level; $R_c = 7$ cm; Configuration I

WL (cm)	Nod Exp. 1	Nod Exp. 2	Nod Exp. 3	Nod Exp. 4	Nod Exp. 5
4	0.140	0.093	0.093	0.279	0.093
5.25	0.279	0.419	0.372	0.837	0.279
6.5	0.372	0.930	0.558	0.837	0.651
7.75	0.605	0.930	2.511	1.302	0.837
9	0.698	1.907	3.813	1.767	1.256
10.25	2.9295	4.0455	3.999	2.046	4.3245
11.5	3.3015	4.557	4.836	6.231	C
12.75	4.836	5.1615	C	C	
14	4.9755	C			
15.25	5.2545				
16.5	C				

Table 14: Damage vs water level; $R_c = 3$ cm; Configuration I

WL (cm)	Nod Exp. 1	Nod Exp. 2	Nod Exp. 3	Nod Exp. 4	Nod Exp. 5
4	0.279	0.000	0.093	0.000	0.093
5.25	0.512	0.093	0.186	0.047	0.140
6.5	0.512	0.233	0.233	0.093	0.186
7.75	0.558	0.651	0.233	0.140	0.372
9	0.651	1.116	0.233	0.186	0.372
10.25	0.744	1.442	0.512	0.233	0.605
11.5	0.977	1.581	0.930	0.419	1.256
12.75	1.070	1.767	0.930	0.465	1.395
14	1.535	C	0.930	0.512	1.814
15.25	1.953		0.930	0.558	1.953
16.5	2.604		1.070	2.046	2.279
17.75	3.023		2.000	3.023	2.372
19	3.069		2.418	C	2.976
20.25	C		C		3.906
21.5					C

Annex II.G Damage due to individual plunges

Table 15: Individual damage vs water level; $R_c = 10$ cm; Configuration I

WL (cm)	Nod Exp. 1	Nod Exp. 2	Nod Exp. 3	Nod Exp. 4	Nod Exp. 5
5.25	0.233	0.326	0.140	0.326	0.140

WL (cm)	Nod Exp. 6	Nod Exp. 7	Nod Exp. 8	Nod Exp. 9	Nod Exp. 10
6.5	0.651	0.837	1.721	0.558	1.302

WL (cm)	Nod Exp. 11	Nod Exp. 12	Nod Exp. 13	Nod Exp. 14	Nod Exp. 15
7.75	0.651	1.953	1.488	0.884	1.070

WL (cm)	Nod Exp. 16	Nod Exp. 17	Nod Exp. 18	Nod Exp. 19	Nod Exp. 20
9	C	3.674	3.860	C	3.116

Annex II.H Damage including reliability intervals

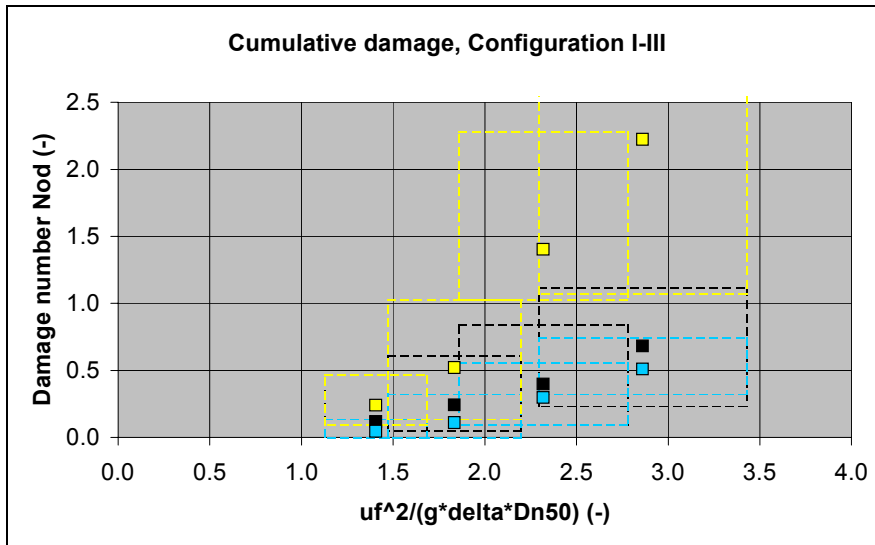


Figure 70: Cumulative damage vs u_f

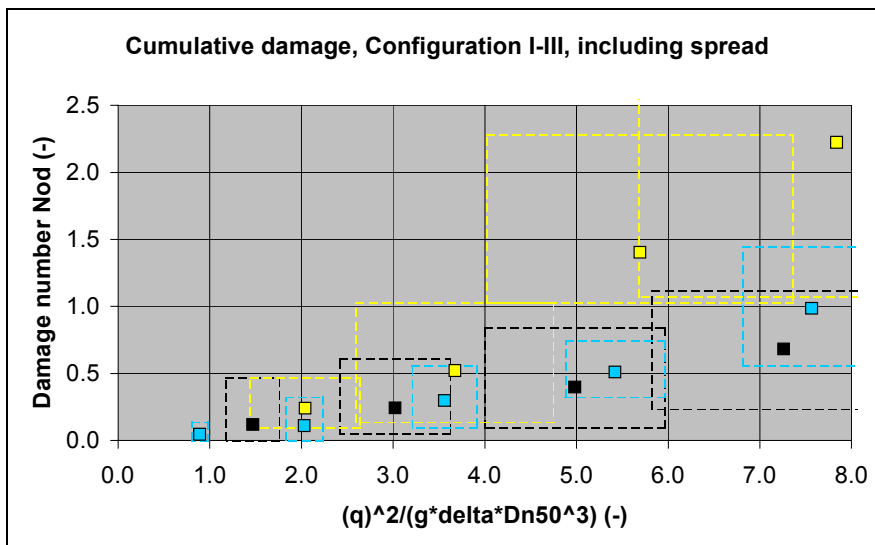


Figure 71: Cumulative damage vs q

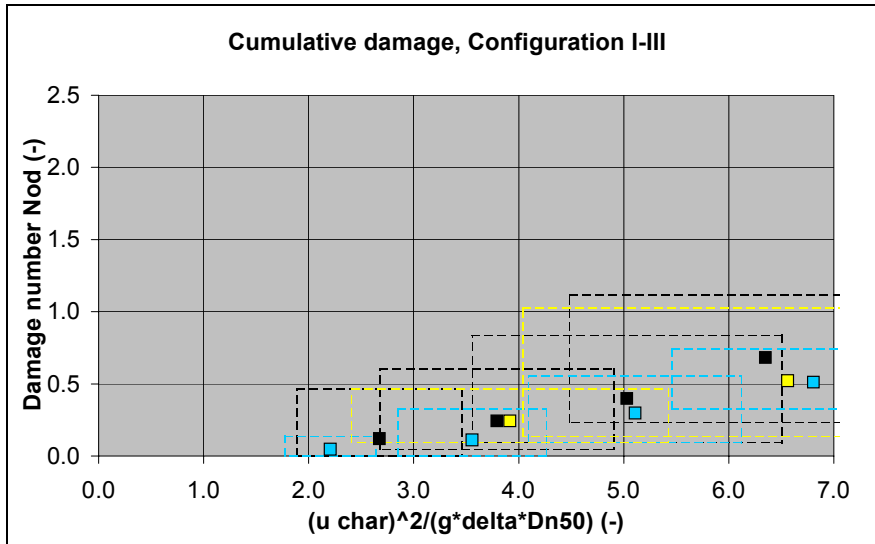


Figure 72: Cumulative damage vs. u_{char}

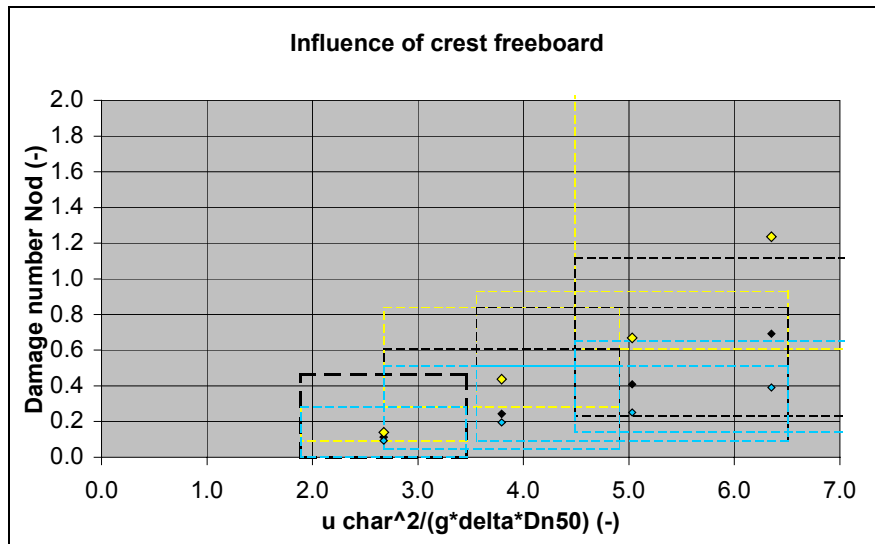


Figure 73: Cumulative damage for three different crest freeboards (Configuration I)

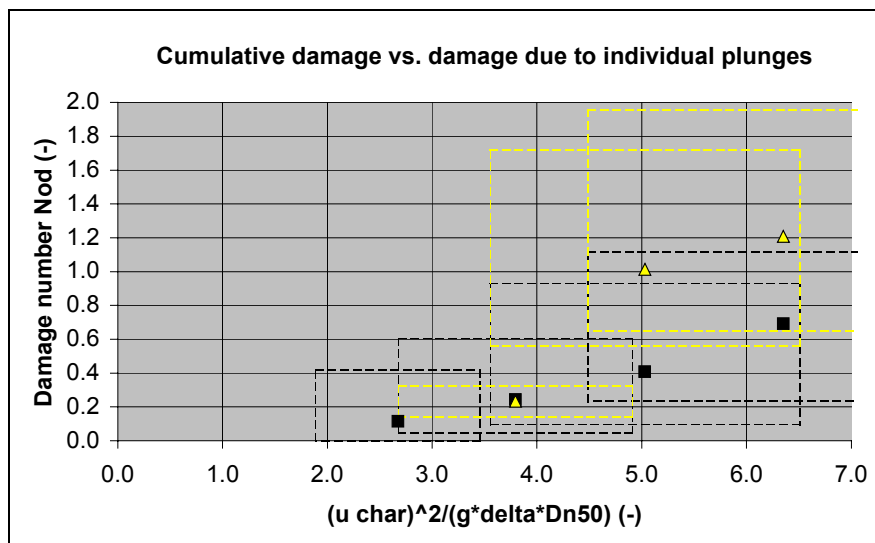


Figure 74: Cumulative damage vs individual damage

ANNEX III - ROUGH ESTIMATES OF DIMENSIONS OF EXPERIMENTAL SET-UP

(in Dutch)

Annex III.A Schatting parameterwaarden

Voordat in Annex III.B de dimensies van de opstelling worden bepaald introduceer ik in deze bijlage de formules die ik heb gebruikt om een schatting te geven van de te gebruiken parameterwaarden.

Overslagvolumes, snelheid en laagdikte

Voor de bepaling van de overslaande volumes, de snelheid en de laagdikte van deze volumes als functie van een inkomende onregelmatig golfveld heb ik gebruik gemaakt van de formules van Van Gent [9]. Deze formules beschrijven de waarden die door 2% van het inkomende golven overschreden worden aan de landkant van de kruin. Het zijn dus de 'grotere plonzen'. Het blijkt dat onder bepaalde aannamen de waarden alleen afhankelijk zijn van $(z_{2\%} - R_c)$ ³³:

$$V_{over} = f(z_{2\%} - R_c)$$

$$u_{over} = f(z_{2\%} - R_c)$$

$$d_{over} = f(z_{2\%} - R_c)$$

Van Gent heeft nog geen formule ontwikkeld voor de bepaling van de overslagtijd.

Overslagtijd

Voor de bepaling van de overslagtijd is gebruik gemaakt van de bevindingen van Perdijk [13] die de overslag van regelmatige golven onderzocht. In feite werd deze formule al gevonden door Roos en Battjes [8]. Het blijkt dat de overslagtijd van regelmatige golven lineair toeneemt met een grotere periode en afneemt met de wortel van de Irribarren parameter:

$$t_{over} = f(T, \frac{1}{\sqrt{\xi}})$$

Hierbij is aangenomen dat de tijdsduur van onregelmatige golven van dezelfde orde grootte is.

³³ Het is belangrijk om te onthouden dat de 2%-overschrijdings-waarden voor V, u en d niet allemaal tegelijk plaatsvinden.

Vorm van overslaande golf

Zowel Perdijk [13] als Van der Meer [14] hebben de vorm van overslaande golven gemeten door middel van laagdiktemeters en snelheidsmeters op de kruin. Perdijk deed dit voor regelmatig overslaande én onregelmatig overslaande golven, Van der Meer alleen voor onregelmatige overslaande golven. Van der Meer bekeek ook het verloop van de vorm op het achtertalud. Hieruit blijkt dat op een vaste plaats het verloop van de laagdikte in de tijd meestal een driehoeksvorm heeft, snel toenemend tot maximaal (t_1) en daarna in een langere tijdsduur afnemend tot nul (t_2 , zie Figure 6 in het hoofdrapport). Voor het verloop van de snelheid geldt meestal een soortgelijk figuur en dus ook voor het specifiek debiet ($q = u \cdot d$). De verhouding $\frac{t_1}{t_2}$ blijkt flink te variëren per golf. Ruwweg is t_1 ongeveer 10 tot 50% van t_2 .³⁴

Uit metingen van Van der Meer blijkt dat de maximale laagdikte op de kruin in de richting van het achtertalud steeds meer afneemt en dat de lengte steeds meer toeneemt. Dit lijkt op een diffusieproces. Volgens dezelfde proeven lijken de snelheden toe te nemen in de richting van het achtertalud, maar omdat de formules van de overslagsnelheden zijn bepaald ter plaatse van de overgang kruin-achtertalud, hoeft dit niet te worden meegenomen in het onderzoek.

Een belangrijke eis aan het fysische model is dat het karakter van de golf uit Figuur 1 wordt nagebootst. Dit betekent dat gedurende een korte periode het specifiek debiet moet toenemen tot maximaal en daarna gedurende een langere periode tot 0. Zo ontstaat de impulsachtige kracht op het achtertalud die een golf veroorzaakt.

Bij een brekende golf ontstaan luchtinsluitingen en roterende bewegingen. Deze processen worden niet meegenomen in dit onderzoek.

Steengrootte armour laag

Het lijkt een goed idee om bij dit onderzoek stenen te gebruiken die al in eerder onderzoek zijn gebruikt. Dit bespaart geld en werk. De stenen van de armour laag van Alwin van den Bosch ($D_n = 3,4$ cm) lijken een goede maat voor de maximale steengrootte. Nu is het de vraag welke waarden hierbij moeten worden genomen voor de hydraulische en structurele parameters en of deze waarden zijn te creëren in een proefopstelling.

Significante golfhoogte H_s

Om de maximale waarden van de overslagparameters te berekenen is gebruik gemaakt van het gegeven dat het in de praktijk gebruikelijk is om bij het ontwerp van lage golfbrekers dezelfde steengrootte voor het voortalud te gebruiken voor het achtertalud. Met behulp van de formule van Van der Meer blijkt dat een voortalud, opgebouwd uit stenen van 0.034 m volledig bezwijkt bij $H_s \approx 0,13$ m. De berekening die hierbij hoort staat beschreven in Annex III.E, maar komt er in het kort op neer dat bij een kruinhoogte gelijk aan 0.08 m (aanname, zie "Kruinhoogte R_c ") en een reductiefactor voor de benodigde steen van 1.1,

³⁴ Persoonlijke schatting

het voortalud ($\tan \alpha = 0.5$) zodanig wordt beschadigd dat $S = 8$. Bij deze berekening ben ik er vanuit gegaan dat de meeste overslag optreedt bij een grote ξ ($> 3,5$) en dat de gemiddelde steilheid van het golfveld niet kleiner is dan 1% ($s_{m, \min} = 0.01$). Voor meer details zie Annex III.E.

Oploophoogte $z_{2\%}$

In Annex III.C staat beschreven dat ervan kan worden uitgegaan dat de maximale $z_{2\%}$ ongeveer gelijk is aan 2.25 maal H_s . Uit berekeningen met behulp van de formule van Van der Meer blijkt dat deze H_s maximaal ongeveer 0.13 m is (bij $\tan \alpha = 0.5$, $s_m = 0.01$ en $\xi_m = 5$). Dit betekent dat de maximale $z_{2\%}$ gelijk is aan 0.29 m. Het is dus zeer onwaarschijnlijk dat $z_{2\%}$ groter is dan 0.29 m bij een steengrootte van 0.034 m. In dit geval is namelijk het voortalud al volledig bezweken.

Kruinhoogte R_c

Ik heb de maximale $z_{2\%}$ berekend bij een kruinhoogte gelijk aan 0.08 m. De maximale waarde van $(z_{2\%} - R_c)$ blijkt dan gelijk te zijn aan 0.21 m. In principe is de minimale waarde van $(z_{2\%} - R_c)$ gelijk aan 0, maar het lijkt me niet nodig om heel kleine plonzen te testen. Vandaar dat de minimale waarde is vastgesteld op 0.05 m.

In het model is de kruinhoogte één van de te onderzoeken parameters. Ik zal deze hoogte variëren tussen 0 en 0.16. De gemiddelde waarde is 0.08 m en bij deze kruinhoogte zijn de overslagparameters berekend. Bij lagere kruinhoogtes en dezelfde $z_{2\%}$ zullen grotere maximale waarden van deze parameters opleveren en grotere kruinhoogtes en dezelfde $z_{2\%}$ juist kleinere waarden. Aangezien ik wil onderzoeken wat het effect is van plonzen op het achtertalud, zal ik echter voor alle kruinhoogtes deze waarden gebruiken. De meeste proeven (75% van het totaal) zullen bij een kruinhoogte van 0.08 m plaatsvinden.

Overslagvolume, snelheid en laagdikte

Het bovenstaande levert de volgende waarden op bij $R_c = 0.08$ m:

$$\begin{aligned} 0.05 < (z_{2\%} - R_c) < 0.21 & \quad (\text{m}) \\ 7 < V_{over} < 120 & \quad (\text{l/m}) \\ 1 < u_{over} < 2.15 & \quad (\text{m/s}) \\ 0.02 < d_{over} < 0.07 & \quad (\text{m}) \end{aligned}$$

Het is dus de verwachting dat bij de maximale waarden van bovenstaande parameters het achtertalud behoorlijk wordt beschadigd.

Omdat de minimale overslagsnelheid in de proef gelijk is aan 1 m/s en de minimale waarde van de overslaglaagdikte gelijk is aan 0.02 m is het Reynoldsgetal voor de stroming op de kruin groter dan 10^4 en is dus de viscositeit ondergeschikt aan de traagheid op de kruin (net zoals in de werkelijkheid):

$$Re = \frac{u \cdot d}{\nu} = \frac{1 \cdot 0.02}{10^{-6}} = 2 \cdot 10^4$$

Dit levert dus geen schaaffecten op.

Overslagtijd

De maximale overslagtijd van een regelmatig golfveld vindt plaats bij een maximale waarde voor de golfperiode en een minimale waarde voor de Irribarren parameter. De minimale overslagtijd van een regelmatig golfveld vindt plaats bij een minimale waarde voor de golfperiode en een maximale waarde voor de Irribarren parameter. Uit berekeningen met een golfhoogte van rond de 20 centimeter en periodes van 1 tot 7 s blijkt dat deze tijdsduur ruwweg ligt tussen 0.5 seconden en 1.4 seconde voor $\tan \alpha = 0.66$ en tussen 0.9 seconden en 2.5 seconden voor $\tan \alpha = 0.2$. De vertaling van de overslagtijd voor regelmatige golven met een golfhoogte van ongeveer 0.2 meter naar de overslagtijd die door 2% van de golven wordt overschreden in een onregelmatig golfveld met $H_s = 0.13$ m, is niet gemakkelijk te maken. In mijn proefopstelling heb ik daarom gekozen voor een zo ruim mogelijke variatie van de overslagtijd:

$$0.5 < t_{2\%} < 2.5 \text{ (s)}$$

Hellingshoek β

De grootte van de hellingshoek β hoeft niet aangepast te worden. In een eerder rapport is al vastgesteld dat deze $\tan \beta$ gevarieerd dient te worden tussen 0.2 en 0.66.

Annex III.B Dimensies proefopstelling

In de volgende paragrafen worden de verschillende onderdelen van de proefopstelling één voor één gedimensioneerd.

Afmetingen van de goot

Breedte

Het overslaand volume is afhankelijk van de breedte van de opstelling. Om de werkbaarheid te vergroten is dus een kleine breedte gewenst. Daarentegen moet de breedte wel zó groot zijn dat randeffecten de proeven niet gaan domineren. Een minimale breedte van 10 à 15 stenen lijkt daarom gewenst. De breedte is zo vastgesteld op 0,5 m. Het overslaand volume is dan maximaal 60 liter. Dit lijkt mogelijk in een model. Een grotere breedte lijkt ook mogelijk.

Hoogte

De hoogte van de golfbreker kan worden vastgesteld aan de hand van de maximale kruinhoogte plus een aantal centimeters onder de waterspiegel. Deze afstand onder water hoeft niet al te groot te zijn, omdat niet is te verwachten dat de grootste schade onder water plaatsvindt. Daarentegen mogen stenen die van het talud naar beneden rollen zich niet opstapelen tot boven de waterlijn waar wel veel schade wordt verwacht. Vandaar dat is gekozen voor een hoogte van de golfbreker van $0,16 \text{ m} + 0,24 \text{ m} = 0,4 \text{ m}$. De goot zal ongeveer 20 centimeter hoger moeten zijn dan de golfbreker. Dat is dus 0,6 m.

Lengte

De golfbreker zelf heeft een maximale lengte van ongeveer 0.8 m (voortalud) + 0.8 m (kruin) + 2 m (achtertalu) = 3,6 m. Daarnaast is ruimte benodigde aan de achterzijde (de opvangbak). De totale lengte van de goot zal dus ongeveer 4 meter bedragen.

Afmetingen van de kruin

In deze proef heeft de kruin één belangrijke functie:

- Plek waar de snelheid en laagdikte gemeten worden (dichtbij de overgang kruin-achtertalu).

Hieruit volgt dat de kruin zal moeten bestaan uit een afsluitende, vlakke plaat met een breedte van 0,5 m en een bepaalde lengte, gelijkgesteld aan 0,8 m. Die lengte is eigenlijk niet van belang voor de proef (aangezien de metingen toch plaatsvinden bij de overgang kruin-achtertalu) en is flink groot gehouden om de invloed van uittree-onregelmatigheden van de pijp bij het achtertalud te voorkomen.

Benodigde hoeveelheid steen

Armour laag

De maximale steengrootte was al eerder vastgesteld op 0,034 m. De effectieve laagdikte kan worden berekend als volgt:

$$t = n \cdot k_t \cdot D_{n50}$$

Hierin is de t de effectieve laagdikte, n de laagdikte in stenen en k_t een coëfficiënt. De Shore Protection Manual zegt dat bij ruwe stenen geldt dat bij $n = 2$ (aannahme van mijn kant) $k_t = 1$. Dit betekent dat $t = 0,068$ m.

Het benodigde aantal stenen kan worden berekend als volgt. De maximale oppervlakte van het achtertalud = $1,02 \text{ m}^2$ (bij $\tan \beta = 0,2$). De totale oppervlakte onder de kruin = $0,15 \text{ m}^2$. De totale maximale oppervlakte (A) is dus $1,17 \text{ m}^2$. Het benodigde aantal stenen kan worden berekend met de volgende formule:

$$N = n \cdot k_t \cdot A \cdot (1 - n_v) \cdot \frac{1}{D_{n50}^2}$$

Hierin is n_v , de volumieke porositeit, volgens de Shore Protection manual gelijk aan 0.37. Dit levert een benodigd aantal stenen op van ongeveer 1300 stenen (!). De meeste metingen zullen plaatsvinden bij een helling met $\tan \beta = 0.5$, waarvoor slechts 700 stenen benodigd zijn. Er zal bedacht moeten worden of het noodzakelijk is de proef bij $\tan \beta = 0,2$ uit te voeren.

In navolging van Van der Meer stel ik in mijn proef dat er schade optreedt als een steen 2 of meer steendiameters verplaatst. Om dit proces aanschouwelijk te maken zal de buitenste steenlaag geverfd worden in verschillende kleuren en in banden van twee steendiameters breed worden gelegd.

Filterlaag + kern

In de proefopstelling zijn de filterlaag en de kern samengevoegd tot één homogeen zandlichaam, afgedekt met zeil. Deze lagen doen dus niet mee in de proefopstelling. Dit is gedaan omdat de snelheden in de filterlaag en de kern min of meer verwaarloosbaar zijn ten opzichte van de snelheden in de armour laag. Ter vergelijking: wanneer de massa van het kernmateriaal gelijk is aan 1/20 van het filtermateriaal en de massa van het filtermateriaal gelijk aan 1/15 van de armour laag, dan is de verhouding van de stroomsnelheden bij hetzelfde verhang 1:0,6:0,4.

Teen

Ik verwacht niet dat er onder water veel schade zal optreden. Voor de zekerheid zal ik echter een teen aanleggen, gemaakt van dezelfde steengrootte als de armour layer, puur ter versterking (breedte = 0,15 m en hoogte = 0,10 m).

Annex III.C Formules Van Gent

De overslagformules van Van Gent zijn gebaseerd op een nieuwe formule voor $z_{2\%}$, de oploophoogte die door 2% van de inkomende golven wordt overschreden. Deze nieuwe formule legt net als de oude formule (CUR/TAW 1992) voor $z_{2\%}$ een verband tussen de waarde van ξ (Irribarren parameter) en H_s (de significante golfhoogte). Het verschil zit 'm erin dat Van Gent ξ berekend met behulp van $T_{m-1,0}$, gebaseerd op de spectraal momenten m_{-1} en m_0 , in plaats van T_p , gedefinieerd in het globale maximum van het energiespectrum. Hierdoor wordt ook de oploophoogte van dubbelgepiekte golfspectra juist beschreven.

Formules van CUR/TAW (1992) voor $z_{2\%}$:

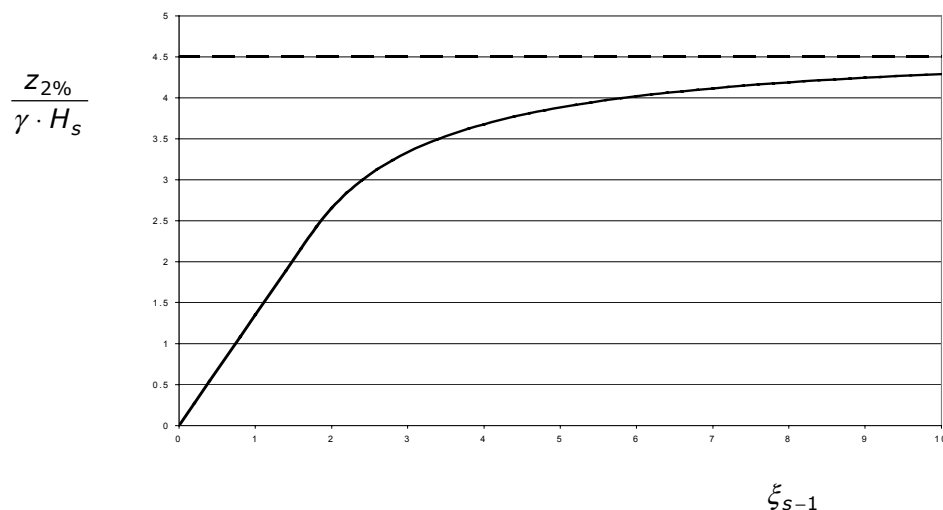
$$\frac{z_{2\%}}{\gamma H_s} = 1.5 \cdot \xi_p, \text{ met maximum } \frac{z_{2\%}}{\gamma H_s} = 3$$

Formules van Van Gent (1999-a) voor $z_{2\%}$:

$$\frac{z_{2\%}}{\gamma H_s} = 1.35 \cdot \xi_{s-1} \text{ voor } \xi_{s-1} \leq 1.74$$

$$\frac{z_{2\%}}{\gamma H_s} = 4.7 - \frac{4.1}{\xi_{s-1}} \text{ voor } \xi_{s-1} \geq 1.74$$

Deze formules zijn als volgt weer te geven in een grafiek:



Voor de berekening van de maximale overslag kan simpelweg gesteld worden dat deze optreedt bij een grote ξ_{s-1} (veel surging golven) en dat deze overslag waarschijnlijk niet veel groter zal worden dan:

$$z_{2\%,\max} = 4.5 \cdot \gamma \cdot H_s$$

Met $\gamma = 0.5$ kan dan gesteld worden dat $z_{2\%,\max} = 2.25$ maal H_s . Deze waarde zal worden gebruikt in verdere berekeningen.

Van Gent geeft op basis van numerieke modellen en fysisch modelonderzoek de volgende formules voor overslaglaagdikte ($d_{2\%}$), overslagsnelheid ($u_{2\%}$) en overslagvolume per strekkende meter ($V_{2\%}$):

$$d_{2\%} = c'_h \cdot \frac{(z_{2\%} - R_c) / \gamma_f}{c''_h + B_c / H_s}$$

$$u_{2\%} = c'_u \cdot (g \cdot \gamma_{f-c})^{0.5} \cdot ((z_{2\%} - R_c) / \gamma_f)^{0.5}$$

$$V_{2\%} = c'_v \cdot \gamma_{f-c}^{0.5} \cdot ((z_{2\%} - R_c) / \gamma_f)^2$$

Hierin is

$d_{2\%}$	laagdikte die door 2% van de inkomende golven wordt overschreden
$u_{2\%}$	snelheid die door 2% van de inkomende golven wordt overschreden
$V_{2\%}$	volumes per m die door 2% van de inkomende golven wordt overschreden
$z_{2\%}$	oploophoogte die door 2% van de inkomende golven wordt overschreden
H_s	significante golfhoogte
R_c	kruinhoogte
B_c	Breedte kruin
γ_f	correctiefactor van de helling
γ_{f-c}	correctiefactor van de kruin
c'_h ; c''_h ; c'_u ; c'_v	constanten

Met behulp van fysische model testen zijn de volgende waarden voor de constanten in deze formules gevonden:

Parameter	c'	c''
$h_{2\%}$	1..7	10
$u_{2\%}$	1.5	-
$V_{2\%}$	1	-

De breedte van de kruin blijkt weinig invloed te hebben op de laagdikte, behalve wanneer deze in waarde meerdere malen groter is dan de significante golfhoogte. Wanneer er verder van wordt uitgegaan dat $\gamma_f = \gamma_{f-c} = 0,5$, dan zijn de hydraulische parameters alleen afhankelijk van de waarde van $(z_{2\%} - R_c)$.

Annex III.D Formules Perdijk

In dit rapport zal ik me beperken tot het behandelen van Perdijks formule voor de tijdsduur van golfoverslag van regelmatige golven, omdat alleen deze formule interessant is voor de proefopstelling.

Perdijk baseert zijn formules voor de tijdsduur van golfoverslag op de oploopformules voor regelmatige golven van Roos en Battjes (1974). De tijdsduur die het golfvront nodig heeft om vanaf SWL op te lopen tot de maximale hoogte is volgens Battjes en Roos gelijk aan:

$$t_m / T = \frac{0.7}{\sqrt{\xi}}$$

Perdijk stelde deze tijdsduur gelijk aan de totale duur van oploop en overslag van lage dijken. Wanneer ik ervan uitga dat in mijn geval de oploop verwaarloosbaar kort is (de kruinhoogte zit behoorlijk laag), dan kan ik stellen dat de formule van Roos en Battjes een aardige schatting is van de overslagtijd.

Annex III.E Stabiliteitsformules Van der Meer

De stabiliteitsformules van Van der Meer (1988) voor het voortalud van golfbrekers onder invloed van een onregelmatig golfveld zijn als volgt gedefinieerd:

$$\frac{H_s}{\Delta D} = 6.2 \cdot P^{0.18} \left(\frac{S_d}{\sqrt{N}} \right)^{0.2} \cdot \xi_m^{-0.5} \quad \text{voor } \xi < \xi_t$$

$$\frac{H_s}{\Delta D} = 1.0 \cdot P^{-0.13} \left(\frac{S_d}{\sqrt{N}} \right)^{0.2} \cdot \xi_m^P \cdot \sqrt{\cot \alpha} \quad \text{voor } \xi > \xi_t$$

met

$$\xi_t = \left[6.2 \cdot P^{0.31} \sqrt{\tan \alpha} \right]^{\left(\frac{1}{P+0.5} \right)}$$

Hierin is

H_s	significante golfhoogte	(m)
Δ	$\frac{\rho_{steen} - \rho_{water}}{\rho_{water}}$	(-)
ρ	soortelijke dichtheid	(kg/m ³)
D	steengrootte armour laag	(m)
P	Permeabiliteit	(-)
S_d	Schadegetal	(-)
N	Aantal golven	(-)
ξ_m	Iribarren parameter	$\frac{\tan \alpha}{\sqrt{\frac{H_s}{g \cdot T_m^2}}}$ (-)
α	Hellingshoek voortalud	(-)

Met bovenstaande formules is berekend welke golfhoogte het voortalud aankan, opgebouwd uit stenen van 3.4 cm. Uiteraard spelen hierin een hoop parameters een rol, waarvan enkele constant zijn gehouden:

Parameter	Waarde	Waarom?
D_n (m)	0,038	Deze waarde is gelijk aan $0,034 \text{ m} * 1.1$. Bij een golfbreker met $R_c/H_s \approx 0,6$ (iteratief bepaald) en $s_p = 0,013$ is de reductiefactor voor de steendiameter ongeveer 1,1.
Δ (-)	1,65	Er wordt bij deze berekening uitgegaan van $\rho_{\text{steen}} = 2650 \text{ kg/m}^3$ en $\rho_{\text{water}} = 1000 \text{ kg/m}^3$
P (-)	0,4	Dit is de waarde voor een klassieke golfbreker met riprap kern
S_d (-)	8-17	Ik wil de waarde van H_s weten waarbij het voortalud bezwijkt. Voor de stijlere taluds betekent $S = 8$ bezwijken, voor de vlakkeren geldt $S = 17$.
N (-)	3000	Een maximum van 3000 golven lijkt mij een aardige representatie van de werkelijkheid.

Bij het bepalen van de H_s die hoort bij de maximale $z_{2\%}$ heb ik gekeken naar verschillende combinaties van $\tan \alpha$ en T_m , waarbij ik ervan ben uitgegaan dat ξ_m een stuk groter dan 3 moet zijn, zodat veel overslag optreedt. De resultaten van deze berekeningen zijn als volgt:

D_n (m)	Δ (-)	P (-)	N(-)	S_d (-)	$\tan \alpha$ (-)	T_m (s)	s_m (-)	ξ_m (-)	H_s (m)
0.0425	1.65	0.4	3000	17	0.2	3.42	0.01	2.00	0.184
0.0425	1.65	0.4	3000	17	0.25	3.23	0.01	2.50	0.164
0.0425	1.65	0.4	3000	12	0.33	2.91	0.01	3.30	0.145
0.0425	1.65	0.4	3000	8	0.5	2.52	0.01	5.00	0.128
0.0425	1.65	0.4	3000	8	0.66	2.35	0.01	6.60	0.125

Uit bovenstaande tabel wordt duidelijk dat een flauwere helling met dezelfde steengrootte een grotere golfhoogte aan kan. Dit wil echter niet zeggen dat bij deze golfhoogte ook het achtertalud maximaal wordt belast. De stabiliteit van het achtertalud wordt bepaald door de grootte van de plonzen die een functie zijn van H_s én ξ . Bij een grote ξ is ook de overslag groot en zal het achtertalud het meest te verduren krijgen. Vandaar dat de significante golfhoogte waarmee de maximale $z_{2\%}$ en dus de grootste plonzen worden berekend, gelijk is gesteld aan 0,13 m ($\tan \alpha = 0,5$ en $\xi_m = 5$).

Nu werkt de formule van Van der Meer met T_m en de daaruit resulterende ξ_m , terwijl Van Gent werkt met $T_{m-1,0}$ en $\xi_{s,-1}$. Het is niet mogelijk T_m om te rekenen naar $T_{m-1,0}$ en dus is invullen van resultaten uit de ene formule in de andere formule erg riskant. Ik ben er echter vanuit gegaan dat wanneer ξ_m behoorlijk groot is, dat dit dan ook geldt voor $\xi_{s,-1}$. Het lijkt in dit geval dus gerechtvaardigd om de uitkomsten van de Van der Meer formule te gebruiken in de formule van Van Gent.